Engineering of corneal stroma and posterior cornea tissues towards applications in corneal transplantation

Submitted in partial fulfillment of the requirements for the

degree of

Doctor of Philosophy in

Biomedical Engineering

Santiago D. Carrasquilla

B.S., Biomedical Engineering, University of Florida

Carnegie Mellon University
Pittsburgh, PA

August 3, 2021

ACKNOLEDGMENTS

As someone said to me, “to get a Ph.D., it takes a village.” Many people have been involved in helping, guiding, and supporting me through this journey. Both, before and through the Ph.D., many teachers, mentors, friends, and family have taken their time and energy to listen to my crazy dreams and ideas. Thank you all, I would not have accomplished this if it were not for you.

First, I would like to thank the people who made this technically possible. My PI, professor Adam Feinberg, for providing financial stability and guidance throughout the project. Thank you for giving me the opportunity to learn and research a tissue not many recognize but many see.

I would like to thank the funding sources, the National GEM Consortium for advocating and giving opportunities to historically underrepresented group to achieve a doctoral degree, and the National Institutes of Health (R01 EY024642-01A1) for caring about corneal health.

Thank you to my committee, Dr. Rachelle Palchesko, Dr. Charlie Ren, Dr. Phil LeDuc, and Dr. Phil Campbell. You were chosen because of your support, acumen, and perspective. Your feedback will always be welcomed. Not in the committee but an integral part of my research, Dr. James Funderburgh and his wife Martha Funderburgh. Jim was always eager to listen what crazy engineering thing I was working on. Thank you, Jim, for your support, teachings, and curiosity. I wish you were here to see the results of those conversations.

I would also like to highlight the people that have been part of my development

as a scientist, student, and person prior to starting the Ph.D. To mind comes several teachers and close friends from from Colombia; who though they might not remember me, they had a significant impact on who I am today. Similarly, I am thankful for the support I had when I first arrived in the US. Theater allowed me to better express myself and get familiar with a new culture, thank you SPHS Theater family. I would like to thank my room mates throughout collage, both at the University of South Florida and the 1133 apartment at the University of Florida. Y'all made my undergrad experience better.

While at CMU I have had the opportunity of creating and sharing many experiences outside of the lab. From my involvement in the Graduate Student Assembly, to helping Tartan Salsa grow and become one of the largest dance groups in Pittsburgh. Thank you Sarah, Brittani, Surya, Josh, Dyviansh, Cole, and all of GSA. Thank you Carmen, Kuai-Kuai, Manuel, Andresa and all of Tartan Salsa. My best and most frustrating memories involve these groups. I have learned and grown because of the people involved in them. Y'all were a source of sanity and support far greater than what you can imagine.

Inside the lab I would not have been able to accomplish this if it weren't for the JAMS (Jaci, Annie, Maria, Santiago) cubicle group and a special thanks to Erica. Being able to share and laugh at our frustrations helped me to keep going. Lastly, Rachelle was more than a mentor to me than she realize.

I want to specially acknowledge Jennifer Bone. Your support throughout the beginning of this adventure helped me more than you can imagine. You belived in me even when I could not, and you guided me through the darkest of times. You made many long nights in the microscope room enjoyable and long days of studing much

much better. Thank you for everything.

I want to acknowledge my mom, dad, and sister. This work is proof of our sacrifice of leaving all behind and gambling on moving to a new country, with new cultures, and a different language. I want to acknowledge that not every immigrant has the opportunity to attend college, and far fewer have the opportunity to complete a Ph.D. None the less, we all sacrificed something, and my family has been there in every turn and hardship. Gracias a todos.

Finally, I would like to thank myself. For staying up late at night writing, or reading, or singing to my cells so that they align and the experiment work out. For keep pushing, even when nothing seemed to go right and there was little time to set-up a new experiment. Because instead of giving up, though I considered it, I decided to persevere and keep pushing and keep going. I want to thank me, for trying to believe in myself even when I could not believe in myself.

This thesis is dedicated to my family, friends, and mentors. To all of those that have supported me and believed in me, and to myself.

ABSTRACT

Blindness and low vision severely diminish the quality of life, and research has shown that going blind is the most feared disability. The cornea is the front-most tissue of the eye, serving to protect the inner parts of the eye and working with the lens to focus light onto the retina. Damage or disease can manifest into an opaque or misshaped cornea. An opaque cornea blocks light from reaching the retina while a misshaped cornea is incapable of focusing light. Both cases can lead to vision loss and corneal-related blindness. Depending on the cause, whole or partial-thickness cornea transplantation, such as deep anterior lamellar keratoplasty (DALK) and Descemet stripping endothelial keratoplasty (DSEAK), can improve the patient's vision. However, donor corneal tissue comes from cadaveric sources and there is an unmet demand for transplantable corneas. Engineered partial thickness or whole corneal scaffolds can help close this gap. The long-term vision of this thesis is to engineer partial-thickness corneal constructs and used them in transplantation procedures. To accomplish this, constructs must be capable of withstanding handling during surgery, be transparent after transplantation, and integrate into the host cornea without causing a pathological host response. In this thesis, I combine biomaterials engineering, protein assembly, and patient-derived corneal stromal stem cells. In chapter 2, I fabricated a multilayered cornea stroma construct with the potential of being used in DALK procedures. In chapter 3, I integrated an engineered endothelium with multilayered stroma constructs to assemble an engineered posterior cornea (EPC). The EPC integrated onto an ex-vivo rabbit cornea after implantation using a DSEAK-like procedure. Lastly, in chapter 4, I initiate the work for a corneal stroma bioreactor that can be used with a multilayered

stroma construct or EPC to understand the effects of pressure on extracellular matrix assembly and fabricate better corneal tissues. This thesis provides valuable data and a platform to build transplantable tissues and models. Future directions include evaluating the multilayered cornea stroma construct in an animal DALK procedure and the EPC on a DSEAK procedure, as well as, generating a whole cornea construct.

TABLE OF CONTENTS

LIST OF TABLES

LIST OF FIGURES

Chapter 1: Overview

The cornea is one of the tissues that permits humans and other living organisms to observe our surroundings. Disease, bacterial and viral infections, and trauma can damage the cornea and cause blindness or visual impairment. For the most severe of cases, whole or partial-thickness cornea transplantation can restore vision. However, demand for donor tissue is not being met with the supply of transplantable corneas. Tissue engineering can help address this demand for transplantable tissue.

This thesis present my work over the last 5 years on developing protocols that combine cell culture, in the form of corneal stroma stem cells (CSSC) and bovine corneal endothelial cells (BCEC), and materials sciences, in the form of fabrication of natural biomaterials scaffolds, to bring about corneal tissues with the potential of transplantation. In chapter 2, I present a general background of the cornea as a whole tissue. I put into perspective the global need to address preventable blindness and visual impairments and emphasize blindness and visual impairments due to corneal-related diseases, such as corneal opacities and refractive errors. Then, I talk about the historical advances, starting from ancient Egypt and ending in the early 1900s, in corneal transplantation and the technologies needed to get to where we are now. Following, I introduce the different transplantation procedures used today, from whole cornea transplantation (penetrating keratoplasty) to the main partial-thickness transplantation procedure. Lastly, I highly major work in the field of corneal tissue engineering, in particular work done using natural biomaterials such as collagen and the amniotic membrane.

Chapters 3, 4, and 5 are the main research chapter of this thesis. Note: Chapters 3 is the chapter closest for publication and I anticipate chapter 4 to closely follow, for these reasons these chapters are presented as research manuscripts with an abstract, although with an extended introduction.

In chapter 3, I concentrate on the development of an engineered stroma tissue. This chapters start by doing a deep dive on the corneal stroma extracellular matrix (ECM) architecture and concentrates on engineered stroma tissues for partial transplantation procedures of the stroma. Chapter 3 lays out the main protocol to transfer protein features, either lines of various dimensions or isotropic controls, over a collagen I (COLI) gel. Furthermore, in chapter 3 I developed and explained the stacking to build multilayered scaffolds. Both protocols are the technical foundation of this thesis and are used extensively throughout chapters 4, and 5. In chapter 3, single-stroma sheets made are formed by highly aligned CSSC that assembled a highly aligned ECM. A multilayered stroma scaffold is achieved by the formation of a slightly rotated second cell layer for each aligned CSSC monolayer and by stacking of single-stroma sheets into a duo-stack and quad-stacks. Note: The work in this chapter is the most developed and closest to be published.

In chapter 4, I expand on the single and multilayered stroma scaffold by integrating a corneal endothelium. Here, I first introduce the endothelium and Descemet's membrane and describe the importance of a healthy endothelium to maintain the proper hydration in the stroma to prevent edema and opacities. I then make a note on the rising interest in the use of DSEAK and DMEK procedure transplant the endothelium. In this chapter, I use the stacking method developed in chapter 3 to

stack an engineered endothelium over a single-sheet stroma, here termed an engineered posterior cornea (EPC), and over a duo-and quad-stack stroma. I assess the ”transplantability” of the EPC by replacing the endothelium of an ex-vivo rabbit cornea with an EPC for 7 days. Although there was a partial attachment of the EPC to the ex-vivo cornea, the results are encouraging and small changes to the tissue and the protocol can enhance the integration of the EPC to the cornea tissue.

Chapter 5 lays out the grown work for future work in developing a corneal bioreactor for the tissues developed in the previous chapters. The motivation for the construction of this bioreactor is to understand how keratocytes in the native stroma assemble a highly aligned, unwoven COLI matrix throughout the development. Using CSSC as a keratocyte proxy, I propose to expose CSSC to various strains that mimic the intraocular pressure and assess how the cell bi-layer changes. Although many pieces of this chapter were affected by the laboratory shutdown caused by the global pandemic, I attempt to give ideas on how to build a corneal bioreactor, drawing inspiration from other groups. I also provide some initial results on CSSC assembly over a suspended COLI gel without any strain. The future work of this chapter was written as a suggestion for the researchers that will take over this work.

To wrap up the main parts of the thesis, chapter 6 is a general summary of the key, take-home messages of each research chapter and provides an encompassing conclusion and future direction of this work.

Lastly, the appendices of this thesis are meant to serve as a record of successful alternative methods and that I believe can be of interest to someone. I wrote each appendix as a draft for a manuscript with the hopes of creating enthusiasm in the reader

for this early work and maybe cause interest in other researchers to continue these works. In appendix A, I build highly regular COLI channels, termed microgrooves, with a planar resolution of 2 μm to align CSSC. While in appendix B, I use a protocol to transfer protein features to both sides of a COLI gel and co-culture CSSCs and BCECs on these double-sided COLI gels.

Chapter 2: Background

2.1. The Cornea

The cornea is the front-most tissue of the eye. It protects the inner tissues, holds two-thirds of the total refractive power, transmits over 90% of the visible light, and provides structural support to the eye globe. A healthy cornea is essential for vision, as it is the window of the eye. Structurally, the cornea is avascular, made of 3 cellularized layers and two basement membranes (Fig. 2.1). Each one the layers have their unique structural and functional characteristics. In order from anterior to posterior: the epithelium has a constant supply of growing cells that provide protection from the outside world and, Bowman's layer provides anchoring points for the stroma and is believed to stabilize corneal shape. The stroma is a dense, collagen-rich tissue that makes up 90% of the cornea and provides most of the cornea's refractive shape. Lastly, Descemet's membrane and the endothelium have the role of regulating hydration and nutrition out of and into the stroma. Finally, the cornea is composed of three major cell types, epithelial cells, stromal keratocytes, and endothelial cells. Both, epithelial and endothelial cells form cellular barriers around the stroma.

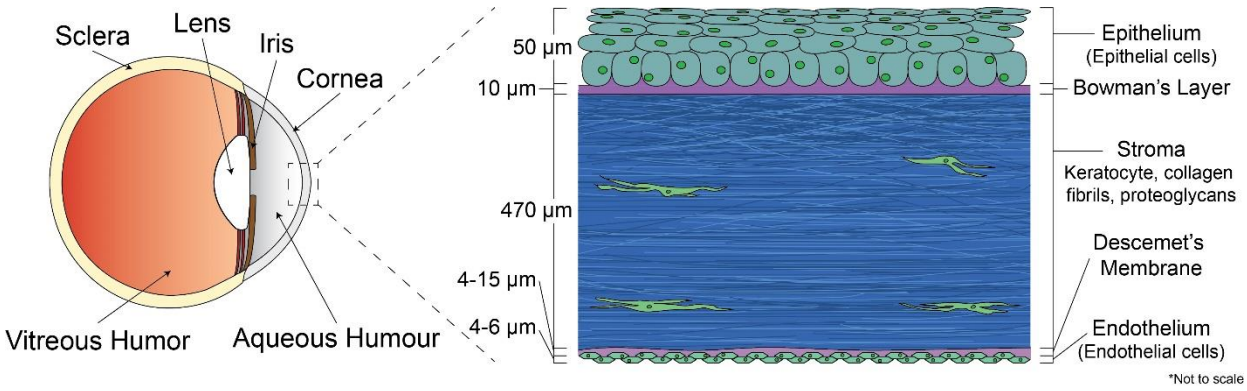

Figure 2.1. Main anatomical components of the eye globe and the cornea.

2.2. Blindness, Visual Impairment, and Corneal Related Blindness

Between the generally accepted five senses of humans, sight is many times considered to be the most important[130]. We rely on sight to navigate and move safely through space, to communicate via written and non-verbal cues, and to appreciate the world around us. Blindness, along with cancer, is the most feared health condition, and vision loss is the most feared disability[134]. Furthermore, developing blindness can lead to a changed perception of self, decreased levels of wellbeing, and an increasing prevalence of depression[125,200].

Latest estimates by the World Health Organization suggest that worldwide 2.2 billion people have a vision impairment or blindness, and at least 1 billion of these cases could have been prevented or can be treated[218]. These 1 billion people include people suffering from unaddressed refractive error (8.8%), cataract (9.4%), glaucoma (7.7%), corneal opacities (4.2%), diabetic retinopathy (3.9%), trachoma (2%), and near vision impairment from unaddressed presbyopia (82.6%)[194,218]. These diseases affect different regions and populations worldwide differently.

The regional difference in access to the infrastructure and supply for treatment are major contributors to this uneven distribution and treatment of eye diseases. Similarly, income level, age, and gender have a significant impact on the accessibility to eye treatments that prevent blindness[218]. The vast majority of blindness and visual impairment cases are concentrated in South, Southeast, and East Asia, with a significant amount of cases in the Sub-Sahara and North Africa, and the Middle East. When compared to the number of patients in high-income countries, high-income countries have a combined blind and visually impaired population 6 to 8 times smaller

than the combined population of countries in South, Southeast, and East Asia[65].

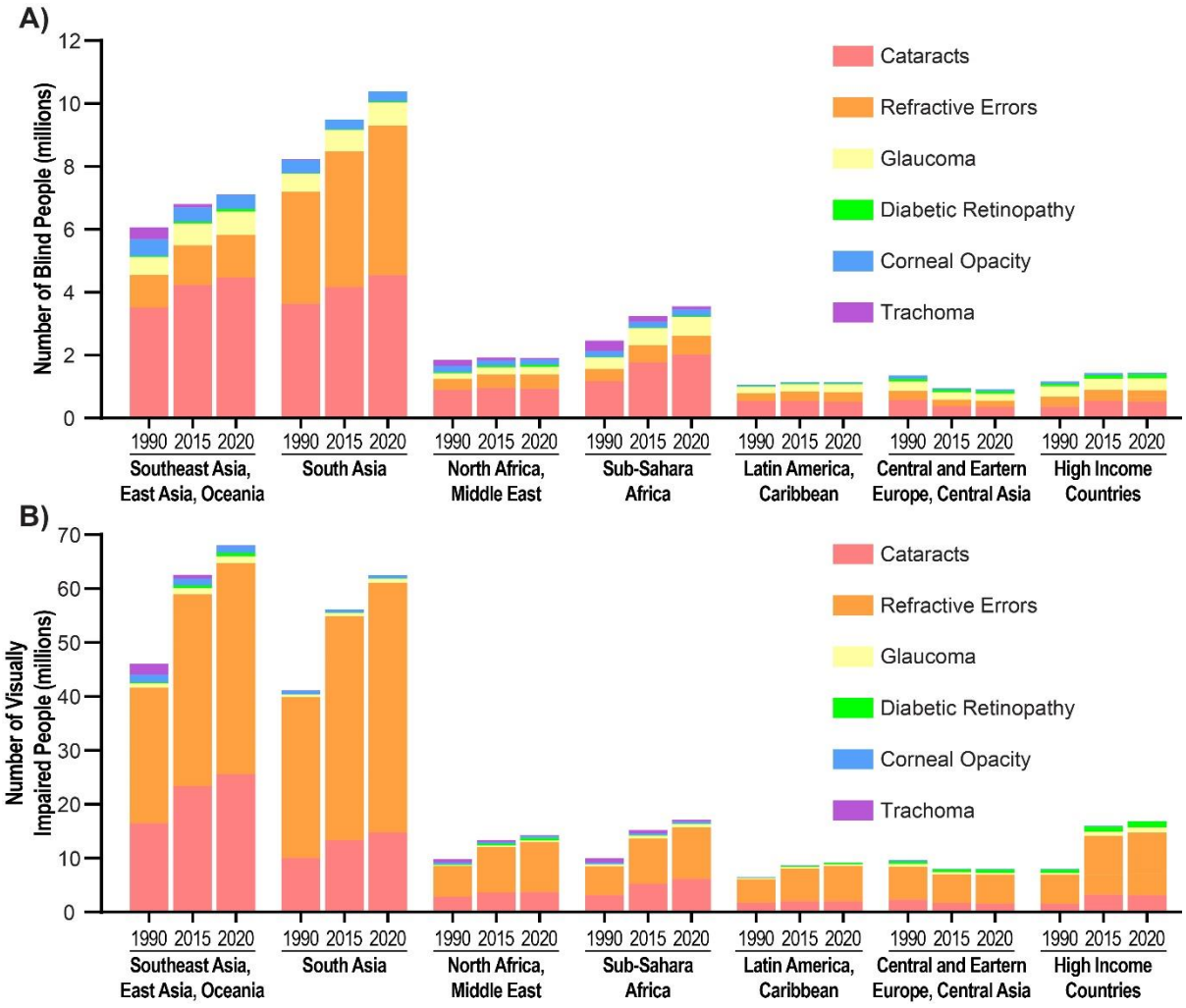

Figure 2.2. Distribution of blindness and visual impairment worldwide from treatable and preventable eye diseases.

The number of people in millions suffering from blindness (A) and visual impairment (B), divided by region. Data for the years 1990 and 2015 were collected from published and unpublished population-based data. 2020 estimates were calculated by fitting a regression model using data from 1980 to 2014. Adapted from Flaxman. S., et al., *The Lancet Global Health,* 2017.[65]

Note that, although trends show an increase in the total number of cases, likely cause by a natural increase in population, the age-standardized prevalence of these

conditions shows a decrease year after year[65]. However, models suggest that new therapies, an increase in facilities and access, and more personal training such as ophthalmologists and surgeons will be needed to continue to provide optimal care and treatments that continue to address blindness and visual impairment[65,194].

Corneal-related blindness, which can be refractive errors and corneal opacities, is the second leading cause of blindness and the leading cause of visual impairment worldwide[194,218], between treatable conditions. Some examples of corneal related blindness include a misshape in the cornea, such as keratoconus, causing refractive errors and problems in focusing a sharp image. Also, the loss of endothelial cells in the endothelium might cause problems in regulating the hydration of the stroma and ultimately cause corneal edema. Corneal edema manifests as a cloudy cornea that inhibits light transmittance and in severe cases causes blindness. Corneal disease from scarring is also one major cause of blindness in children and young adults.

2.3. Over 100 years of Corneal Transplantations

Understanding the corneal structure and its functions, how to treat corneal diseases and eventually transplant the cornea, are challenges that have inspired scientists, philosophers, and physicians for centuries. For example, trachoma is one of the oldest recorded diseases of mankind, first reported and treated in Egypt in 1900 BCE with copper sulfate scarification, a procedure that remained unchanged until the late 1930's[215]. Similarly, Egyptians resorted to rubbing soot or other exotic ingredients onto the eye to treat corneal disorders due to smallpox, or injury[149].

In ancient Greece, Aristotle proposed, in great contradiction with many of his contemporaries, that the eye was a sensing organ that receives rays and was affected by light to create an image, intromission[9]. However, it was Galen, a believer of extramission (the idea that a light source inside the eye interacts with the outside world to create an image), who described and named most of the parts of the eye, such as the retina, cornea, iris, uvea, tear ducts, and eye lids, as well as the vitreous and aqueous humour, and identify cataracts as a disease capable of interfering vision[71]. Galen also proposed, although believed not to test, superficial keratectomy to restore corneal aberrations[34,71].

The idea of regaining sight via transplantation of the eye or the cornea only lived in fairytales and legends. Such is the legend of Saint Lucy, patron saint of ophthalmology, who removed her eyes to escape from unwelcomed attention and then was rewarded with more beautiful eyes due to her virtue. It was not until the late 1700s when a serious discussion and consideration of transplanting the cornea started to gain traction in Europe.

In the late 1700s, surgeons and ophthalmologists started to give serious consideration to the cornea. For example, Erasmus Darwin proposed in the 1760s to cut out the opaque any opaque section of the cornea and allow the cornea to heal into a transparent scar[34,149]. Also, French cataract surgeon Guillaume Pellier de Quengsy published in 1789 the first known monograph for ophthalmic surgery[178]. In it, Quengsy describes a procedure where an opaque cornea is removed and substituted by a glass lens supported by a silver ring and sutured into the sclera using a cotton thread[26,139]. However, there is little evidence that either of these procedures was carried out.

Then, in the XIX century major advances in the technology surrounding corneal transplantation happened rapidly, but with little long-term success. Karl Himley postulated in 1813 to transplant clear animal corneas to opaque corneas of other animals, which was carried out experimentally by Franz Reisinger, his pupil, in 1824 using rabbits[149,181]. Here, although healing occurred, none of the corneas remained clear. It was not until 1837 when the first reported successful cornea transplantation took place on a pet gazelle by Samuel Bigger using the cornea of another gazelle[16,34].

From these early experiments and few successes, interest in cornea human transplantation started to grow and in 1838 the first pig to human corneal transplantation took place. The New York-based ophthalmologist Richard Kissam performed transplanted a donor pig cornea onto a human. Although there was an early improvement in visual acuity, the cornea opaqued within the first night, and by the first month, the graft had been completely absorbed[34,117].

The remaining of the century was filled with little success that shed important knowledge on the collective understanding of the cornea and on the development of

tools that have advanced the field. The introduction of general anesthesia in 1846, the accurate microscopic description of the cornea by Sir William Bowman in 1847, and the development of circular trephine by Arthur von Hippel in 1886, are some examples of the interest in the development of a lamellar graft for partial transplantation of cornea and anatomy of the cornea.

Using the knowledge of over 2000 years of fail attempts and discoveries, the first fully successful human-to-human transplantation of a whole cornea happened in the early XX century. Eduard Konrad Zirm performed the first penetrating keratoplasty in 1905 where the graft remained clear after 6 months post operation[149,239]. And the subsequent introduction of corticosteroids and antibiotics to address allograft rejection made corneal transplantation a popular and successful treatment to restore vision.

In the following decades, corneal scientists, ophthalmologists, and surgeons have been able to improve this surgical technique by introducing different trephines including laser-guided trephination, develop new transplantation techniques for precise removal and implantation of different corneal layers, as well as optimizing donor tissue preservation and preparation and develop new materials, both synthetic and biological, to expand the supply of corneal tissue.

For a more in-depth exploration of the history of corneal research and procedures, the author recommends the reviews by Crawford, et al.[34] and Moffatt, et al.[149] Since these reviews show a Euro-centric view, the author also recommends Chirila, et al.[25] for the historical perspective in Japan.

2.4. Corneal Transplantation Procedures

In the most severe cases of corneal damage, corneal transplantation is the only way to restore vision. Current corneal transplantation techniques can be divided into four main types that vary in invasiveness. From most to least intrusive: penetrating keratoplasty, deep anterior lamellar keratoplasty (DALK), Descemet's stripping automated endothelial keratoplasty (DSEAK), and Descemet's membrane endothelial keratoplasty (DMEK).

Whole corneal transplantation, also known as penetrating keratoplasty (Fig. 2.3A), is the most invasive procedure to restore corneal health. Using a healthy whole donor cornea, the patient's whole cornea is cut out using a trephine of an appropriate diameter, and the new tissue is radially sutured in place to minimize post-operative astigmatism[41]. With the rise of less invasive and more selective transplantation procedures, penetrating keratoplasty is primarily used for cases with significant corneal scarring, opacities, edemas where the status of the endothelium is unknown, corneal ectasias such as keratoconus, infectious ulcerations, and cornea perforations. The main drawbacks of penetrating keratoplasties are the relatively long recovery period, sometimes taking years, the frequent postoperative refractive error, and a higher risk of allograft rejection[29,98]. Because of these complications, new surgical methods were developed to leave intact healthy layers of the cornea while selectively replacing the diseased layers

The objective of DALK is to preserve a patient's healthy endothelium and Descemet membrane. DALK is a partial-thickness transplantation procedure where a section of the corneal stroma is replaced without disturbing the native endothelium and

Descemet membrane (Fig. 2.3B). A trephine of the right diameter is used to make a partial incision on the cornea. The anterior stroma is then removed manually and replaced with a graft prepared from a donor whole cornea where the donor endothelium and Descemet membrane have been separated from the anterior stroma[41]. DALK is particularly useful in procedures involving a healthy endothelium and an opaque cornea[203], corneal ectasia, corneal scars that do not affect the whole cornea, and stromal dystrophies[41,66]. Leaving the host endothelium intact significantly increases a successful outcome and faster recovery. However, DALK is more complex than penetrating keratoplasty and in the case of damage to the Descemet membrane during the operation, the procedure needs to be converted to penetrating keratoplasty. The "big bubble" technique has gained popularity in DALK procedures because makes dissection more consistent[8]. This procedure consists of separating the stroma from the Descemet membrane by injecting an air bubble in between the layers of the cornea. Then, donor stroma tissue can be introduced in the pocket created by the bubble. On aspiration of the air, the donor tissue is locked in-place. This technique has been proven to be faster, safer and easier to perform than previous DALK methods[8,79,164].

DSAEK (Fig. 2.3C) and DMEK (Fig. 2.3D) attempt to transplant the posterior layers of the cornea, that is, the endothelium and Descemet membrane. In both procedures, a small incision in the cornea-scleral region of the eye is performed to be able to access the posterior cornea. The endothelium and Descemet membrane are removed from the patient. In DSEAK, the donor tissue includes the endothelium, Descemet membrane, and about 100 to 200 μm-thickness of the posterior stroma. In DMEK, the donor tissue does not contain the stroma. In both procedures, the donor

tissue is folded and inserted through the small incision and a bubble of air or 20% sulfur hexafluoride in the anterior chamber supports the graft against the cornea to promote adherence to the tissue[41]. Both procedures are particularly useful to treat endothelial dystrophies, such as Fuchs disease, and various endothelial dysfunctions. DSAEK has better postoperative visual acuity than DALK, however, the interface between the native stroma and the graft stroma can cause interference. DMEK offers the fastest recovery period and superior visual acuity than any other keratoplasty technique to date. Both of these techniques have a higher-level technical difficulty than DALK and penetrating keratoplasty. The tissue grafts can be thin, fragile, and hard to handle, and some post-operative complications include graft dislocation and lifting.

Like in section 2.3., to read on the historical perspective and the development of these techniques the author points to the review by Baydoun, L., et al.[14] and Hos, D., et al[95].

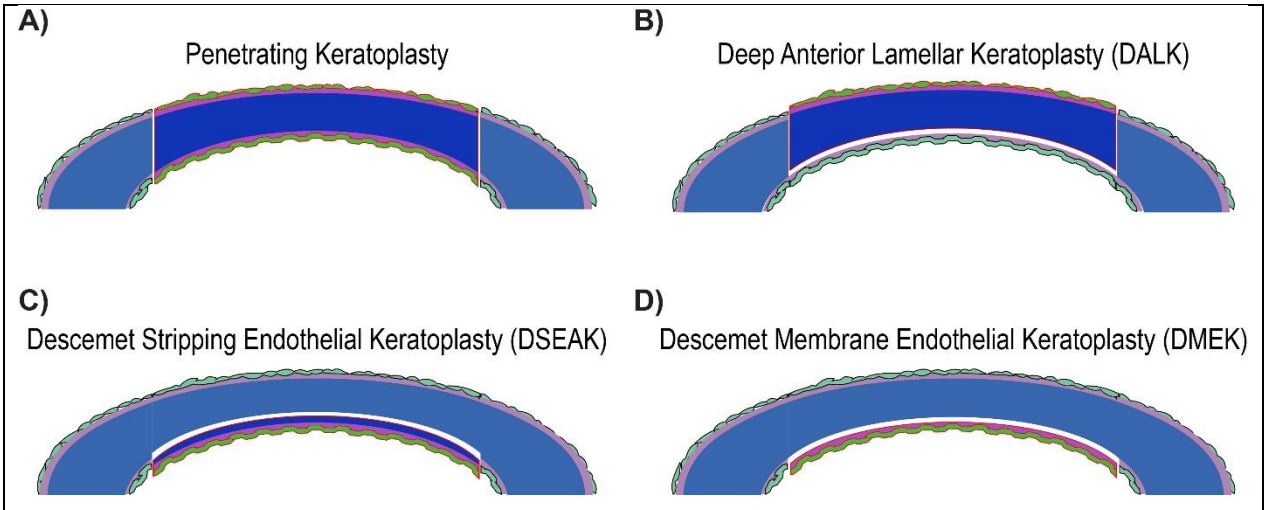

Figure 2.3. Schematic of the main corneal transplantation procedures.
From most to least intrusive, penetrating keratoplasty (A), Deep Anterior Lamellar Keratoplasty (DALK; B), Descemet Stripping Endothelial Keratoplasty (DSEAK; C), Descemet Membrane Endothelial Keratoplasty (DMEK; D)

2.4.1. A Note on Engineered Corneal Constructs from Synthetic Materials: Keratoprosthesis

The only artificial cornea procedure currently available is a Keratoprosthesis. Through this procedure, the whole cornea is removed and often replaced with the Boston Type I Keratoprosthesis, the most used artificial cornea device in the US. The Boston Type I consist of plastic polymethylmethacrylate front and backplates that sandwich corneal tissue that serves to suture the device to the eye, and a titanium locking c-ring that prevents intraocular disassembly of the device. Because of the high level of care needed postoperatively, this procedure is specially reserved for patients with a history of multiple failed transplantations, patients with autoimmune diseases, and severe acid and alkali ocular burns.

There are several long-term risks for Keratoprosthesis. Because these involve a synthetic, foreign body with vastly different mechanical and chemical properties to biological materials, there is a high risk of postoperative glaucoma and endophthalmitis, and due to the hard plastics, general monitoring of eye health becomes harder to assess, in particular the measurement of the interocular pressure. Other risk factors include stromal melt, retinal detachment, and vitreous hemorrhage. Due to the substantial risks, close monitoring and a large group of specialists are needed for successful postoperative management.

2.5. Engineered Corneal Constructs from Natural Biomaterials

Engineered corneas can help address the gap between demand and supply of transplantable corneal tissue. Engineers and scientists have been developing new and exciting approaches to bring about a scaffold that of withstanding handling during transplantation, be transparent after transplantation, and integrate into the host cornea without causing a pathological host response.

Natural biomaterials have been used in combination with keratocytes or corneal fibroblasts to give rise to desired functional characteristics, such as transparency and mechanical strength, to build a corneal scaffold. For example, silk fibroin is a natural biomaterial isolated from silkworms cocoons that can be easily molded into mechanically strong, micropatterned sheets that can control the direction of cell growth[75,223]. Additionally, recent work has shown how multiple corneal cells can be incorporated into silk-based, multilayered constructs to model diabetic corneal neuropathy [37,73]. Alternatively, allogenic amniotic membranes, which are composed of epithelium, basement membrane, and stroma, serve as an initial platform for cell growth because of their low immunogenicity and resemblance to the cornea basement membranes[54,125]. Other alternatives to allogenic corneas are decellularized xenogeneic tissues because these can be produced in abundance, retain major structural components of the cornea, and can be readily decellularized and recellularized with human keratocytes to make them immune match the patient[125].

However, none of these materials have emerged as a clear candidate that recreates the complex biophysical and mechanical properties of the cornea. Silk lacks specific cell-binding motifs that keratocytes and other cells use to bind to the ECM. The

amniotic membrane lacks mechanical strength and there is a high ECM compositional and structural donor-to-donor variability. Furthermore, there is little evidence that the amniotic membrane is better than existing treatments for various corneal conditions[125,185]. Lastly, the use of decellularized xenogeneic corneal tissues presents significant structural variabilities, requires expensive and extensive testing to prevent possible disease transmission, and, in some regions, cultural stigmas prevent people from cross-species transplantation. Overall, although scaffold-based approaches using natural biomaterials have demonstrated acceptable levels of cell adhesion, proliferation, and differentiation, some still lack suitable mechanical stability, optical transparency, and the vast majority fail to mimic the natural microenvironment[22,123,125]. These drawbacks result in post-operative complications such as delayed rejection[27], immunological and foreign body response, incomplete epithelization[120], and inflammation.

A successful bioengineered cornea can also be used for in-vitro disease and developmental studies and several groups have taken the lead in this area. For example, research done by Deardorff and colleagues shows that a benchtop, tunable in-vitro silk model of the corneal epithelial, stroma, and neuronal components can potentially be used to describe diabetic neuropathy and cellular dysfunction occurring in hyperglycemia.[37] Similarly, work done by Sharif and colleagues suggests that the use of corneal stromal-nerve in-vitro models allows for differentiation of tissue-specific cells that more accurately replicate the interaction between the stroma and nerve network, and can help identify structural and cellular changes taking place in corneal diseases[189]. Taken together, these and other models[175,182,188] suggest that developing and

characterizing cornea-accurate 3D in-vitro models might provide clues for the expansion of new disease therapies, reduce drug development cost, and shed light on new mechanisms in disease progression. However, these in-vitro models are limited by the interaction between cellular components and the scaffold materials. For example, in the silk-based diabetic neuropathy model presented by Deardorff, et al., the neuronal-epithelial interaction is restricted by the slow neuronal innervation and growth into the silk material. For this model to be more accurate the total culture time for neuronal innervation would exceed 8 weeks, which is longer than the embryonic corneal maturity time of 2 months[37].

Chapter 3: Engineering a Multilayered Cornea Stroma Scaffold with Controlled Cell and Extracellular Matrix Architecture

3.1. Abstract

Nearly 10 million people worldwide suffer from cornea-related blindness caused by trauma, viral and bacterial infections, chemical burns, or corneal diseases. These conditions, along with an unhealthy endothelium, can lead to scar formation, opacities, and refractive errors in the corneal stroma. Transplantation of healthy donor tissue via keratoplasty of the whole cornea, sections of the endothelium and stroma, or small segments of the stroma can address some of these optical diseases; however, access to suitable donor tissue varies by location, leaving millions in need of therapy. Previously, corneal stroma stem cells (CSSC) have been used to produce thin (4 μm) scaffold-free engineered corneal stromal constructs, but this construct is often fragile to stack, which might make this procedure not appropriate if one wants a thicker construct. In this study, surface-modified collagen I (COLI) gels were used to generate single-corneal stroma sheets (single-sheets) that can be easily stacked and handled without altering cell organization. CSSC were cultured and differentiated to keratocytes on COLI substrates with laminin (LAM) or fibronectin (FN) protein lines to direct parallel cell alignment and extracellular matrix (ECM) organization, like the ECM organization found in the native corneal stroma. CSSC-derived keratocytes expressed keratocan and assembled COLI and collagen V (COLV), both found in the native stroma. Before stacking, keratocytes in single-sheets were organized into two highly aligned cell layers rotated on average 30° from each other. Single-sheets were successfully stacked into double-layered constructs (duo-stacks) and, duo-stacks were successfully stacked into

four-layered constructs (quad-stacks) without affecting cell organization. Single-sheets, duo-, and quad-stacks had an average thickness of 20, 40, and 80 µm, respectively. Using a surface modified-COLI scaffold to align CSSC and bring about single-sheets and multi-layered scaffolds of thicknesses of up to 80 µm have the potential for targeting different keratoplasty procedures.

3.2. Introduction

The cornea is a collagen type I (COLI) rich tissue composed of an epithelial layer that provides protection, a thick stroma that provides mechanical integrity, and an endothelial layer that regulates hydration.[36,83,142,145] These layers work in unison to create a transparent tissue that allows for vision and helps focus light onto the retina. Trauma, chemical burns, and viral and bacterial infections can lead to scar formation, opacities, and uncorrected refractive errors that decrease visual acuity and may produce corneal blindness.[158,166] To restore or improve vision, procedures using cadaveric donor tissues range from whole cornea penetrating keratoplasty (PK) for severe cases, Descemet stripping automated endothelium keratoplasty (DSAEK) for patients with a dysfunctional endothelium, and deep anterior lamellar keratoplasty (DALK) that transplants sections of the stroma for patients with a functional endothelium.[39,72,125] However, access to donor-grade corneas varies by location, and although overall supply has increased, strict qualifications for corneal tissue to be deemed acceptable for donation have kept the supply of transplantable corneal tissue from meeting demand [57,125]. This unmet demand could be addressed by using various ongoing engineering approaches to produce transplant-quality corneal constructs. Some of these include but are not limited to xenotransplantation, decellularization and recellularization of xenografts[125], and engineering of artificial corneas from synthetic[80] or natural biomaterials[37,99,113,114,160,165,197]. Likewise, piece-wise approaches of engineering the cornea have been explored because of the cornea's complexity and the different functions each part contributes to the whole cornea.

3.2.1. The Corneal Stroma Structure

The stroma often serves as a popular starting platform to engineer a corneal scaffold because the stroma makes up approximately 90% of the total thickness of the cornea and in transplantation procedures, it is either used alone or in combination with other corneal layers. However, replicating the corneal stroma's intricate and highly regulated ECM architecture is remains an engineering challenge. A tightly regulated COLI-rich ECM brings about the corneal transparency[69,83,142,147]; cellular components, primary keratocyte, help maintain the stromal structure and respond to injury; and the interweaving and layering of lamellae provide strength and distribute forces[63,142,145]

3.2.1.1. Collagen fibrils and proteoglycans in the corneal stroma

Collagen in the stroma is important in establishing transparency and help resist tensile forces. Collagen accounts for 68 to 71% dry weight of the stroma. COLI is the most abundant type of collagen in the stroma proper. The structure of the COLI fibril is precise and highly regulated in the cornea, found to be 22.7 $\pm$ 1.8 nm in diameter with adjacent fibrils located at a distance between 19.6 to 20.9 nm. COLV is a minor fibrillar collagen[68] often found buried within the COLI fibril in the stroma. In vitro studies of COLV suggest that protruding NH_2-terminal domains cause steric hindrance and limit the COLI fibril diameter.[17,145] Lastly, collagen VI (COLVI), the second most abundant collagen in the stroma, forms 100 nm long filaments that bridge COLI fibrils and stromal lamellae together[42,145].

Proteoglycans are macromolecules with a glycosaminoglycan side chain and a protein core that modify the structure and function of collagen fibrils. Dermatan sulfate

and keratan sulfate are the predominant glycosaminoglycans in the bovine, rabbit, chicken, and human cornea.[36,148] The main functions proteoglycans serve in the cornea are to regulate tissue volume by maintaining the spatial order and diameter of collagen fibrils,[231] to regulate collagen fibril assembly, and aid in the configuration of the developing cornea.[226] From a mechanical perspective, proteoglycans also provide some viscoelasticity and help resist compressive forces.[36,90]

For a more in-depth explanation, the author points to an excellent review by Meek K.M. on the collagen and proteoglycan distribution in the cornea.[145,147] Similarly, Dawson D.G., Ubel J.L., and Edelhauser H.F. have an in-depth review on the physiology of the cornea and the sclera, found in chapter 4 of “Adler’s Physiology of the Eye”. [36] Lastly, Muller L.J., et al. provides an extensive explanation of the three-dimensional organization of collagen and proteoglycans in the stroma.[151]

3.2.1.2. Cellular Components in the Corneal Stroma

Keratocytes, the main cell type in the stroma proper, are dendritic cells of neural crest-derived mesenchymal fibrocyte-origin that populate about 3 to 5% per volume of the corneal stroma.[123,171] Throughout the adult life of most vertebrates, keratocytes remain in a quiescent state, showing little to no apoptotic nor mitotic behavior, until the environment is perturbed by trauma or infection. This suggests that, unlike the metabolically active epithelial cells, the stroma and keratocytes are not in a constant state of cellular and ECM destruction and renewal. Confocal microscopy of healthy human corneas has shown that keratocytes are spatially distributed, with cell densities averaging 20,000 keratocytes/mm^3 in the central stroma and 35,000 keratocytes/mm^3 in the anterior-most layers of the stroma.[167]

Ultimately, collagen fibril arrangement and proteoglycan support, and maintenance by cellular components, keep a tight balance on the ECM structure to produce a transparency tissue. The homogenous diameter and spacing of each parallel collagen fiber, as well as the lattice structure created by these fibers, gives rise to the destructive interference of scattered light and constructive interference of forward-moving light[69,142,150]. When this interfibrillar distance is disturbed, as is the case of corneal edema, the cornea becomes opaque, and transparency is lost.

3.2.1.3. Corneal Stroma Lamellae Structure

Now that an in-depth description of the fibril structure of the stroma has been presented, it is of great interest to talk about the microstructure and the organization of lamellae. The stroma is made up of COLI-rich layers, called lamellae (singular is lamella), which in the total thickness of the stroma there are about 200 to 300 lamellae, each with a thickness of 0.2 to 2.5µm [36,145]. These lamellae interweave one another and the direction of the fibril that makes them up align at preferential angles depending on the location and depth in the stroma[146] and lamellae are believed to distribute the load from the intraocular pressure and balance the swelling pressure from the epithelium and endothelium fluid exchanges[183]. Though mechanical testing of the cornea shows its viscoelastic behavior[49] and several finite element analyses have been made to model several of the cornea's biological phenomena[51], little is known about the source and the means for which this mechanical behavior arises.

The lamellae build up the stromal tissue and make large cross-angles from lying one on top of another. Studies by Petsche, et al. show that transverse shear stiffness of the anterior cornea is about an order of magnitude greater than the posterior cornea[170].

Concerning the interweaving of lamellae, Radner, et al. used SEM and TEM imaging to study the cross-angle distribution of lamellae in the whole cornea[179]. In their study, three different dimensional organizations are exhibited by lamellae. First, a lamella can split along the anterior-posterior axis with the split along the central part of the lamella. Second, a lamella can split horizontally. Third, a lamella splitting along the anterior-posterior axis with the split happening in the margins of the lamella. Putting these three types of dimensional organization together, a complex structure, with interweaving lamellae is sketched [179] (Fig. 3.1). In the same study, Radner compares the frequency distribution of cross angles within layers. For layers in the posterior-most part of the stroma, the areas closer to the limbus exhibit a cross angle <30°, while in the rest of the stroma no significant difference was found between cross angles of lamellae.

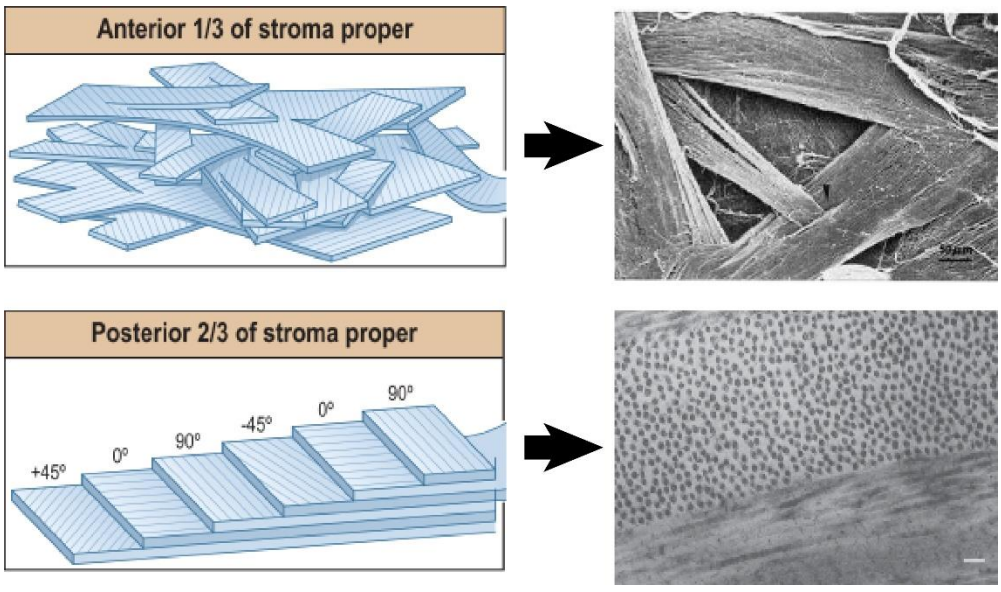

Figure 3.1. Schematic and imaging of the anterior and posterior parts of the stroma. Schematic of the different parts of the stroma taken from Dawson and Ubels[36], with permission from Elsevier. SEM of stroma surface taken from Radner et al.[179], with permission from Wolters Kluwer Health, Inc. TEM of the stroma taken from Meek[145], with permission from Springer Nature.

3.2.2. Corneal stroma transplantation procedures and tissue sources

The need for stromal tissue in three out of the four common transplantation procedures (fig. 1.3a-c) makes the stroma a popular target in developing corneal scaffolds. However, the stroma's intricate structure and unique properties make it a major tissue engineering challenge. The stroma is an avascular, collagen I (COLI)-rich tissue that makes up about 90% of the total corneal thickness. Lamellae interweave in the anterior stroma and form a multilayered crisscrossing structure in the posterior stroma that provides corneal strength and maintains corneal structure [36,145,147,152]. Each lamella is composed of highly aligned COLI fibrils packed into a lattice structure where stromal proteoglycans tightly regulate COLI fibril diameter and spacings. The lattice structure and fibril spacings of the COLI fibrils give rise to tissue transparency.[69,142,145,147] Lastly, corneal stromal cells, known as keratocytes, are quiescent cells that secrete proteoglycans and other collagens to maintain the aforementioned structures and address tissue damage. To engineer these parameters; crisscrossing of COLI lamellae; highly aligned and regulated fibril architecture; and maintenance of the tissue via keratocytes; researchers aim to use different bioengineering techniques that combine biomaterials and cell approaches to develop architecturally and biologically accurate tissue models that can be used for disease, maturation, and transplantation studies. The ideal corneal stroma alternative needs to be transparent in the visible range, have enough strength to withstand the intraocular and outside pressures, be capable of interacting with the other corneal layers, either in vitro or in vivo, and do not cause a pathological host response[141]

3.2.3. Engineering methods of corneal stroma tissues

The stroma often serves as a starting platform because the stroma makes up approximately 90% of the total thickness of the cornea and it is either used in combination with other corneal layers or alone for the different transplantation procedures. Some engineering approaches use natural biomaterials to host cells that can assemble a stromal equivalent [160]. For example, silk fibroin [37,80,209] and collagen type III scaffolds [58,80,101] have been used to grow endothelial and stromal cornea constructs when combined with corneal stem cells. However, silk fibroin and collagen III approaches present some limitations that could affect the properties and materials-host interaction in a transplantable corneal stroma construct. Silk fibroin needs biochemical modifications, typically with an RGD-peptide, to promote cell adhesion and proliferation [73,208,232]. Similarly, collagen type III requires chemical modifications to increase the scaffold's mechanical strength to sustain sutures and handling typically used in corneal transplantation [58,80]. To circumvent material modifications and better match the stromal ECM, approaches that employ COLI as the main scaffold have become common. For example, vitrification of COLI [21,211] and compressed COLI [94] are some promising examples of using COLI to fabricate an engineered stromal construct. Alternatively, approaches using corneal stromal stem cell (CSSC), a group of specialized stem cells that reside in the corneal limbus and have the potential of differentiating into keratocytes, show that aligned CSSC can assemble a COLI-rich ECM that mimics the structure of the native stroma[197,222,223]. Taken together, however, these approaches require scaffold functionalization, which might affect material-host interaction, or lack the mechanical strength to be able to be handled and transplanted.

3.2.4. The use of corneal stroma stem cells as a healthy source of keratocytes

Primary keratocytes exhibit low proliferation and slow ECM deposition when cultured ex vivo[55,123,153,214]. Many groups have used corneal fibroblasts as a cell source, however, fibroblasts are representative of some corneal pathologies. To circumvent the use of corneal fibroblasts, corneal stroma stem cells (CSSC), a specialized group of mesenchymal cells located in the anterior limbal region of the human stroma [45,171] can be easily isolated, expanded in vitro, and under the right conditions express keratocyte-like genes and produce relevant ECM proteins[197,220,222]. When CSSC are compared to corneal fibroblasts, CSSC assemble an ECM composed of the major types of collagen and proteoglycans found in the native stroma.[220]

3.2.5. Cell alignment to guide assembly of an aligned extracellular matrix

We and others have shown that by aligning CSSC and other ECM-producing cells, a highly aligned matrix is deposited. Recently, Syed-Picard, et al., demonstrated that CSSC cultured on PDMS channels coated with FN build their matrix and form scaffold-free tissue sheets. Inspection of this matrix by transmission electron microscopy shows that collagen fibrils are uniform in diameter at 30.87 $\pm$ 6.22 nm and collagen V and keratocan were expressed after 12 days in keratocyte differentiation medium (KDM)[197]. However, these scaffold-free tissues lack strength and could not be readily handled, making stacking of the tissues arduous (conversation with the authors). Likewise, CSSC culture on PEUU fibers showed similar results. Here the PEUU fibers were electro-spun into an aligned substrate that induced alignment of CSSC. CSSC then deposited a highly aligned, COLI-rich matrix measuring 8 to 10 μm[222]. The

drawback here is that the PEUU substrate was ~200 µm thick, meaning that unless the deposited ECM is detached from the substrate, the construct would be difficult to stack into a multilayered component with dimensions like the stroma, as suggested by the authors. Stroma-like ECM has also been demonstrated from aligned CSSC over silk fibroin[223].

Our goal was to build a construct that recapitulates the stromal architecture using proteins found in the native or developing stroma towards the application of DALK and other corneal transplantation procedures. Here I have developed a scaffold to guide CSSCs to build a stroma construct with defined extracellular matrix (ECM) architecture and can layer these to assemble stroma constructs of defined thickness. To do this, I leveraged previous advances in CSSC culture, differentiation, and ECM assembly [45,171] and surface-initiated assembly (SIA) of ECM scaffolds to engineer cornea stroma tissue[62,161,163]. Specifically, I engineered sheets of compressed COLI patterned with micropatterned fibronectin (FN) or laminin (LAM) lines to align CSSCs and guide them to assemble a highly aligned COLI-rich ECM. These engineered stroma sheets were then stacked into two layers (duo-stack) or four layers (quad-stack) to create thicker tissue constructs. This required determining the relationship between CSSC seeding density and alignment on the micropatterned lines, as well as the effect of different micropatterned line widths and spacings and ECM protein type. Then, I differentiated CSSC to keratocytes and analyzed the composition and structure of the cell-assembled ECM. Finally, I stacked engineered stroma sheets into duo-stacks and quad-stacks and measured the thickness and transparency. Overall, I show that micropatterned FN and LAM lines on COLI scaffolds can serve to guide CSSC alignment and that this

alignment further guides the assembly of a stromal-like ECM from differentiated keratocytes. Engineered stroma sheets and multilayered constructs were robust and capable of being handled, rolled, unrolled, and further stacked without tearing the constructs. These results suggest that CSSC, on the COLI-protein scaffolds, assemble engineered stroma sheets with an ECM equivalent in architecture and composition to the native stroma, and these sheets can be easily stacked into larger multilayered stromal constructs with tunable thickness.

3.3. Materials and Methods

3.3.1. Fabrication of Polydimethylsiloxane (PDMS) Stamps

PDMS stamps were prepared using traditional photolithography steps as described in published methods [186]. Briefly, a computer-aided design file was generated with lines of widths and space of 10 by 10, 20 by 20, and 30 by 30 µm, and transparency photomasks were ordered (CAS/Art Services Inc). A glass wafer was cleaned with ethanol, dried with filtered air, and treated with a Bunsen burner flame to activate the wafer surface. The wafer was then placed on a spin-coater, and SPR 220.3 photoresist (Microchem) pipetted on the treated surface. The wafer was spun for 30 sec at 5000 rpm to achieve a uniform photoresist coating and baked on a hot plate for 90 seconds at 115°C. The then-baked wafer was moved under a UV lamp and aligned with the transparency mask and the UV source. The wafer was exposed to UV light for 50 seconds and exposure was checked under a microscope. The exposed wafer was then baked for 90 seconds at 115°C on a hot plate, placed on SPR developer solution (Microchem) for 40 sec, and submerged in two consecutive water batches for 40 seconds each. The final wafer was then dried with nitrogen and inspected under a microscope. Sylgard 184 Poly(dimethylsiloxane) (PDMS; Dow Corning) was mixed 10 parts elastomer to 1 part curing agent in a planetary mixer (THINKY ARE-250) mixer for 2 minutes at 2000 rpm and degas for 2 minutes at 2000 rpm, poured over the wafer done previously, degassed for another 15 minutes for any remaining air, and cured overnight at 65°C. Finally, the stamps were cut out of the wafer and stored for further use.

3.3.2. Fabrication of COLI-Protein Scaffolds

Protein lines and isotropic controls were transferred to a compressed COLI scaffold using SIA techniques [62,186] which was further adapted as previously described [161]. Briefly, a 6 mg/ml COLI gel was assembled from a higher concentration stock solution (>9mg/ml, BD Biosciences). Two hundred µL of COLI solution was pipetted over a glass coverslip with a silicone mold that defined the shape of the gel as a 9 mm diameter circle (Fig. 3.2A.i). The COLI solution was gelled at 37°C in a humidified incubator for three hours (Fig. 3.2A.ii). Following gelation, the silicone molds were removed, the gels rinsed three times with deionized water, and dried in a cell culture hood (Fig. 3.2A.iii-iv). The compressed COLI gel was stored at room temperature until use.

LAM (Thermo Fisher) or FN (Corning) proteins were fluorescently labeled with AlexaFluor 555 SE tag (Thermo Fisher) according to the manufacturer's protocol; by the reaction of the succinimidyl ester groups in the dyes and the primary amines in the proteins. First, FN or LAM lines of width and spacings of 10 by 10 (FN 10 by 10; LAM 10 by 10), 20 by 20 (FN 20 by 20; LAM 20 by 20), and 30 by 30 µm (FN 30 by 30; LAM 30 by 30), or FN isotropic controls (FN Iso) were microcontact printed on a poly(N-isopropyl acrylamide) (PIPAAm, mixed 2% w/v in butanol, Scientific Polymer Products) coated coverslip. This was done by sonicating PDMS stamps with channels of line widths and spacings, or flat features in a 50% ethanol solution for 30 minutes, and then dried with nitrogen. The stamps were incubated for 60 minutes with either LAM or FN at a concentration of 50 µg/mL, both mixed at 1:1 fluorescently-labeled to unlabeled protein (Fig. 3.2B.i). Excess protein was removed from the stamps by submerging the stamps

in distilled water and dried with nitrogen. Then, stamps were placed in conformal contact with the PIPAAm-coated coverslip, features down for 60 minutes (Fig. 2.2B.ii). The stamps were then carefully removed from the PIPAAm-coated coverslips to prevent the tearing of the PIPAAm surface. A detailed description of these steps can be found in Sevcik, et al, 2017.

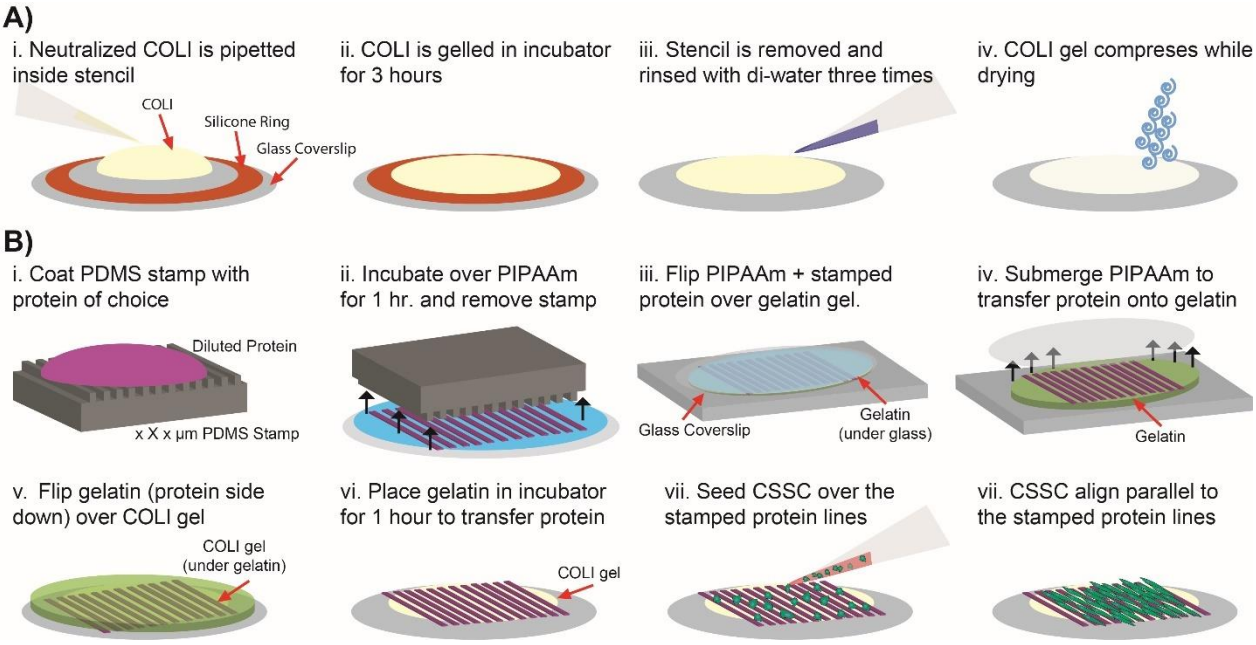

Figure 3.2. Schematic of fabrication of COLI-Protein Scaffold.

(A) Fabrication of compressed COLI gel by dehydration of the COLI gel. (i-ii) COLI solution is neutralized, pipetted into a silicone mold, and allowed to gel in a 37°C incubator for 3 hours. Then, (iii-iv) the silicone ring is removed, the gels are rinsed with di-water three times and allowed to dry inside a cell culture hood. (B) Surface initiated assembly of protein lines over a compressed COLI gel. (i-ii) Protein features are stamped over PIPAAm coated coverslip using micro-contact printing. (iii-iv) The PIPAAm is flipped over a gelatin gel, as an intermediate step, and upon submersion in room temperature water, the PIPAAm dissolves, leaving the protein features on the gelatin gel. (v – vi) Then, the gelatin gel is flipped over a compressed COLI gel, placed a 37°C, thus melting the gelatin and transferring the protein lines to the COLI gel. (vii-viii) Cells are seeded and cultured.

Next, 20% gelatin type A (Thermo Fisher) gels were prepared by pipetting 200 µL of 20% gelatin solution warmed to 60°C on a 20 mm diameter silicone ring on a microscope slide. This was then followed by a 10-minute incubation at room temperature and the removal of the silicone ring. The coverslips prepared previously were placed ECM-side down over the gelatin gels and immersed in distilled water at room temperature to dissolve the PIPAAm and transfer the protein lines onto the gelatin (Fig. 3.2B.iii-iv). The gelatin was peeled off the microscope slide and placed protein-side down onto the compressed COLI (Fig. 3.2B.v). These completed COLI + protein constructs were then incubated in a humidified incubator at 37°C for 45 minutes, rinsed with warm 1xPBS thrice, and incubated again for 45 minutes and rinsed with warm PBS to remove any residual gelatin (Fig. 3.2B.vi). These were then dried in a biosafety hood and stored at room temperature. Lastly, the top of 15 mL centrifuge tubes were cut off and sealed around the COLI + protein constructs with vacuum grease, restricting the seeding area. COLI constructs were put in 6 well plates, covered with 1xPBS, and sterilized with UV light for 15 minutes before usage.

3.3.3. Corneal Stroma Stem Cell Isolation and Culture

Isolation of CSSC was performed as previously described [13,45,197]. Briefly, cornea-scleral tissues from human donors younger than 60 years with <5 days of preservation were obtained from the Center for Organ Recovery and Education (www.core.org), after the center corneal tissue had been removed for transplantation. The rims were rinsed, and the remaining endothelial cell layer, Descemet's membrane, conjunctiva, and trabecular meshwork were removed. The limbal tissue was dissected, cut into 3 mm fragments, and digested overnight in 0.5 mg/mL collagenase L solution at

37°C. Fractions were pipetted and further digested for 30 to 45 minutes. The remaining digest was filtered through a cell strainer, and the cells were centrifuged at 1500 rpm for 5 minutes. The resulting CSSC were plated onto a 25 cm^2 tissue culture flask in stem cell growth medium (GM) containing 2% (v/v) fetal bovine serum, Dulbecco's Modified Eagle Medium-LowGlucose-GlutaMax (Gibco), 400 mg/L MCDB-201 (Sigma Aldrich), 1mg/mL of AlbuMax Lipid-Rich BSA (Gibco), 0.1 mM L-ascorbic acid-2-phosphate (Sigma Aldrich), 0.1X insulin-transferring-selenium (Gibco), 10 ng/mL recombinant rat platelet-derived growth factor-BB protein (R&D Systems), 10 ng/mL recombinant human epidermal growth factor (R&D Systems), 100 nM dexamethasone (Sigma Aldrich), 1x penicillin-streptomycin 100x (Corning CellGro), and 1:1000 gentamycin (50 mg/mL) (Gibco) (Table 3.1). CSSC were expanded using TrypLe (Thermo Fisher) and passaged at ~1000 cells/cm^2. COLI scaffolds were seeded with CSSC derived from a single donor cornea at passage 2-5.

3.3.4. Seeding and Culture of CSSC on COLI-Protein Scaffolds

CSSC were seeded onto COLI-protein scaffolds FN 10 by 10 or FN Iso at 10,500, 30,000, 50,000, or 100,000 cells/cm^2. CSSC were cultured in GM until confluency, and then the culture medium was switched to keratocyte differentiation medium (KDM) containing advanced Dulbecco's Modified Eagle Medium (Gibco) with 1 mM L-ascorbate acid-2-phosphate (Sigma Aldrich), 10 ng/mL recombinant human fibroblast growth factor 2 (Cell Sciences), and 0.1 ng/mL recombinant human transforming growth factor β3 (R&D Systems) (Table 3.2; Fig. 3.3). KDM was replaced every 2 days for 10 days. The alignment of CSSC was calculated at the day of confluency and at the end of the differentiation.

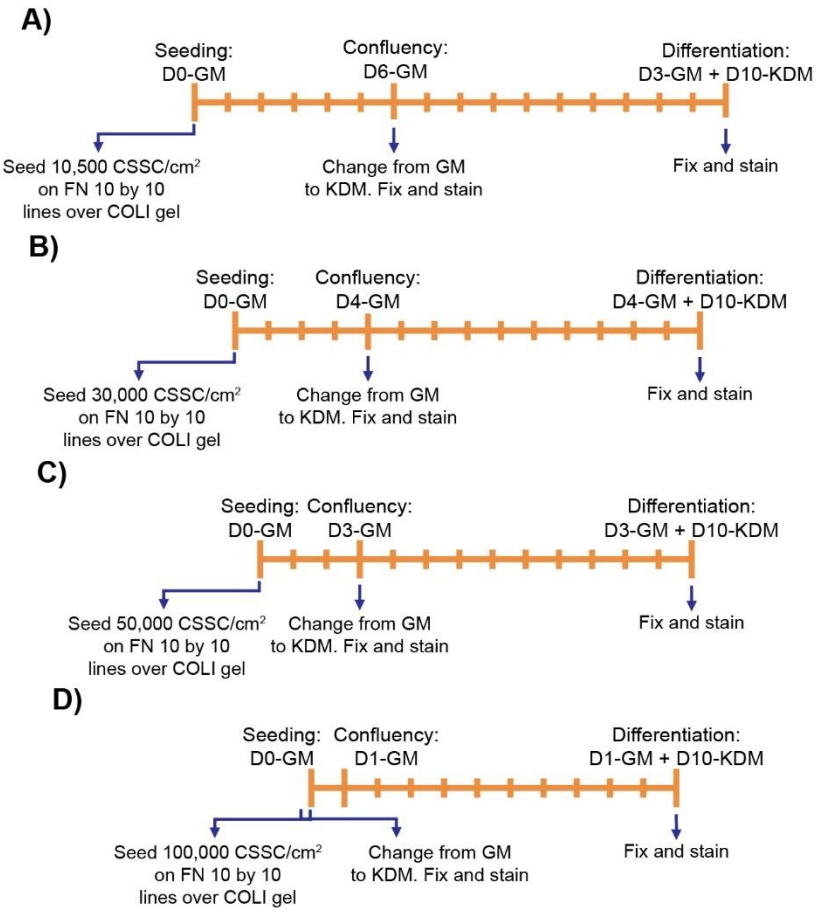

Figure 3.3. Different CSSC seeding concentrations and differentiation timelines.
(A) Seeding of 10,500 CSSC/cm^2. (B) Seeding of 30,000 CSSC/cm^2. (C) Seeding of 50,000 CSSC/cm^2. (D) Seeding of 100,000 CSSC/cm^2

CSSC were seeded at 50,000 cells/cm^2 onto COLI-protein scaffold LAM 10 by 10, FN 20 by 20, LAM 20 by 20, FN 30 by 30, and LAM 30 by 30. In this case, CSSC were cultured in GM for 3 days, at which point the medium was switched to KDM. The medium was replaced every 2 days for 10 days (D10-KDM) (Fig. 3.3C). This seeding concentration and the schedule were used for all remaining experiments.

Table 3.1. Ingredients and Concentrations for Corneal Stroma Stem Cell Growth Media

Ingredient	Brand	Cat. Number	Preparation to Working Solution	Storage	Volume/ 500 mL total media (mL)	Concentration
DMEM, low glucose, GlutaMAX™ Supplement, pyruvate	Gibco	10567014	N/A	2-8C up to 12 months	286.14	0
MCDB-201	Sigma	M6770-1L	Dilute as manufacture recommendation	Liquid medium at 2-8C in the dark	190.76	400mg/L
Fetal Bovine Serum					10	0.02
AlbuMAX Lipid-Rich BSA	Gibco	11020021	Dissolve 10 mg/100mL	Store 25mL aliquots at -20C	5	1 mg/mL
L-Ascorbic Acid 2-Phosphate sesquimagnesim salt hydrate	Sigma	A8960	Dissolve 182 mg in 10 mL of water. Makes 50mM	Reconstituted: store in 4C. Powder: Store in -20C	1	0.1 mM
Insulin-Transferrin-Selenium (ITS)	Gibco	41400045	N/A	Store in 4C	0.5	0.1X
Recombinant Rat PDGF-BB Protein	R&D System	520-bb-050	(10ug/ml) Dissolve 50 ug in 5 mL of 4mM HCl + 0.1% BSA	0.5mL aliquots store in -80C	0.5	10 ng/mL
human Epidermanl Growth Factor	Sigma	E9644	Mix into 0.01mg/mL in 10mM acetic acid + 0.1% BSA	Store at 4C for up to a month. For extended storage, freeze in -20C in aliquots of 0.5mL	0.5	10 ng/mL
Dexamethasone	Sigma	D4902	Dissolve 0.1mg in 0.1mL of 100% ethanol. Then add 4.9 mL of medium. This makes 50uM solution	0.5mL aliquots store in -20C	0.1	10^-8 M
Penicillin-Streptomycin 100x			N/A	0	5	1X
Gentamicin (50 mg/mL)	Gibco	15750060	N/A	Room temp. in a dark room	0.5	1 to 1000

Table 3.2. Ingredients and Concentrations for Corneal Keratocyte Differentiation Media – Base (KDM Base)

Ingredient	Brand	Cat. Number	Preparation to Working Solution	Storage	Volume/ 500 mL total media (mL)	Concentration
Advanced DMEM	Gibco	12491	N/A	2-8C up to 12 months	245	0
GlutaMax Supplement 100x	Gibco	35050-061	N/A	Room Temp	2.5	1 to 100
Penicillin-Streptomycin 100x	0	0	0	0	2.5	1X
Gentamicin (50 mg/mL)	Gibco	15750060	N/A	Room Temp	0.25	1 to 1000

Table 3.3. Ingredients and Concentrations for Corneal Keratocyte Differentiation Media – Use (KDM)

Ingredient	Brand	Cat. Number	Preparation to Working Solution	Storage	Volume / 50 mL total media (mL)	Concentration
KDM Base	N/A	N/A	N/A	2-8C up to 12 months	50	0
L-Ascorbic Acid 2-Phosphate sesquimagnesium salt hydrate	Sigma	A8960	Dissolve 182 mg in 10 mL of water. Makes 50mM	Reconstituted: store in 4C. Powder: Store in -20C	1	1mM
Recombinant Human FGF2/FGF-Basic147	Cell Sciences	CRF001C	Add sterile di water to a concentration of 0.1mg/mL. The vial comes with 1mg. Dissolve 1 mg in 10 mL	Reconstituted: store in -20C. Powder: store in -20C	0.005	10ng/mL
Recombinant Human TGF-Beta 3 Protein	R&D Systems	243-B3-002	(2ug/ml) Dissolve 2 ug (the vial) in 1mL sterile filter 4mM HCl+0.1% BSA	12 months from date of receipt, -20 to -70 °C as supplied. 1 month, 2 to 8 °C under sterile conditions after reconstitution. 3 months, -20 to -70 °C under sterile conditions after reconstitution.	0.0025	0.1ng/ml

3.3.5. Stacking of Engineered Stroma Sheets into Duo- and Quad-stacks

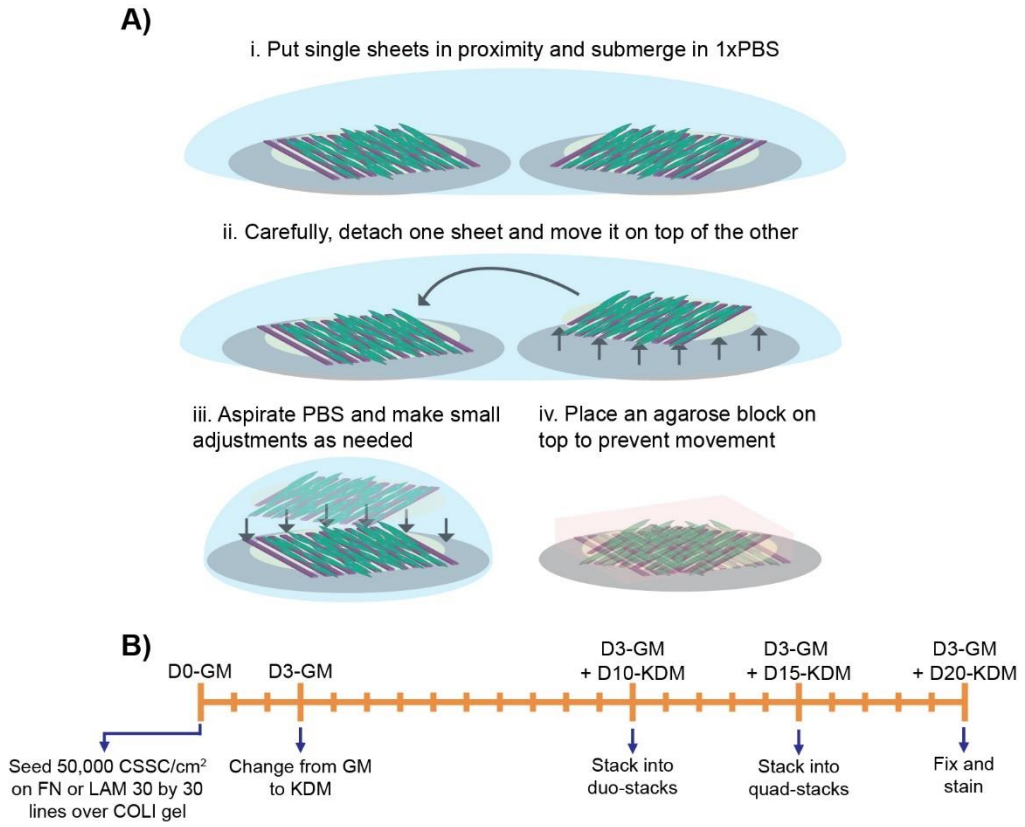

Figure 3.4. Schematic of Stacking of Engineered Stroma Sheets.
(A) Stacking of single stromal sheets at desired angles is achieved by (i) submerging the single sheets on PBS and (A.ii) manually lifting and accommodating the single sheets over one another. (iii) Carefully, the PBS is aspirated, allowing the sheets to get into contact. (iv) A 1% agarose block is then used to prevent the sheets from sliding.

At D10-KDM, engineered stroma sheets cultured on FN 30 by 30 were stacked to create a duo-stack. Before seeding, the direction of the protein lines was marked on the coverslip. Engineered sheets were placed in proximity to one another and submerged in 1xPBS (Fig. 3.4A.i). Carefully, one of the sheets was peeled off the coverslip, allowing it to float in the PBS. The floating sheet was moved and placed right over the adjacent single sheet (Fig. 3.4A.ii). Slowly, the PBS was aspirated, allowing the single sheets to touch and stack. Before all PBS was aspirated, the top sheet was rotated such that the

direction of protein lines between the sheets are perpendicular to one another (Fig. 3.4A.iii). Finally, a 1% agarose block was placed over the stack to prevent sliding between the sheets. (duo-stack; Fig. 3.4A.iv). Duo-stacks were cultured in KDM, replacing the medium every 2 days for 5 days. To create four-layered constructs (quad-stacks), two duo-stacks were mechanically picked up, stacked, and rotated using the same process as before. Quad-stacks were then cultured in KDM, with medium replacement every 2 days for 5 days (Fig. 3.4B).

3.3.6. Immunostaining and Microscopy

Engineered stroma sheets were rinsed with 1xPBS, and then fixed with 4% paraformaldehyde in 1xPBS for 12 minutes and washed for 5 minutes with 1xPBS thrice. Five percent normal goat serum in 1xPBS was used to block any non-specific binding. Samples were incubated with rabbit anti-keratocan (1:200, Thermo Fisher), rabbit anti-alpha smooth muscle actin (1:200, Thermo Fisher), mouse anti-human fibronectin (1:200, HFN 7.1, Development Studies Hybridoma Bank), or rabbit anti-collagen type V (1:200, EMD Millipore Corp.) in 1% Bovine Serum Albumin in 1xPBS overnight at 4°C. Following, the samples were washed for 5 minutes with 1xPBS thrice and incubated with secondary antibody AlexaFluor 633 goat anti-rabbit (1:200, Thermo Fisher) or AlexaFluor 633 goat anti-mouse (1:200, Thermo Fisher) when appropriate, diamidino-2-phenylindole (DAPI, Thermo Fisher) to stain nuclei, and Phalloidin 488 (1:200, Thermo Fisher) to stain actin filaments for 1 hour. Samples were washed for 5 minutes with 1xPBS thrice again and mounted on microscope glass slides with Prolong Anti-Fade (Life Technologies). Mounted samples were imaged on a Zeiss LSM 700 confocal microscope. Two-photon microscopy was perform using a Nikon Eclipse Ti2

multiphoton microscope at a wavelength of 810-830 nm for the generation of second-harmonic signaling from aligned COLI fibrils. When available, images were taken such that the protein lines run vertically.

Duo- and quad-stacks were fixed, washed, and blocked as above. However, after blocking, stacked samples were incubated with DeadRed 488 (Thermo Fisher) to stain nuclei, and phalloidin 633 (1:200, Thermo Fisher). Samples were then washed and mounted as above.

3.3.7. Gene Expression

Engineered stroma sheets of CSSC at D10-KDM cultured on FN 30 by 30 or LAM 30 by 30 were rinsed with 1xPBS, the samples carefully detached from the glass coverslip, and placed in a 1.5 mL Eppendorf tube each. One mL of TRIzol (Life Technologies) was added to the samples and vortex mixed for 10 to 20 seconds. CSSC were homogenized by passing each sample through a 20-gauge needle until the gels were fully dissolved. Samples were then allowed to sit for 5 minutes at 20°C before 200 µL of chloroform (Sigma Aldrich) was added to each tube. Samples were then shaken for 15 seconds, allowed to sit for 2 minutes, and centrifuged at 12,000 g for 15 minutes at 20°C. New Eppendorf tubes were properly labeled and filled with 500 µL of 70% ethanol. Carefully, the upper aqueous phase of each sample was transferred to the ethanol-filled Eppendorf tubes. An RNeasy Mini-Prep Kit (Qiagen) was then used to further isolate RNA according to the manufacturer's protocol. Final RNA concentration was measured with the NanoDrop-2000c Spectrophotometer (Thermo Fisher).

Reverse transcription of 600 ng of total RNA was done with the SuperScript III

Reverse Transcription Kit (Invitrogen) following the manufacturer's protocol. Real-time PCR of the cDNA was done using TaqMan gene expression assay primers and TaqMan Universal Master Mix (Applied Biosystems). Primers used were keratocan (KERA, Hs00559942_m1; All primers from Life Technologies), alpha-smooth muscle actin (α-SMA, Hs00426835_g1), PAX6 (Hs01088114_m1), aldehyde dehydrogenase (ALDH, Hs00964880_m1), and COLI (Hs00164004_m1). For endogenous control, 18S (Hs99999901_s1) was used in all samples. All values were normalized to CSSC grown on a tissue culture plate (TCP) for 5 days in GM.

3.3.8. Orientational Order Parameter as a Measure of Alignment

The alignment was quantified by finding the largest eigenvalue of the orientational order tensor, defined as the 2D orientational order parameter (OOP) [81]. Actin alignment for all samples at D10-KDM was measured using a custom MATLAB (MathWorks) algorithm that calculates the OOP of the given image were 0 meaning isotropy and 1 perfect alignment, as in previously published methods [61]. To quantify the OOP, samples were imaged on the Zeiss LSM 700 confocal; 9 images per sample and 9 samples per condition.

3.3.9. Transparency and Transmittance

Light absorbance of the engineered stroma sheets, duo-stacks, and quad-stacks was measured by a Molecular Devices SpectraMax i3x spectrophotometer at D10-KDM, 5 days after stacking into a duo-stack, and 5 days after stacking into a quad-stack, respectively. The transmittance of a compressed-COLI scaffold was used as a reference. Constructs were rinsed once with 1xPBS and submerged in 1xPBS during

the measurement. Absorbance was measure from 240 to 1000 nm wavelength in 20 nm steps for each construct. From the measured absorbance, the transmittance was calculated as described by other groups [64].

3.3.10. Statistical Analysis

All the results are expressed as mean ± sample standard deviation. Two-way ANOVA followed by post-hoc Sidak's multiple comparison test was used to compare the OOP of CSSC seeded at the various seeding concentration on the FN 10 by 10 and FN Iso. conditions. $p<0.05$ was deemed significant. Similarly, a two-way ANOVA with a post-hoc Sinak's multiple comparison test was used to compare the OOP of CSSC cultured on FN and LAM lines of dimensions 10 by 10, 20 by 20, and 30 by 30 µm. A one-way ANOVA with a post-hoc Tukey's multiple comparison test was used to compare the gene expression of the different conditions and to compare the angle differences between the bottom and top layers of the single sheets. An unpaired student t-test was used to compare the alignment of the bottom and top cell bilayers. A sample size of 9, each made of 9 different fields of view, was used to compare OOP-based seeding density, line width and protein type, and rotational shift based on protein type. Also, a sample size of 3 with 3 virtual replicates was used to compare the expression of each gene. For all statistical analyses, $p<0.05$ was deemed significant. All statistical analysis was performed on GraphPad Prism 8.3.0.

3.4. Results

3.4.1. Effects of CSSC Seeding Density on CSSC Alignment

To form a highly aligned ECM structure, I needed to organize CSSC into highly aligned sheets. I first tested how the initial seeding density affects the alignment of the CSSC on the COLI gels. I cultured the CSSC on FN 10 by 10 lines and an initial seeding density of 10,500 cells/cm^2 because previous work using FN coated PDMS channels of 10 µm wide by 10 µm space by 5 µm has shown promising results in creating a highly aligned stromal tissue [197]. Similarly, CSSC cultured on patterned silk substrates or poly (ester urethane) urea fibers at an initial density of 50,000 cell/cm^2 have shown promising results in creating an aligned stroma tissue [220,223]. Lastly, 30,000 and 100,000 cells/cm^2 were chosen as in-between steps and an extreme condition. For each seeding density, CSSC were seeded on FN Iso., as a control, and FN 10 by 10 in GM until confluency, and then cultured in KDM for 10 days before fixing and staining.

Regardless of seeding density, the CSSC had a random orientation when cultured in the Iso. control as evidenced by the confocal imaging of the actin. In contrast, when CSSC were cultured on the FN 10 by 10 lines, the cells aligned parallel to the lines as evidenced by the actin fibers from the confocal images (Fig. 3.5A). Quantification of the CSSC alignment, via OOP, highlighted that CSSC seeded at 50,000 cell/cm^2 on the FN 10 by 10 lines had a significantly higher OOP than CSSC seeded at the other concentration on the FN 10 by 10 lines (Fig. 3.5B). Furthermore, a pair-wise comparison between the two 50,000 cells/cm^2 groups showed that CSSC seeded on the FN 10 by 10 lines had a significantly higher OOP than CSSC seeded on the FN Iso. stamp.

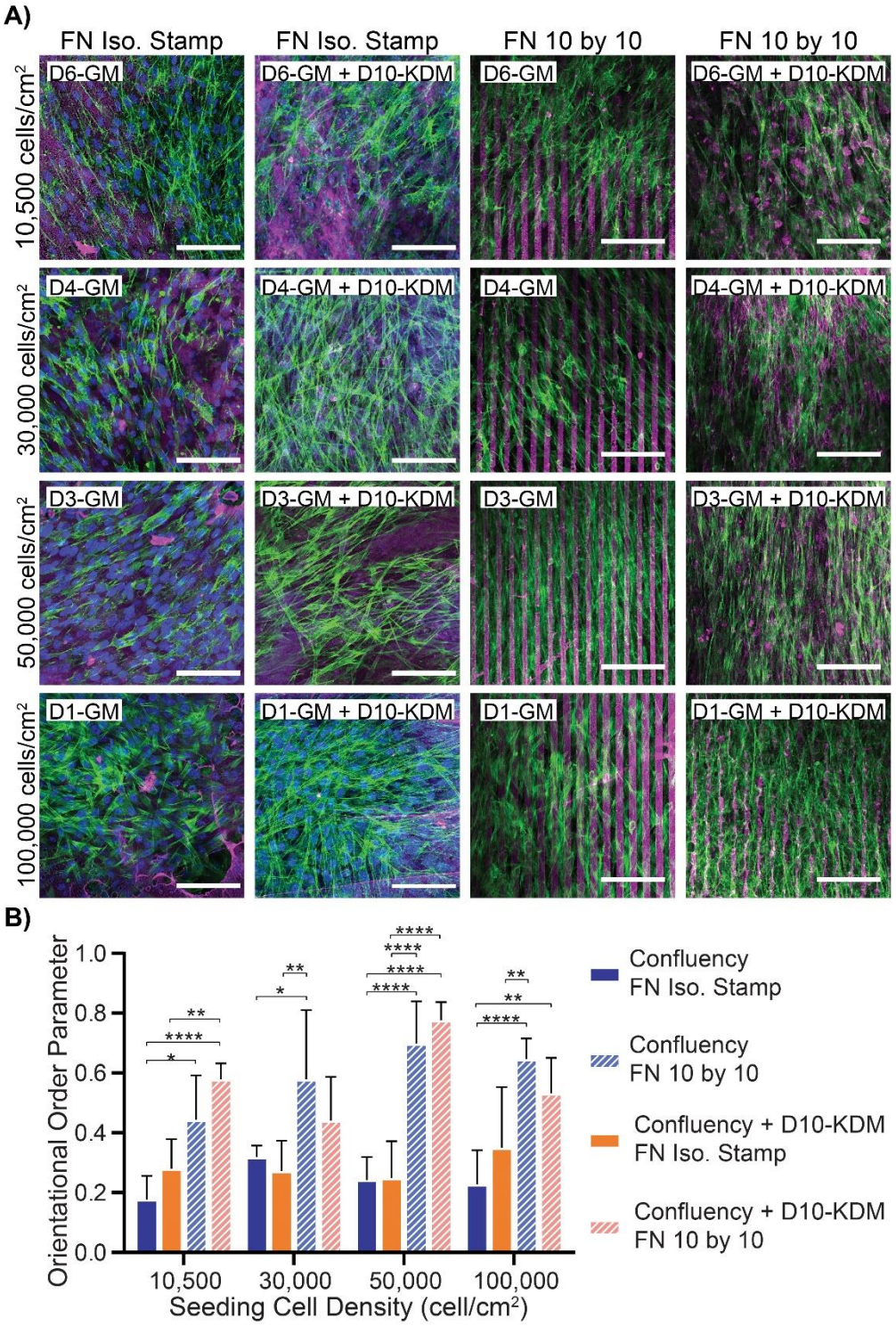

Figure 3.5. CSSC alignment as a function of seeding density on 10 by 10 FN lines.

(A) Confocal images of CSSC at confluency and 10 days after media change at 10,500, 30,000, 50,000, and 100,000 cells/cm^2. (B) Orientational order parameter of CSSC as a function of cell density.

Interestingly, a pair-wise caparison between the FN 10 by 10 and FN Iso. stamp on CSSC seeded of 10,500 cells/cm^2 also showed a significant difference in OOP (Fig. 2.5B). I believe that CSSC seeded at 100,000 cells/cm^2 on the FN 10 by 10 lines did not align because seeding at higher concentrations caused multi-layering with no apparent alignment and the CSSC disregarded the FN protein pattern. Also, I believe there was little alignment in CSSC seeded at 30,000 cells/cm^2 on the FN 10 by 10 lines because, as these cells started to divide, the cell-cell interactions started to guide cell organization rather than the cell-FN interactions. These events might lead to a lower and more variable OOP for these two conditions. Based on these results, I used an initial seeding density of 50,000 cells/cm^2 for all subsequent experiments.

3.4.2. CSSC Alignment on Lines of Different Protein and Dimensions

Following, I decided to assess how CSSC OOP differs between lines of various widths and spacing made of LAM or FN since both of these proteins are present in the early development of the cornea [40] and FN has been used to anchor CSSC to different engineered substrates.[197] CSSC were seeded on FN or LAM lines of 20 by 20 and 30 by 30 µm and LAM lines of 10 by 10 µm. Cells were grown until confluent in GM, and then cultured for another 10 days in KDM. The alignment of CSSC on the FN and LAM lines appeared by CSSC confluency, 3 days in GM, and was significantly different than the FN Iso. Condition. Similarly, at D10-KDM CSSC were aligned parallel to the FN and LAM lines as shown in the FN and LAM 30 by 30 lines (Fig. 3.6A). Statistical analysis of the OOP showed no significant difference between the alignment of cells cultured on FN or LAM, nor between lines of different widths and spacing (Fig. 3.6B). I continued all experiments using the 30 by 30 conditions using both FN and LAM.

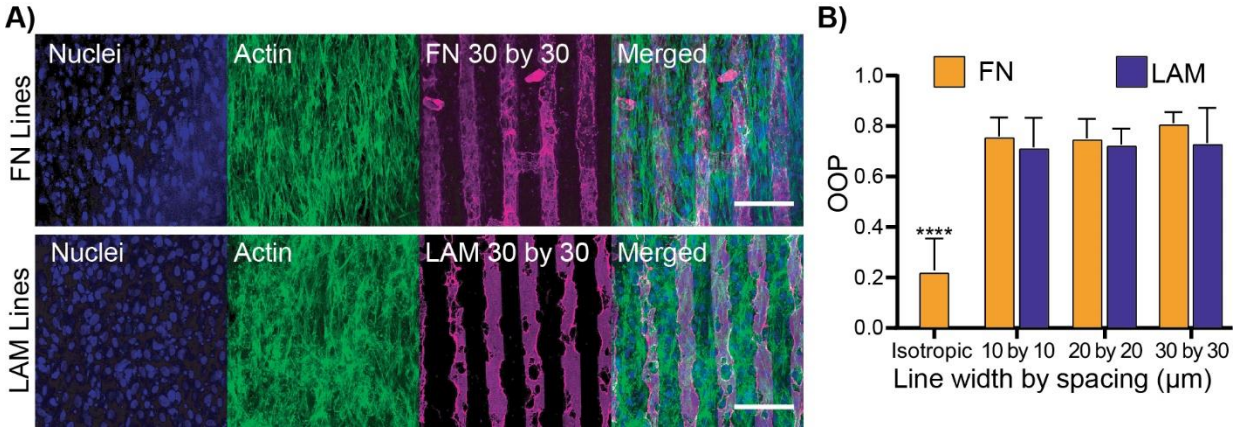

Figure 3.6. CSSC alignment is independent of using FN or LAM protein.
(A) Confocal images of CSSC nuclei (blue), actin (green), and 30 by 30 μm protein lines (magenta). (B) Quantification of the actin orientational order parameter of CSSC cultured over FN and LAM 10 by 10, 20 by 20, and 30 by 30. An ANOVA test showed no significant difference in alignment between these groups.

3.4.3. ECM Structure and Keratocyte Gene Expression

Once I identified the substrate conditions that resulted in the maximum alignment of CSSC, I investigated the gene expression and composition of the cell-assembled ECM. Second-harmonic generation microscopy was used to identify COLI and immunofluorescence was used to identify KERA and COLV in the ECM. On both, FN and LAM lines, COLI fibrils ran parallel to the CSSC actin filaments (Fig. 3.7A, B), while COLI assembled by CSSC cultured on FN Iso. was randomly organized. These results suggest that cell orientation influences ECM orientation and that one way to achieve the highly aligned stromal COLI matrix is by first aligning CSSC and allowing them to assemble their matrix. Similarly, I observed via fluorescent microscopy KERA and COLV in the assembled ECM, two common and important ECM proteins in the native stroma. This suggests that by D10-KDM, CSSC cultured on FN (Fig. 3.7A) and LAM

(Fig. 3.7B) lines build and ECM with the proteins found in the native corneal stroma.

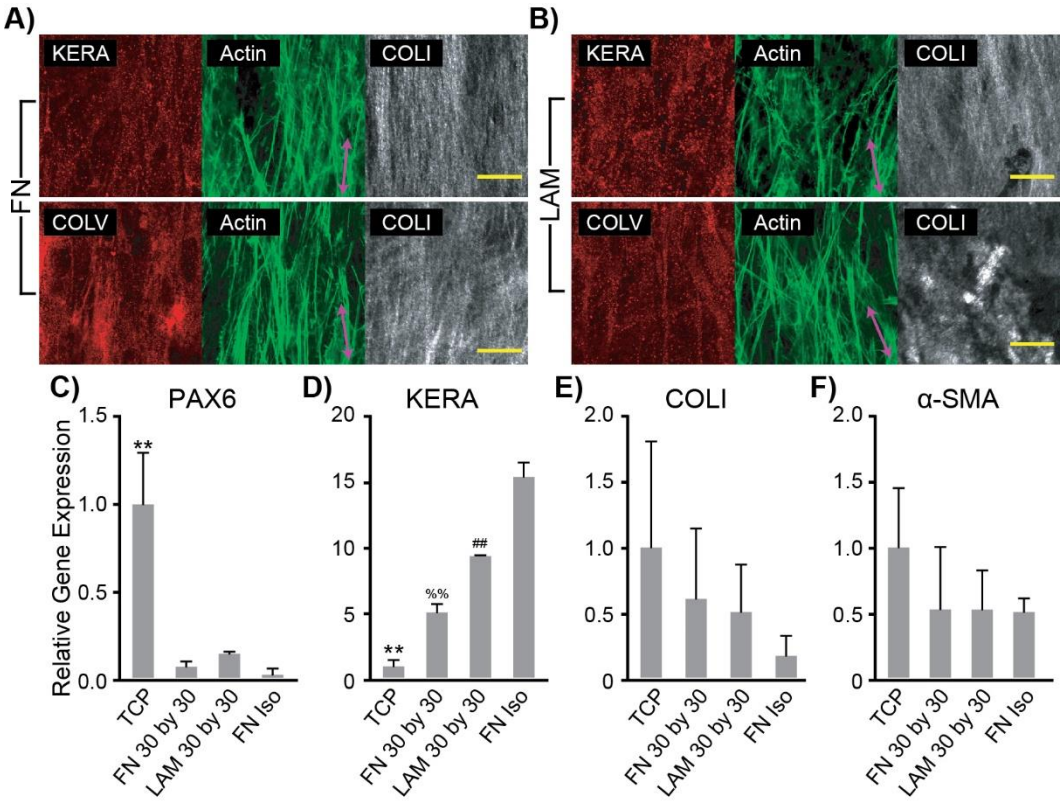

Figure 3.7. CSSC alignment is independent of using FN or LAM protein.
Confocal and second harmonic imaging of CSSC-assembled ECM and qPCR of keratocyte differentiation markers. Confocal imaging of assembled COLV and KERA proteins by CSSC cultured on FN (A) and LAM (A) lines. Second-harmonic imaging of COLI suggests high alignment of COLI fibrils running parallel to the CSSC actin filaments. The scale bar is 25 µm. Relative PAX6 (C), KERA (D), COLI (E), and α-SMA (F) gene expression of CSSC seeded on tissue culture plate (TCP), FN lines, LAM lines, and FN Iso. stamps. Gene expressions are relative to TCP. The relative expression of PAX6 was significantly higher on TCP than any of the other groups (** $p<0.005$, n=3). Relative KERA expression in TCP was significantly lower than FN 30 by 30, LAM 30 by 30, and FN Iso (**$p<0.005$, n=3), also KERA expression in FN 30 by 30 was LAM 30 by 30, and FN Iso (%%$p<0.005$, n=3), and KERA expression in LAM 30 by 30 was significantly lower than FN Iso (##$p<0.005$, n=3),FN 30 by 30 significantly lower No significant difference was observed between groups in the relative expression of COLI nor α-SMA.

CSSC are a group of specialized stem cells that reside in the corneal limbus and

have the potential of differentiating into keratocyte, corneal stroma cells that maintain the structure of the stromal ECM in the healthy cornea. I performed qPCR and compared the expression of PAX6, an early stem-cell marker, KERA, a keratocyte marker and important glycoprotein that help maintain COLI fibril architecture, COLI, and αSMA, a fibroblast marker often used to identify a diseased keratocyte state, for FN lines, LAM lines, and FN Iso. samples on D10-KDM relative to CSSC cultured on TCP, which could be understood as a “pre-experimental, stem-cell state”. I observed a significant decrease in PAX6 expression between the FN lines, LAM lines, and FN Iso. groups to TCP (Fig. 3.7C) and a significant increase in KERA expression between FN lines, LAM lines, and FN Iso. to TCP. Also, a significant difference in KERA expression between the FN Iso. group and FN and Lam lines groups was observed, which could be attributed to higher cell-cell contact in isotropic cell organization. Taken together, lower expression of PAX6 and greater expression of KERA on the FN lines, LAM lines, and FN Iso. groups compared to the “pre-experimental, stem-cell state” TCP group, suggests that, by D10-KDM, CSSC have departed their stem cell state and have differentiated to keratocytes (Fig. 3.7D). Although I observed a decrease in the relative COLI gene expression between the groups, there was no significant difference (Fig. 3.7E). Similarly, I observed no significant difference in α-SMA expression between the groups, suggesting that CSSCs are not approaching a fibroblastic state (Fig. 3.7F).

3.4.4. Formation of Distinct Cell Layers on a Single Stroma Sheet

While further characterizing the cell and ECM organization, I noticed that CSSC on single sheets were organized into distinct cell bilayers. At D10KDM cells cultured over the protein lines showed two distinct cell layers with high actin alignment and well-

defined orientations. CSSC actin showed that cells located closer to the FN lines were aligned parallel to the lines, as demonstrated before, while a second cell layer of highly aligned and rotated CSSC were present just above the previous cell layer (Fig. 3.8D, E). It is important to highlight that the second cell layer, furthest from the protein lines, had an OOP of 0.791 $\pm$ 0.071, which was not significantly different from the OOP of the first cell layer, however, this was significantly different from the OOP of CSSC on FN Iso. To further understand and measure the rotational shift between the cell bilayers, z-stack images were taken such that the FN lines run vertically. This allowed us to use the normalized angle frequency of the actin filaments, calculated by the OOP algorithm, across the thickness of both cell layers. As expected, the normalized angle frequency of the first cell layer was 90°, because these cells were parallel to the FN lines, and as I moved from the first to the second cell layer, the normalized angle frequency shifted to 120° (Fig. 3.8F). This smooth transition was observed regardless of protein type (FN or LAM). However, this shifting between the first and second layers was not present in the CSSC cultured on FN Iso. (Fig. 3.8A-C). The rotational shift between the first and the second cell layers were 32.67 $\pm$ 6.63°, 24.92 $\pm$ 5.64°, and 2.41 $\pm$ 13.95° for the FN lines, LAM lines, and FN Iso. groups, respectively. Statistical analysis of the rotational shift between the three groups showed that both FN and LAM lines have a significantly higher shift than the FN Iso. group, while no significant difference in the rotational shift was found between the FN and LAM lines conditions (Fig. 3.8G). Lastly, I found no significant difference in distance between the cell bilayers between the FN and LAM line conditions (Fig. 3.8H).

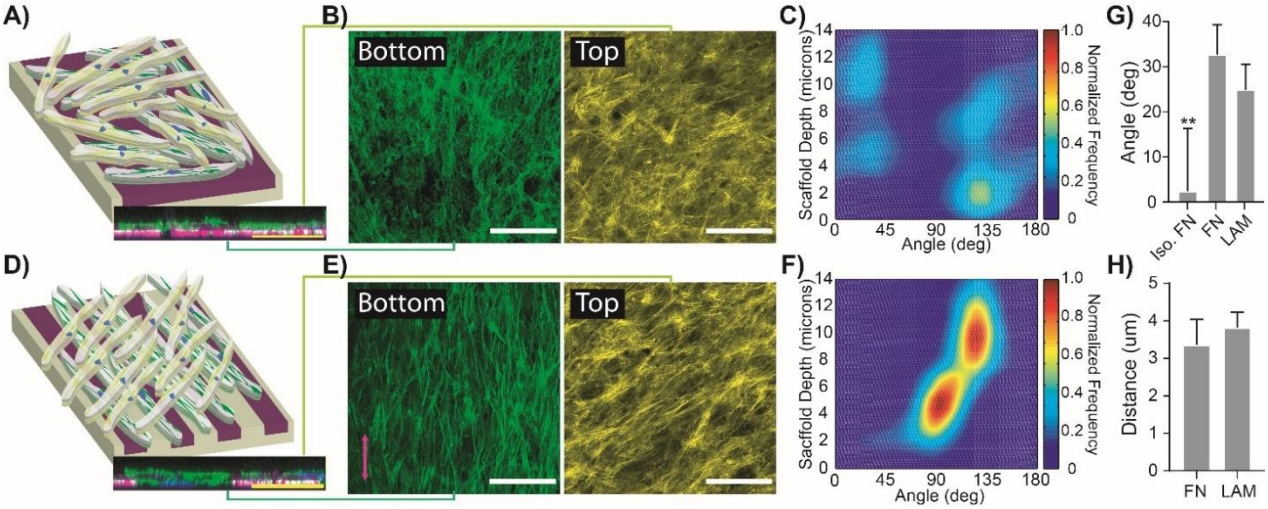

Figure 3.8. CSSC build a highly aligned second cell-layer that is rotated from the cell-layer when the first layer is aligned.

(A) Schematic of cell organization of two cell-layers on an FN iso. stamp with confocal z-stack, scale bar is 25 µm. (B) Corresponding confocal images of actin architecture on the bottom cell-layer closest to the stamp (green) and top of the cell-layer (yellow). (C) Normalized angle preference of the actin filaments across the thickness of the two cell-layers on the FN Iso. (n=9). (D) Schematic of cell organization of the two cell-layers on FN 30 by 30 lines with confocal z-stack. (E) Corresponding confocal image of actin architecture on the bottom cell-layer closest to the protein line (green; magenta arrow representing the direction of FN lines) and top of cell-layer (yellow). (F) Normalized angle preference of the actin filaments across the thickness of the two cell layers on the FN 30 by 30 (n=9). (G) Measured angle difference between the bottom and top layers for CSSC cultured over FN Iso. stamp and FN and LAM lines. The angle difference is significantly different between the FN Iso. group and the two other groups (**p<0.005, n=9). (H) The average distance between points of highest alignment of the two cell-layers on FN and LAM lines (n=9). Scale bars are 100 µm.

3.4.5. Stacking and Characterization of Duo-stacks and Quad-stacks

To target different transplantation procedures, I produced corneal stroma constructs of different thicknesses by manually stacking single sheets into duo-stacks, and duo-stacks into quad-stacks (Fig. 3.4). A 1% agarose block was used to maintain the contact between the layers until cell adhesion had occurred. Duo-stacks (Fig. 3.9A),

and quad-stacks (Fig. 3.9B) were imaged using confocal and second-harmonic generation microscopy. The measured actin orientation across the thickness of each construct shows that the distinct cell layers and rotations from individual single-sheets are maintained after stacking into duo-stacks (Fig. 3.9C) and quad-stacks (Fig. 3.9D). As expected, the thickness of the quad-stack, 84.07 $\pm$ 5.68 µm, is twice the thickness of the duo-stack, 39.83 $\pm$ 2.57 µm, and four times the thickness of the single sheets, 21.23 $\pm$ 2.28 µm (Fig. 3.9E). Lastly, the transmittance of the duo-stacks and quad-stacks was significantly lower than that of the single-sheet and COLI gel from 240 to 960 nm wavelength, while the transmittance of the engineered stroma sheet was significantly lower than the COLI-gel between the 300 nm and 740 nm (Fig. 3.9F). Single stacks were strong enough to be dragged, moved, and rolled with tweezers to create duo-stacks. Similarly, after 5 days of further culture, duo-stacks could be handled with tweezers to create quad-stacks. I attempted to create quad-stacks from stacking four single sheets, however as the third and fourth layers were placed on top of the construct, the adjacent second layer slid because there was no anchorage to the layer below. The staining of the FN lines showed single sheets and duo-stacks could be easily rotated to recreate the crisscrossing pattern of native stromal lamellae of the human cornea at desired angles. Fluorescent staining and second harmonic generation showed that the integrity of the single sheets was maintained in the duo- and quad-stacks and there was a little infiltration of the CSSC into the compressed COLI gels.

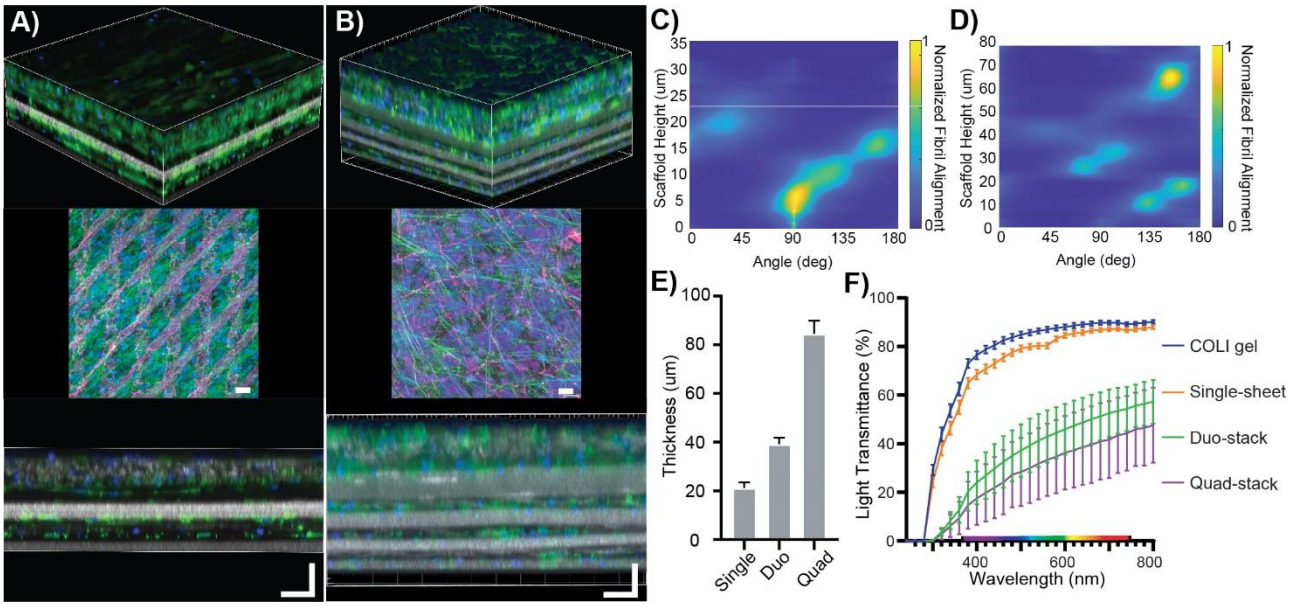

Figure 3.9. Stacking of single sheets into duo- and quad-stack.

Perspective, top, and side view of a duo-stack (A) and quad-stack (B). For each condition, the cell layers made of cell nuclei (blue) and actin (green) are divided by the COLI gels (white). Only on the top-view, the FN lines (magenta) are shown. Top-view scale bars are 20 μm and side view scale bars are 20 μm in each direction. Normalized angle preference of the actin filaments across the thickness of the duo-stack (C) and quad-stack (D). (E) The measured thickness of the single sheet, duo-stack, and quad-stacks. (F) The measured light transmittance of the COLI gel, single sheet, duo-stack, and quad-stack.

3.5. Discussion and Future Directions

Here, I demonstrated a methodology to engineer multilayered corneal stroma constructs from stacking single layers of COLI scaffolds with ECM assembled by CSSC that includes COLI fibrils that run in parallel and corneal-specific proteoglycans. As demonstrated before, the alignment of the CSSC is an important step to guide the parallel assembly of COLI fibrils. In this approach, cell alignment is accomplished by transferring SIA fabricated FN or LAM lines onto a flat COLI substrate and seeding of CSSC at 50,000 cells/cm^2. Because the height of the protein lines is 5 nm[161], I believe the cells are not sensing the height difference between the COLI substrate and the protein lines and, therefore, this is a different approach to align CSSC or keratocytes from modifications to the topography or physical structure of the substrate. For example, PDMS grooves or channels have been used for a scaffold-free approach[197] as well as grooves made out of silk-fibroin[73,232]. Similarly, fibrils in a fibrillar substrate can be arranged to guide cell organization via a physical cue. For example, microfluidics[118], cyclic stretching[154], and electrospinning[219] have been used to align COLI fibers, and electrospinning is readily used to align fibrous poly(ester urethane) urea [220,222] and polylactic acid fibrils[216]. These methods may cause transparency problems if stacked due to gaps between the scaffolds and uneven thicknesses.

This approach presents the advantage of potentially being specific to the patient and the clinical procedure. I can achieve a patient-specific approach using CSSC. CSSC can be easily collected from an incision in the limbus and used to differentiate keratocytes with a lower chance of immune rejection than otherwise. In this paper, I used CSSC from two different patients, and the results presented here were consistent

from both cell sources. Although a multi-patient comparison might be needed, the results here suggest that CSSC from different patients will align, self-organize, and assemble a COLI-rich single sheet. Furthermore, because I can build constructs that range from 20 to 80 µm in thickness, this approach allows me to engineer stroma that can be specific to the procedure and need of the patient.

Something to note is that although both FN and LAM are present at very low quantities in the native-adult cornea stroma [119], these two proteins have major functions in embryonic development of the stroma and ECM assembly. For instance, there is strong evidence that the presence of a preformed FN matrix is essential for COLI assembly [195,204]. In developmental studies of the avian corneal stroma, FN has been found within the matrix of the primary stroma and later loss in corneal stroma differentiation [40]. In development, FN may aid in the migration of corneal precursor cells and when migration is no longer necessary or possible, FN disappears from the stroma and is only present in Descemet's membrane [124]. In the SIA process I employed, protein-surface interactions unfold the protein and trigger assembly of FN [62]. Here, I observed that the width of the FN lines in the duo- and, especially, in the quad-stacks was smaller than the FN lines at the beginning of the experiment. This can be attributed to the remodeling of the FN lines by keratocytes, suggesting that adult physiological levels of FN can be achieved if the cells are cultured for a longer time. Similarly, LAM can be found in the developing cornea. LAM has been localized in the basement membranes and, in smaller quantities, in the epithelium, and neural crest cells, the precursor cells of keratocytes, have a strong affinity towards LAM.

Here, I developed a methodology that takes advantage of the regenerative

potential of CSSCs to build a laminar structure of the native cornea stroma at two scales. The first scale is at the cell-assembled bi-layers of cells, rotated from one another, and highly aligned. Although this event of bi-cell-layering and rotation has been observed before in CSSC [220,223], to my knowledge, this work is the first to measure the rotational angle and distance between these bi-layers. It is important to highlight that this rotational effect was only present when the first layer of CSSC was cultured on the protein lines. I believe that as the first layer of cells starts to assemble the ECM, the fibers on the same plane as the cells are assembled parallel to the cell while the fibers build immediately over the cells are rotated. This causes that any cell the migrates on top of the first cell layer align to rotated fibers assembled by the previous cell layer. This bi-layer self-assembly supports the premise that CSSC have an un-tapped regenerative potential and future steps will investigate how to guide CSSC to assemble more than two cell layers. Furthermore, future experiments will look into how different stimuli, such as pressure, biochemical composition, and cell density, affect the rotational angle and distance between these bi-layers.

The second scale is formed by the stacking of single-stroma sheets into duo- and quad-stacks. Different approaches to achieve a multilayered structure that replicates the crisscrossing laminar structure of the stroma have been extensively used before. The most straightforward and most used method has been manually stacking single sheets of thin stromal constructs. For example, Ghezzi, et al. cultured CSSCs on a single film made out of silk and then stacked them one by one into a total of 7 films that measured on average 150 µm after 9 weeks in culture [73]. However, there seems to be low integration and/or binding between the single sheets, evidenced by gaps between single

sheets. In this approach, there is strong evidence of sheets binding to each other, evidenced by the lack of gaps in the confocal images of the multi-stacks and by how stacking of duo-stacks into quad-stacks did not damage or separated the sheets in the duo-stacks. Follow-up experiments include both an ex-vivo and in-vivo component. For example, long-term experiment looking into cell migration and assembly of ECM between adjacent single sheets via cell tracking and immunostaining, and characterization of the binding strength between the single sheets by peeling.

Similarly, Fernández-Pérez, et al. cast corneal stromal cells encapsulated in a COLI hydrogel to bind different layers of decellularized lenticules from porcine corneas [64]. The multilayered construct achieved in Fernández-Pérez, et al. were made of 4 gels and 5 sheets and decreased in thickness from 245.2 $\pm$ 66.50 to 187.9 $\pm$ 27.44 µm after 3 weeks of culture. In comparison, the quad-stacks developed here were made of 4 COLI scaffolds, and each scaffold with a cell assembled bi-layer. After 23 days of culture and stacking, the total thickness of the quad-stack averaged 80 µm. This method has greater resolution, that is, the single sheet, the smallest unit in the multilayered construct, is thinner than the ones presented by Fernández-Pérez, et al. This presents an advantage because more targeted and less invasive transplantation techniques will need thinner and smaller tissues, while I can further stack quad-stacks to build larger multilayered constructs.

However, some disadvantages and limitations remain in this approach. First, the use of a COLI gel with randomly organized fibrils and high cell density could limit light transmittance. When I test for the transmittance, there is a significant decrease as more single sheets are stacked, however transmittance of the stromal after implantation is

unknown. Cells can remodel the COLI structure and dehydration of the tissue by the endothelium can increase the transparency of the implanted construct, as has been observed previously in the literature [160]. Also, a limitation of this approach to mimic the structure of the whole cornea is that the cornea stroma structure changes depending on depth. However, this technique allows us to stack the sheets at different angles at different depths so I can address this in the future if in vivo testing reveals it is necessary for a clear cornea.

To better understand these limitations and address some of the disadvantages, I proposed the following steps of this research. The scaffolds build here were able to sustain handling and rolling, however, it might be beneficial to measure the mechanical properties of the different multilayered constructs. Similarly, I would like to expand the culture time beyond the scope of this paper to allow keratocytes to reassemble and organize the fibrils in the COLI scaffold. To address how this construct will be transplanted, I propose transplantation into an ex-vivo cornea stromal pocket or partial transplantation. From this ex-vivo model, I will assess cell migration into and out of the transplant, keratocyte gene expression, ECM remodeling, and epithelization of the corneal epithelium.

I believe this platform can be expanded by adding an engineered endothelial layer or use to better understand the relationship between strain/pressure and formation of the cell bi-layer explored here. Previous work from the Feinberg lab using similar fabrication techniques has shown that I can assemble an engineered corneal endothelium on a COLI sheet[161]. While not straightforward, I could leverage this work and culture an endothelium on one side of the engineered stroma to engineer a DSEK

like a graft. I will assess the barrier function of the added endothelial layer by measuring the transendothelial electrical resistance and immunostaining of gap junction and cadherins, endothelial and keratocyte gene expression and viability, and transplantation into an ex-vivo cornea. I believe that the platform presented here can be used to study the relationship between strain/pressure and the formation of the cell bi-layer explored here. The constructs can be loaded into systems that can induce relevant physiological pressure. I will study the rotational angle of the cell-assembled cell layers, COLI content and assembly, and gene expression.

3.6. Conclusion

In this study, surface-modified COLI gels were used to generate single-corneal stroma sheets (single-sheets) that can be easily stacked and handled without altering cell organization. I show that micropatterned FN and LAM lines on COLI scaffolds can serve as an early guide for CSSC alignment and that this alignment guides assembly of a stromal-like ECM from differentiated keratocytes. CSSC-derived keratocytes expressed keratocan and assembled COLI and COLV, both found in the native stroma. Engineered stroma sheets and multilayered constructs were robust and capable of being handled, rolled, unrolled, and further stacked without tearing the constructs. These results make animal in-vivo studies and further understanding of the self-rotating assembled ECM possible next steps.

Chapter 4: Bioengineering Integrated Corneal Stroma and Endothelium Tissue Towards Application in Posterior Cornea Transplantation

4.1. Abstract

The corneal endothelium and Descemet membrane are the posterior-most layer of the cornea. Endothelial cells are non-proliferative cells that form a thin monolayer that maintains hydration and controls nutrient transport into the stroma by a mechanism that pumps excess fluid into the anterior chamber. On the other hand, Descemet's membrane is a dense sheet of extracellular matrix (ECM) composed of laminin (LAM), collagen IV (COLIV), and other proteins that support endothelial cells in the posterior of the cornea. Disease and damage to the endothelium can cause severe swelling to the stroma and cause blindness in the form of corneal edema. Currently, the only way to repair the endothelium is via whole or partial corneal transplantation, with a preference for partial corneal transplantation to avoid unnecessary damage to a healthy stroma and epithelium. Here, I developed a transplantable engineered posterior cornea (EPC) that consists of an engineered endothelium anchored to an engineered corneal stroma. A collagen I (COLI) gel with a dense, 5 nm thick layer of COLIV and LAM was used to mimic Descemet's membrane and serve as a scaffold to culture corneal endothelial cells. Similarly, corneal stroma stem cells (CSSC) were seeded and differentiated to keratocyte over a COLI gel with fibronectin lines to bring about a cell-assembled, highly aligned, COLI-rich ECM analogous to the corneal stroma. Here, I develop a protocol to stack these layers into a posterior corneal stroma. Furthermore, I demonstrate that an engineered endothelium can be stacked on to a thick (80 μm) engineered stroma. Serving as a proof of concept for a possible engineered whole cornea. Lastly, the EPC

attached to an ex-vivo rabbit cornea denuded from the native endothelium. Suggesting that this engineered construct has the potential of being transplantable. Future work will include refining the co-culture environment to optimize endothelial cell and keratocyte viability and function. Similarly, this work can be supplemented by an animal model where a DSEAK procedure is employed.

4.2. Introduction

4.2.1. The Corneal Endothelium and Descemet's Membrane

The posterior-most layers of the cornea are the endothelium and Descemet's membrane. The endothelium is a 4 to 6 µm thick monolayer[212] of polygonal-shaped endothelial cells arrangement in a cobblestone formation responsible for maintaining proper water content in the stroma. At birth, endothelial cells appear at a density of 3,000 to 5,000 cells/mm^2 spread over the whole endothelium[108,126]. Human endothelial cells are arrested in the G1 phase of the cell cycle and have a limited capacity for mitosis to replace the damage and regenerate the endothelium, making the endothelium fragile[104,212]. Instead, endothelial cells enlarge to maintain an intact monolayer. The corneal endothelium has an ATP-based pump-leak mechanism that regulates hydration by being permeable to nutrients into the stroma and actively pumps ions to move water out of the stroma into the anterior chamber[10]. This mechanism gives rise to transparency by maintaining an unsaturated level of water-glycosaminoglycan binding[67]. When this mechanism is disrupted, either by trauma, loss of endothelial cell density from age, or other diseases, the water content in the stroma increase causing edema, thus disrupting transparency.

4.2.2. Diseases and Disorders of the Corneal Endothelium

Cell density is one of the most important factors affecting the function of the corneal endothelium. During normal aging and disease, such as Fuch's Dystrophy, the underlying Descemet's membrane gradually thickens, and the endothelial cell density decreases[50,103]. Once the cell density decreases below ~500 cells/mm^2 the pump mechanism of the endothelium is no longer sufficient to maintain fluid out of the stroma,

leading to swelling, edema, and ultimately blindness[18,52]. In the case of damaged endothelium, a whole or partial cornea transplant can recover vision.

4.2.3. Transplantation Procedures and Shortage of the Corneal Endothelium

Many patients with endothelial dysfunction have viable stromal and epithelial tissues. In these cases, DMEK or DSEAK are performed, in which just the donor endothelium and Descemet's membrane are removed and substituted with a donor endothelium and Descemet's membrane (DMEK) or a donor endothelium and Descemet's membrane with a section of the posterior stroma (DSEAK; Fig. 2.3). Partial transplantation procedures that target the endothelium were the most common type of keratoplasty performed in 2015 worldwide and are becoming more widely used and available in the US[56,57]. These procedures, allow the patients to retain most of their cornea and have rejection and failure rates much lower than for penetrating keratoplasties[7,56,57]. Furthermore, low endothelial cell density is one of the main reasons that donor corneas are deemed unsuitable for transplant, highlighting the importance of the endothelium for normal corneal function[105,106,168].

4.2.4. Approaches to Engineer a Corneal Endothelium and Posterior Cornea

For a tissue-engineered corneal endothelium, the construct must support the formation of a high-density cell monolayer suitable for transplantation and ideally can be implanted using current surgical techniques. Common starting materials include silk fibroin and the amniotic membrane. Silk fibroin is a natural material produced from silkworm cocoons and has been used clinically for sutures because of its mechanical strength for centuries[92,137]. Silk's biodegradability and optical properties are easily tunable by controlling the fabrication process[169,205] and can be molded into different

shapes and patterns to control cell growth and organization[75,143]. On the engineering of the corneal endothelium, silk provides a strong scaffold that can be handled, however, silk needs to be functionalized first to enable and enhance endothelial cell growth[110,111,138]

The amniotic membrane is the innermost layer of the fetal membrane. It is composed of epithelial cells and planted on a basement membrane[35,47]. In ophthalmology, the amniotic membrane is a promoter of epithelialization[217], suppresser of inflammation[190], and an inhibitor of scarring[28] and angiogenesis[115]. The amniotic membrane has been used primarily for the treatment of epithelial diseases and trauma, and examples of its use in engineered endothelial constructs are limited. However, work by Zhao, et al., on the transplantation of corneal endothelium constructs into rabbit[235] and primates[234] suggests that the amniotic membrane is a promising scaffold material to increase the supply of endothelium tissues because the structure of the amniotic membrane is similar to the Descemet membrane. Taken together, an engineered basement membrane that recapitulates the structure and protein composition of Descemet membrane can enhance endothelial growth and be incorporated into larger corneal constructs.

Here, I developed a corneal endothelial construct, made entirely of native extracellular matrix proteins, that can be manipulated and has the potential of being transplanted into an in-vivo cornea. In this chapter, I expanded on the stacking platform used in Chapter 2 to bring about the duo- and quad-stack stroma by integrating an engineered endothelium to stromal constructs of various thicknesses. The presence of tight junctions and regular cobblestone organization of the endothelium suggests that

healthy endothelial cells were present and integrated within the various stroma constructs. An engineered posterior cornea (EPC), composed of the engineered endothelium and a single-sheet stroma, was transplanted onto an ex-vivo rabbit cornea and successfully integrated with the rabbit stroma tissue.

4.3. Materials and Methods

4.3.1. Surface Initiated Assembly of FN Lines for Engineered Stroma Scaffold

To build the engineered stroma scaffold, protein features were transferred to a COLI gel as previously described in section 3.3.1. and 3.3.2. of this thesis as well as in published method[62,161,186].

To make the engineered stroma, PDMS stamps with channels 10 µm wide and 10 µm apart were made by following traditional photolithography[186]. Briefly, a computer-aided design file with lines of widths and space of 10 by 10 µm was generated and transparency photomasks were ordered (CAS/Art Services Inc). A glass wafer was cleaned with ethanol, dried with filtered air, and treated with a Bunsen burner flame to activate the wafer surface. The wafer was then placed on a spin-coater, and SPR 220.3 photoresist (Microchem) pipetted on the treated surface. The wafer was spun for 30 sec at 5000 rpm to achieve a uniform photoresist coating and baked on a hot plate for 90 seconds at 115°C. The then-baked wafer was moved under a UV lamp and aligned with the transparency mask and the UV source. The wafer was exposed to UV light for 50 seconds and exposure was checked under a microscope. The exposed wafer was then baked for 90 seconds at 115°C on a hot plate, placed on SPR developer solution (Microchem) for 40 sec, and submerged in two consecutive water batches for 40 seconds each. The final wafer was then dried with nitrogen and inspected under a microscope. Sylgard 184 Poly(dimethylsiloxane) (PDMS; Dow Corning) was mixed 10 parts elastomer to 1 part curing agent in a planetary mixer (THINKY ARE-250) mixer for 2 minutes at 2000 rpm and degas for 2 minutes at 2000 rpm, poured over the wafer done previously, degassed for another 15 minutes for any remaining air, and cured

overnight at 65°C. Finally, the stamps were cut out of the wafer and stored for further use.

For the engineered stroma, protein lines were transferred to a compressed COLI. Briefly, a 6 mg/ml COLI gel was assembled from a higher concentration stock solution (>9mg/ml, BD Biosciences). Two hundred µL of COLI solution was pipetted over a glass coverslip with a silicone mold that defined the shape of the gel as a 20 mm diameter circle (Fig. 3.1A.i) The COLI solution was gelled at 37°C in a humidified incubator for three hours (Fig. 3.1A.ii). Following gelation, the silicone molds were removed, the gels rinsed three times with deionized water, and dried in a cell culture hood (Fig. 3.1A.iii-iv). The compressed COLI gel was stored at room temperature until use.

FN (Corning) protein was fluorescently labeled with AlexaFluor 555 SE tag (Thermo Fisher) according to the manufacturer's protocol; by the reaction of the succinimidyl ester groups in the dyes and the primary amines in the proteins. First, FN lines of width and spacings of 10 by 10 µm were microcontact printed on a poly(N-isopropyl acrylamide) (PIPAAm, mixed 2% w/v in butanol, Scientific Polymer Products) coated coverslip. This was done by sonicating PDMS stamps with channels of line widths and spacings, or flat features in a 50% ethanol solution for 30 minutes, and then dried with nitrogen. The stamps were incubated for 60 minutes with FN at a concentration of 50 µg/mL, mixed at 1:1 fluorescently-labeled to unlabeled protein (Fig. 3.1B.i). Excess protein was removed from the stamps by submerging the stamps in distilled water and dried with nitrogen. Then, stamps were placed in conformal contact with the PIPAAm-coated coverslip, features down for 60 minutes (Fig. 3.1B.ii). The stamps were then carefully removed from the PIPAAm-coated coverslips to prevent the

tearing of the PIPAAm surface. A detailed description of these steps can be found in Sevcik, et al, 2017[186].

Next, 20% gelatin type A (Thermo Fisher) gels were prepared by pipetting 200 µL of 20% gelatin solution warmed to 60°C on a 20 mm diameter silicone ring on a microscope slide. This was then followed by a 10-minute incubation at room temperature and the removal of the silicone ring. The coverslips prepared previously were placed ECM-side down over the gelatin gels and immersed in distilled water at room temperature to dissolve the PIPAAm and transfer the protein lines onto the gelatin (Fig. 3.1B.iii-iv). The gelatin was peeled off the microscope slide and placed protein-side down onto the compressed COLI (Fig. 3.1B.v). These completed COLI + protein constructs were then incubated in a humidified incubator at 37°C for 45 minutes, rinsed with warm 1xPBS thrice, and incubated again for 45 minutes and rinsed with warm PBS to remove any residual gelatin (Fig. 3.1B.vi). These were then dried in a biosafety hood and stored at room temperature. COLI constructs were put in 6 well plates, covered with 1xPBS, and sterilized with UV light for 15 minutes before usage.

4.3.2. Surface Initiated Assembly of COLIV and LAM for Engineered Basement Membrane (EBM)

To fabricate the EBMs used for endothelial cell culture, SIA was used to transfer a thin layer of COLIV + LAM onto a compressed COLI gel as described in published methods[161]. Briefly, a compressed COLI gel was made by following the manufacturer's protocols to prepare a 6 mg/mL COLI solution from a higher concentration stock solution (>9 mg mL−1, BD Biosciences). Forty µL of COLI solution was pipetted onto a glass coverslip with a silicone mold on top to define the shape of the gel as a 9 mm

diameter circle. The COLI solution was gelled for three hours in a humidified cell culture incubator at 37 °C, resulting in auto-compression of the gel[20]. Following gelation, the silicone molds were removed, and the gels were rinsed 3 times with di-water before drying in a cell culture hood.

Subsequently, SIA was performed to transfer a flat, featureless COLIV + LAM protein onto the COLI gel. This was done by microcontact printing a LAM (50 µg/mL; Life Technologies) + COLIV (50 µg/mL; From human placenta; Sigma Aldrich) solution using featureless (flat) PDMS stamps onto a poly(N-isopropylacrylamide) (PIPAAm; 10% in butanol; Polysciences) coated coverslip. Briefly, PDMS stamps were sonicated in a 50% ethanol solution for 60 minutes, dried using a nitrogen gun, and incubated with the LAM and COLIV mixture for 1 hour. The stamps were then rinsed, dried, and brought into conformal contact, ECM side down, with the PIPAAm-coated coverslip for 1 hour. After 1 hour, the PDMS stamps were carefully picked up from the PIPAAm-coated coverslips.

Next, 20% gelatin type A (Thermo Fisher) gels were prepared by pipetting 200 µL of 20% gelatin solution, warmed to 60°C, onto a 20 mm diameter silicone ring on a microscope slide. This was then followed by a 10-minute incubation at room temperature, to allow the gelatin to gel, and remove the silicone ring. The LAM+COLIV over PIPAAm coverslips prepared previously were placed ECM-side down over the gelatin gels and immersed in distilled water at room temperature to dissolve the PIPAAm and transfer the flat protein onto the gelatin. The gelatin was peeled off the microscope slide and placed protein-side down onto the compressed COLI. These completed COLI + protein constructs were then incubated in a humidified incubator at

37°C for 45 minutes, rinsed with warm 1xPBS thrice, incubated in PBS again for 45 minutes to remove any residual gelatin (Fig. 3.1B.vi). The constructs were then dried in a biosafety hood and stored at room temperature. Lastly, the tops of 15 mL centrifuge tubes were cut off and sealed around the COLI + protein constructs with vacuum grease, restricting the seeding area. COLI constructs were put in 6 well plates, covered with 1xPBS, and sterilized with UV light for 15 minutes before usage.

4.3.3. Isolation and Culture of CSSC and Bovine Endothelial Cells (BCEC)

4.3.3.1. Isolation, Culture, and Seeding of CSSC

Isolation of CSSC was performed as previously described [13,45,197]. Briefly, cornea-scleral tissues from human donors younger than 60 years with <5 days of preservation were obtained from the Center for Organ Recovery and Education (www.core.org), after the center corneal tissue had been removed for transplantation. The rims were rinsed, and the remaining endothelial cell layer, Descemet's membrane, conjunctiva, and trabecular meshwork were removed. The limbal tissue was dissected, cut into 3 mm fragments, and digested overnight in 0.5 mg/mL collagenase L solution at 37°C. Fractions were pipetted and further digested for 30 to 45 minutes. The remaining digest was filtered through a cell strainer, and the cells were centrifuged at 1500 rpm for 5 minutes. The resulting CSSC were plated onto a 25 cm^2 tissue culture flask in corneal stroma stem cell growth medium (GM) containing 2% (v/v) fetal bovine serum, Dulbecco's Modified Eagle Medium-LowGlucose-GlutaMax (Gibco), 400 mg/L MCDB-201 (Sigma Aldrich), 1mg/mL of AlbuMax Lipid-Rich BSA (Gibco), 0.1 mM L-ascorbic acid-2-phosphate (Sigma Aldrich), 0.1X insulin-transferring-selenium (Gibco), 10 ng/mL recombinant rat platelet-derived growth factor-BB protein (R&D Systems), 10 ng/mL

recombinant human epidermal growth factor (R&D Systems), 100 nM dexamethasone (Sigma Aldrich), 1x penicillin-streptomycin 100x (Corning CellGro), and 1:1000 gentamycin (50 mg/mL) (Gibco) (Table 3.1). CSSC were expanded using TrypLe (Thermo Fisher) on FN coated tissue culture flask and passaged at ~1000 cells/cm^2.

CSSC were seeded onto COLI scaffolds with FN lines of 30 by 30 µm (width by the spacing) at 50,000 cells/cm^2. CSSC were cultured in GM until confluency, 3 days, and differentiated by switching to keratocyte differentiation medium (KDM), containing advanced Dulbecco's Modified Eagle Medium (Gibco) with 1 mM L-ascorbate acid-2-phosphate (Sigma Aldrich), 10 ng/mL recombinant human fibroblast growth factor 2 (Cell Sciences), and 0.1 ng/mL recombinant human transforming growth factor β3 (R&D Systems) (Table 3.2). KDM was replaced every 2 days for 10 days. After 10 days in KDM, engineered corneal stroma sheets were ready to be imaged or stacked with the engineered endothelium. COLI scaffolds were seeded with CSSC derived from a single donor cornea at passage 2-5.

4.3.3.2. Isolation and Culture of BCEC

Bovine corneal endothelial cells were isolated as in published protocols[162]. Briefly, corneas from whole bovine eyes (Pel-Freez Biologicals, Rogers AR, USA) were dissected and soaked for 20 minutes in PBS containing 1% penicillin/streptomycin/ amphotericin B and 0.5% gentamicin. Corneas were incubated, endothelial side up, in a 12-well spot plate with approximately 300 mL of TrypLE Express at 37°C for 20 minutes. Endothelial cells were released into the TrypLE Express by gently scraping with a rubber scalpel, combined, and then centrifuged for 5 minutes at 1500 rpm. The cells were designated as passage 0 (P0), resuspended in low glucose DMEM with 10% FBS,

1% penicillin/streptomycin/amphotericin B, and 0.5% gentamicin (EndoM), and cultured in standard tissue culture flasks coated with COLIV. All experiments used endothelial cells of passage P1 to P3.

BCEC were seeded at 100,000 cells/cm^2 on the EBM previously developed. The BCEC were kept in culture for up to 10 days with media changes every 2 days. After 10 days of culture, the engineered endothelium was ready to be stained and imaged or stacked with an engineered corneal stroma sheet.

4.3.4. Coculture of CSSC and BCEC

The culture of BCEC in vitro can be challenging because BCEC can undergo a rapid endothelial-mesenchymal transition (EMT) in KDM. A coculture maintenance media was developed by optimizing BCEC viability and expression of ZO-1. Because I also wanted to optimize CSSC differentiation and keratocyte phenotype, I used the KDM as a starting point. Over a COLI EBM, fabricated as described above, 100,000 BCEC/cm^2 were culture and in low glucose EndoM for 5 days, refreshing the media every 2 days. Then, the media was changed to KDM, KDM without TFG (TGF$^-$), KDM without FGF (FGF$^-$), KDM without TGF and FGF (TFG$^-$ FGF$^-$), or KDM supplemented with 2% FBS (FBS$^+$) for another 5 days. Finally, the samples were fixed and stained for nuclei, actin, and ZO-1. Extra samples of BCEC cultured in KDM were cultured for another 5 days in EndoM (Recovery) and then fixed as stained as before. To assess the effect of the candidate media on CSSC, once a media was selected from BCEC culture, CSSC were cultured over a COLI gel with 30 by 30 µm FN lines in GM and differentiated in KDM as described above.

4.3.5. Stacking of Single-Sheet Engineered Stroma and Engineered Endothelium

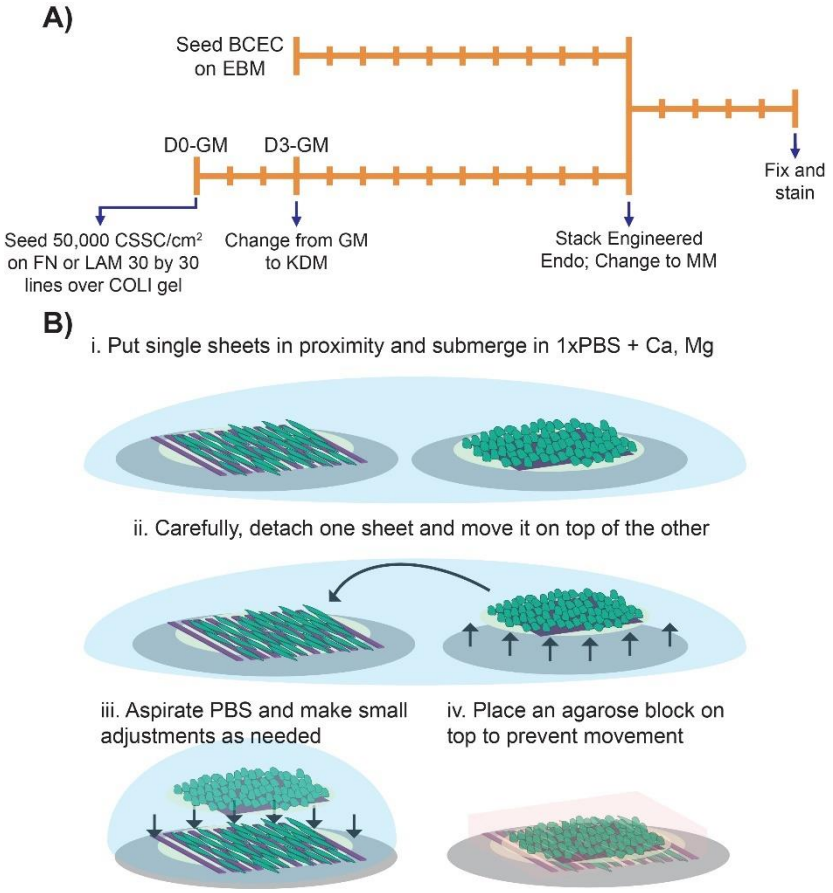

Figure 3.1. Stacking of engineered corneal endothelium over single-sheet stroma. (A) Timeline to culture and stack the engineered endothelium over the single-sheet stroma. (B) The engineered endothelium and single-sheet stroma are placed in proximity and submerged in 1xPBS (i). The endothelium is peeled off and transported over the single-sheet stroma (ii). As the PBS is removed, the endothelium lands over the stroma (iii). An agarose block is used to prevent shifting and enhance contact between the tissues (iv).

The engineered endothelium and single-sheet stroma were cultured separate and on day 10 of culture for the endothelium and day 10 of differentiation for the stroma. Stacking of the endothelium over the stroma was performed as described in section 3.3.5. (Fig. 3.1A). Briefly, single-sheet stroma and the engineered endothelium were

placed near one another submerged in 1xPBS supplemented with Calcium and Magnesium (Fig. 3.1B-i). Carefully, the engineered endothelium is peeled off the glass coverslip and moved over the single-sheet stroma (Fig. 3.1B-ii). As the PBS is aspirated, small adjustments were made to allow the endothelium to land over the single-sheet stroma (Fig. 3.1B-iii). Finally, a 1% agarose block was placed on top of the stack to prevent shifting and movement between the engineered tissues (Fig. 3.1B-iv). The agarose block was removed 3 days after stacking and the constructs were cultured for 2 more days.

The posterior cornea constructs were then mounted onto a transwell-like insert (CellCrown 24NX, Scaffdex) to assess the handling of the construct and visual transparency. Briefly, the construct is submerged in 1xPBS+Ca+Mg and then peeled off the coverslip. The construct is then flipped over such that the endothelium is facing down. Carefully, the construct is “fished out” using the CellCrown insert, and the construct is moved such that the endothelium is centered and taught. Finally, the construct is locked in place as manufacturers protocol.

4.3.6. Stacking of Multilayered Engineered Stroma and Engineered Endothelium

BCEC were seeded on EBMs at least 10 days before stacking over the duo-stack and quad-stack. Engineered multilayered stroma constructs were fabricated as described in section 4.3.5. Briefly, engineered stroma sheets cultured on FN 10 x 10 μm lines were picked up, stacked, and rotated with tweezers, creating a double-layered construct (duo-stack; Fig. 3.3). Duo-stacks were cultured in KDM, replacing the medium every 2 days for 5 days. To create four-layered constructs (quad-stacks), two duo-

stacks were mechanically picked up, stacked, and rotated. Quad-stacks were then cultured in KDM, with medium replacement every 2 days for 5 days. Stacking of the engineered endothelium was carried out as described in section 4.3.4. and performed 5 days after stacking CSSC into a duo-stack (Fig. 4.2A) and 5 days after stacking duo-stacks into a quad-stack (Fig. 4.2B).

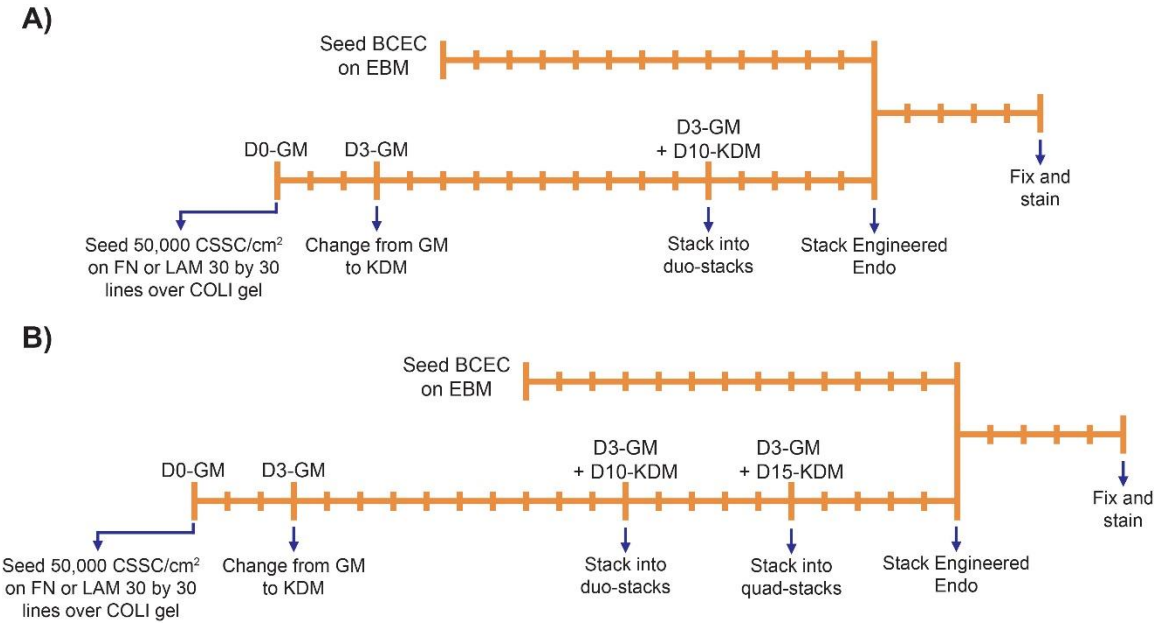

Figure 4.2. Timeline for seeding and stacking of engineered endothelium over-engineered multilayered stroma.

Stacking of engineered endothelium over a stoma duo-stack (A) and quad-stack (B).

4.3.7. Transplantation of Integrated Engineered Stroma and Endothelium to Ex-vivo Rabbit Cornea

To assess as proof of concept whether the engineered endothelium can survive a transplantation procedure and attach to the native cornea, I performed a DSEAK like procedure where the native endothelium and Descemet membrane from a rabbit ex-vivo cornea was removed and an EPC (engineered endothelium + a single-sheet stroma)

was attached. Briefly, whole rabbit eyes (Pel-Freez Biologicals, Rogers AR, USA) were ordered, and the corneas were dissected. The corneas, endothelium side-up, were rinsed with 1xPBS +Ca, +Mg, containing 1% penicillin/streptomycin/ amphotericin B and 0.5% gentamicin. Then, the native endothelium and Descemet membrane were removed. An engineered endothelium with a single-sheet stroma construct was carefully laid over the rabbit cornea (engineered endothelium-side up) and a 1% agarose black was placed on top to prevent shifting or moving. The cornea was then cultured in low glucose DMEM with 2% FBS, 1% penicillin/streptomycin/ amphotericin B, and 0.5% gentamicin for 7 days. The agarose block was removed after 4 days of culture.

Positive control of intact ex-vivo rabbit cornea and negative control of a rabbit cornea without replacement of the endothelium were culture for 7 days using the same media as above. Similarly, a fourth group where the native endothelium was removed and replaced with a 10 µm-thick COLI gel was prepared and cultured.

4.3.8. Immunostaining H&E staining, and Microscopy

All engineered endothelium and the different stacked constructs were immunostained as follows Samples were fixed in 4% paraformaldehyde in 1xPBS+Ca,+Mg supplemented with 1:1000 Triton-x for 12 minutes and washed for 5 minutes with 1xPBS+Ca+Mg three times. Tight junctions were stained using a primary antibody cocktail of mouse anti-ZO1 (1:200; Thermo Fisher) in 1% Bovine Serum Albumin in 1xPBS overnight at 4°C. The following day, samples were rinsed for 5 minutes three times with 1xPBS+Ca+Mg and stained using a second antibody cocktail containing AlexaFluor 555 goat anti-mouse (1:200; Thermo Fisher), Phalloidin 488 for staining of actin filaments, and diamidino-2-phenylindole (DAPI, Thermo Fisher) for

staining of cell nuclei for 1 hour at room temperature. Finally, samples were washed for 5 minutes with 1xPBS three times and mounted on microscope glass slides with Prolong Anti-Fade (Life Technologies). Mounted samples were imaged on a Zeiss LSM 700 confocal microscope. For second-harmonic generation microscopy, I replaced DAPI with TO-PRO-3 Iodide (632/661) – 1 mM Solution in DMSO (1:1000 in 1xPBS; Thermo Fisher).

Ex-vivo corneas were fixed in 4% paraformaldehyde in 1xPBS for 24 hours at 4°C and rinsed with 1xPBS+Ca+Mg for 30 min three times. Fixed corneas were processed for paraffin histology. Five µm paraffin sections from the ex-vivo corneas were deparaffinized and stained with H&E to visualize whole tissue morphology.

Samples were imaged on a Zeiss LSM 700 confocal microscope and a Nikon Eclipse Ti2 multiphoton microscope. Two-photon microscopy was performed using a wavelength of 810-830 nm for the generation of second-harmonic signaling from aligned COLI fibrils. Visualization of H&E staining was done using an EVOS FL Auto 2 microscope.

4.3.9. Transparency and Transmittance

Light absorbance of the engineered endothelium stacked over a stroma sheet was measured by a Molecular Devices SpectraMax i3x spectrophotometer 5 days after stacking into an EPC. Constructs were rinsed once with 1xPBS supplemented with Calcium and Magnesium and submerged during the measurement. Absorbance was measure from 240 to 1000 nm wavelength in 20 nm steps. From the measured absorbance, the transmittance was calculated as described by other groups[64].

4.4. Results

4.4.1. Coculture of CSSC and BCEC Using a Maintenance Media (MM)

CEC can undergo EMT under certain conditions. EMT has been observed with TFGβ1, basic-FGF, and FGF2 supplemented medium on rabbit CEC[127,128,225], and BCEC[91,162], and human CEC[24]. Here I isolated and expanded BCEC in co-culture with corneal stromal stem cells (CSSC). The differentiation medium for CSSC (KDM) contains both FGF2/basic-FGF and TGFβ3, which could cause EMT of BCEC. To generate an optimal co-culture that maintains CSSC differentiation and prevents EMT, I cultured confluent BCEC on KDM, KDM without TGF (TGF^-), KDM without FGF (FGF^-), KDM without TGF and FGF (TFG^- FGF^-), and KDM supplemented with 2% FBS (FBS^+) for 5 days. An extra group was assigned as “Recovery” for BCEC that were culture in EndoM for 5 days after exposure to KDM.

Staining of BCEC with ZO1 and actin suggests that in TGF^-, BCEC produces little tight junctions between cells and the signature cobblestone arrangement of endothelial cells is lost. Although to a lesser extent, this was also present for BCEC cultured in FGF^-, and TGF^- FGF^-. BCEC cultured on KDM, although a more regular ZO1 stain was present, this ZO1 stain was not consistent throughout the monolayer, and it seemed like some BCEC had started to lose their polygonal shape. Lastly, BCEC cultured in FBS^+, have the most consistent ZO1 stain while maintaining cobblestone formation throughout the endothelial monolayer (Fig. 4.3A). This suggests that FBS^+ is the best candidate to serve as a maintenance medium for CSSC and BCEC co-culture.

To further assess FBS^+ as a co-culture maintenance medium, CSSC were seeded on a COLI scaffold with 30 by 30 μm FN lines, cultured in GM, and differentiated

in KDM. The medium was then switched to FBS^{+} for 5 days. From fluorescent staining of the CSSC for actin, the morphology of the CSSC remained relatively unchanged from culturing in KDM. The staining of alpha-smooth muscle actin (αSMA) shows no distinguishable signal suggesting a fibroblastic change on the CSSC (Fig. 4.3B).

The intermittent tight junction in the mediums without growth factors can be attributed to how to FGF2 is linked to the modulation of EMT in vivo. For example, FGF2 can inhibit EMT by repressing TGFβ1 signaling[31], and there is evidence suggesting that the small quantities of FGF2 present in Descemet's membrane assists in maintaining CEC polygonal shape[127,129]. This suggests that BCEC might tolerate small quantities of FGF2 before going EMT. Similarly, KDM was supplemented with FBS because the major difference between KDM and EndoM is the presence of FBS in EndoM. Previous experiments showed that BCEC grows in GM, which is supplemented with 2% FBS, thus I hypothesize that at 2% FBS BCEC will be able to grow and that the presence of serum might promote tight junction formation.

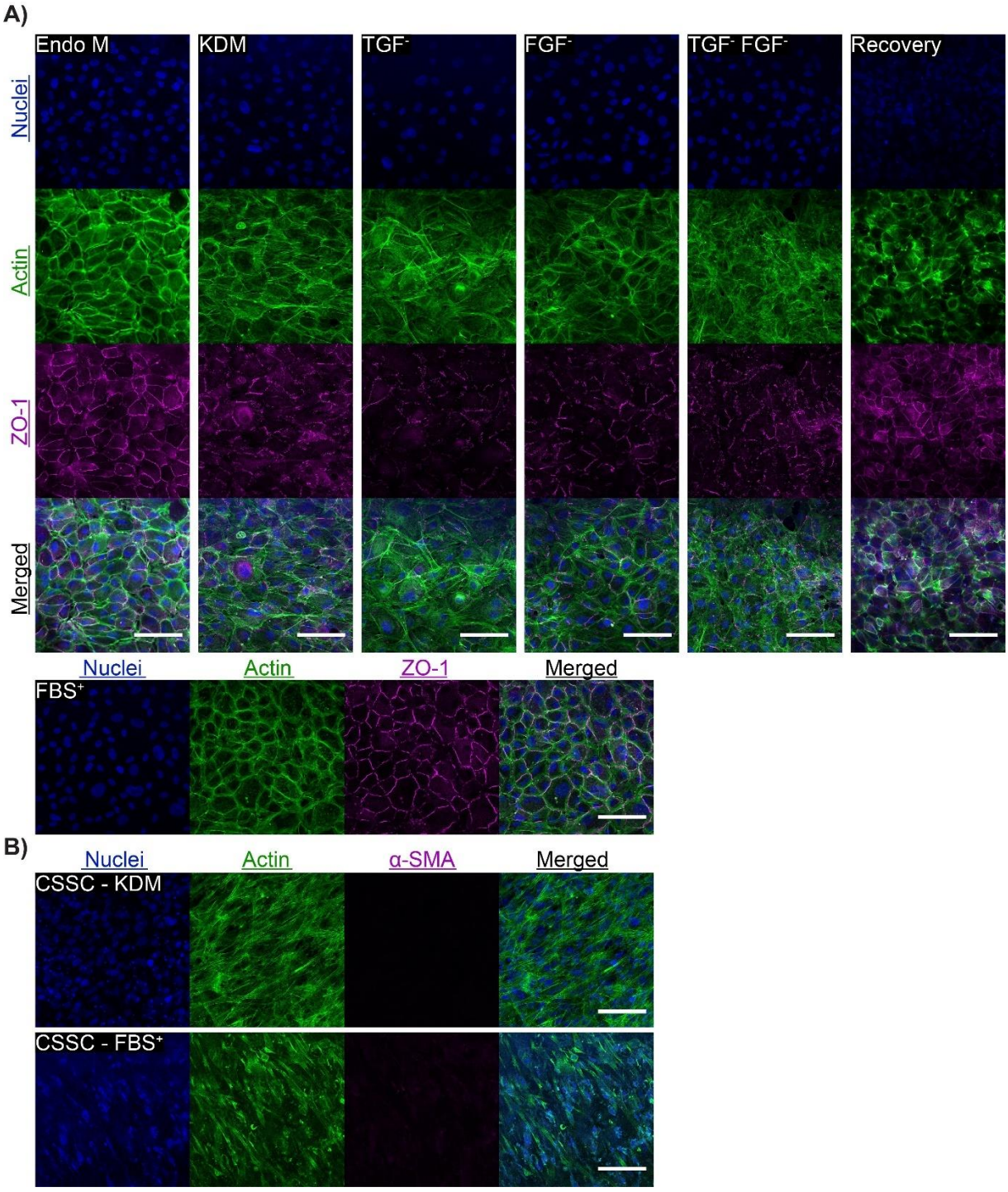

Figure 4.3. Assessment of co-culture maintenance media on BCEC and CSSC.

(A) BCEC were exposed to the different media compositions; EndoM (control), KDM, TGF^-, KDM FGF^-, TGF^- FGF^-, FBS^+, and exposure to EndoM for 5 days after exposure to KDM (Recovery). Nuclei (blue), actin (green) and ZO-1 (magenta). (B) CSSC-derived keratocyte in KDM+FBS. Nuclei (blue), actin (green), α-SMA (magenta). All scale bars are 100 µm.

4.4.2. Integrated single-sheet Engineered Stroma and Endothelium

Upon developing a co-culture maintenance medium, the engineered endothelium, previously developed in the Feinberg lab[161], was co-culture with the engineered stroma developed in chapter 3 of this thesis. A single-sheet stroma was prepared by seeding CSSC over a COLI gel with 30 by 30 µm FN lines and then differentiating the CSSC to keratocytes. Parallelly, an engineered endothelium was culture by seeding BCEC over the EBM at least 10 days before stacking. The engineered endothelium was then manually stacked over the single-sheet stroma.

The engineered endothelium was easily stacked over the single-sheet stroma without tearing or damaging the scaffold (Fig. 4.4A.i). As shown by the photographs, the EPC can be handled and mounted onto a CellCrown insert without causing damage to the engineered endothelium or the single-sheet stroma (Fig. 4.4A. ii-iii). This suggests that the binding between the CSSC in the single-sheet stroma and the COLI of the EBM can prevent the delamination of the different tissues.

Fluorescent staining of the construct suggests that distinct endothelial and stromal layers are present. ZO1 and the cobblestone arrangement of endothelial cell suggests a healthy endothelium. Furthermore, endothelial cells appear to be evenly and widely distributed throughout the whole construct. Also, on the stroma-side of the construct, CSSC aligned and assembled a highly aligned and rotated cell bilayer. This is a promising result because this behavior was also present in the experiments in Chapter 3, which mimics the native lamellar architecture of the stroma (Fig. 4.4B-C) Taken together, these results suggest that the EPC is made of a healthy endothelium, with a stroma that mimics the native architecture, and can be picked up and handled

with ease and without tears.

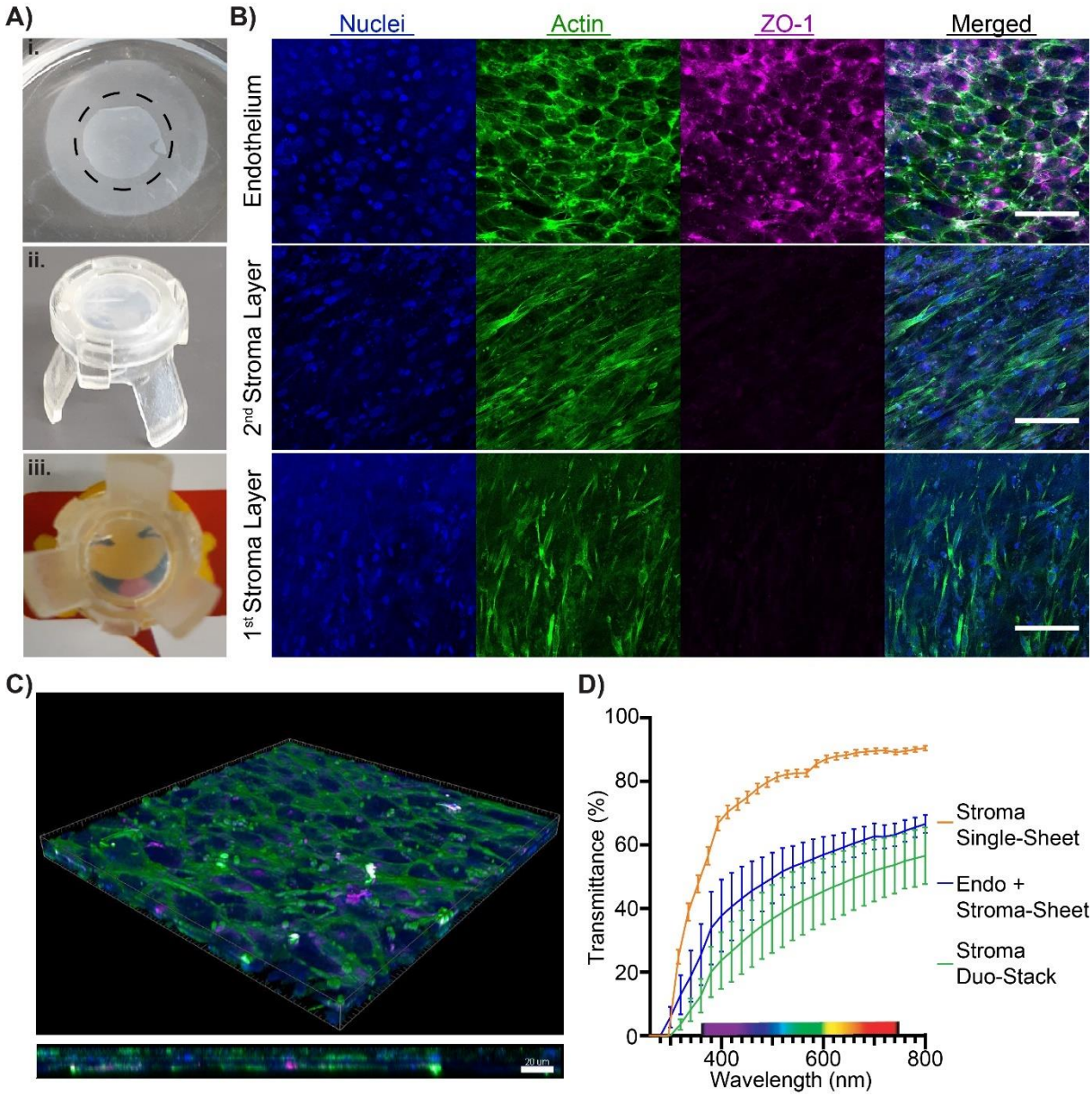

Figure 4.4. Integrated engineered endothelium with single-sheet stroma.
(A) Image showing the engineered stroma over the single-sheet stroma (i). The EPC can be manipulated and mounted on a transwell (ii). Construct is transparent enough to visualize images through it (iii). (B) Fluorescent staining of the EPC Slides showing the engineered endothelium, the first and second CSSC-assembled cell layers. Nuclei (blue), actin (green), ZO-1 (magenta). Scale bar 100 µm. (C) Perspective and side view of the EPC. Scale Bar 20 µm. (D) Measured transmittance of the EPC and comparison with a single-sheet stroma, and a stroma duo-stack.

Lastly, the transparency of the EPC was measured and compared with the transparency of a single-sheet stroma and a duo-stack stroma. Although no statistical significance was found between the EPC and the duo-stack stroma, it seems like the transparency of the EPC falls between the transparency of the single-sheet stroma and the duo-stack. It might be expected that the transparency of the EPC is lower than the single-sheet stroma because the former is made of two COLI gels with randomly arranged fibrils; randomly arranged COLI fibrils refract more light than COLI fibrils with a high degree of alignment, tight spacing, and regular diameter, which are major contributors to stroma transparency. On the other hand, the higher transparency of the EPC to the duo-stack stroma might arise from the difference in thickness of the engineered layers. The EPC had a thickness of 26.52 $\pm$ 2.38 μm, while the thickness of the duo-stack was 39.83 $\pm$ 2.57 μm.

4.4.3. Integrated Multilayered Engineered Stroma and Endothelium

In Chapter 3, I developed a multilayered stromal construct that partially mimics the lamellar structure of corneal stroma and is composed of single-sheet stroma with CSSC that express native stromal ECM proteins. Here, an endothelial layer was added to a duo-stack and a quad-stack stroma.

Fluorescent microscopy shows an endothelial layer with evenly distributed tight junctions, shown by the ZO1 stain (magenta), and a cobblestone monolayer, shown by the actin stain on constructs with the duo- and quad-stack stroma (green; Fig. 4.5). The keratocytes on the stroma side appear dendrite-like, like native keratocytes. Lastly, COLI imaging using second harmonic generation microscopy shows sharp separation between the endothelial and stromal layers. These results serve as a proof-of-concept

that a thicker corneal construct with multiple cell types can be developed. An area that still needs further development is to fine-tune a co-culture media or environment that permits maintenance of endothelial cells, permit keratocytes to reassemble the stromal layers, and can readily integrate a corneal epithelium.

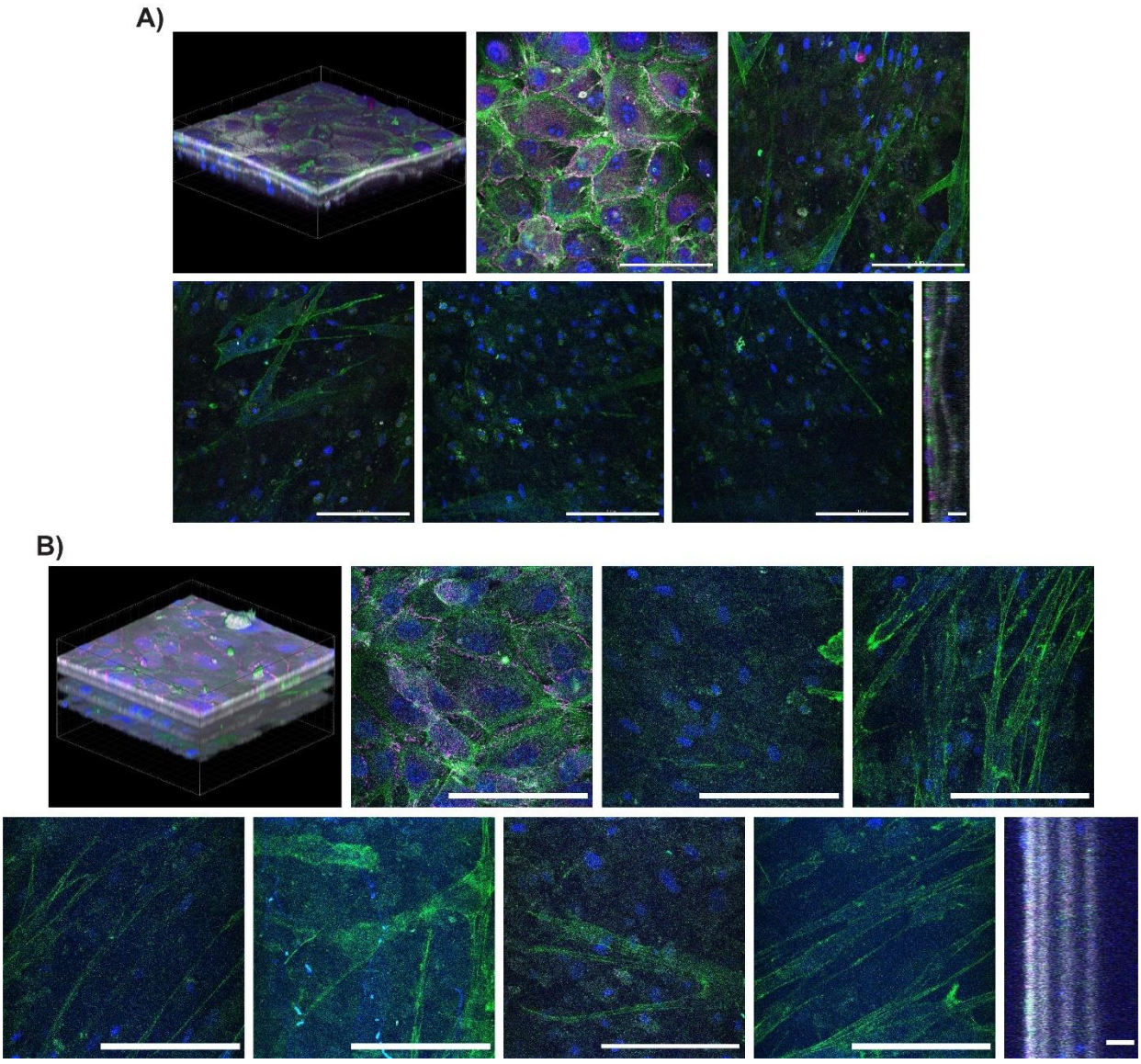

Figure 4.5. Integrated Multilayered Engineered Stroma with Endothelium

(A) Stacking of duo-stack stroma with engineered endothelium. (B) Stacking of quad-stack stroma with engineered endothelium. SB 200 µm. SB for side projections: 20 µm.

4.4.4. Transplantation of EPC to Ex-vivo Rabbit Cornea

Rabbit eyes were dissected, and the corneas were separated into four groups: intact control, endothelium-denuded control (Denuded Control), replacement of the endothelium with a COLI gel, and replacement of the endothelium with an EPC developed in section 4.4.2, and all cultured for 7 days. It is important to note that after the 7 days cultivation period, the samples replaced with a COLI gel suffered from delamination and detachment of the COLI gel, making these not viable for histology or further processing, and suggesting that a cellular component might be needed to facilitate integration and attachment of the tissues.

Photographs of the Intact Control, Denuded Control, and the EPC Show that there is little visual difference between the samples (Fig. 4.6A). Likely due to the samples being cultured by being submerged in media. Histology H&E stain of the various samples shows significant swelling in all the samples, averaging more than 1000 µm (Fig. 4.6B-D). This swelling might also be due to submerging the samples in media. Although integration of the EPC with the rabbit cornea was not consistent throughout the full length of the tissue, some areas, specifically closer to the central cornea, were attached to the rabbit tissue. It is important to note that the observed endothelium in the Intact Control (Fig. 4.6B) appears to be similar in thickness to the engineered endothelium in the transplanted sample (Fig. 4.6D).

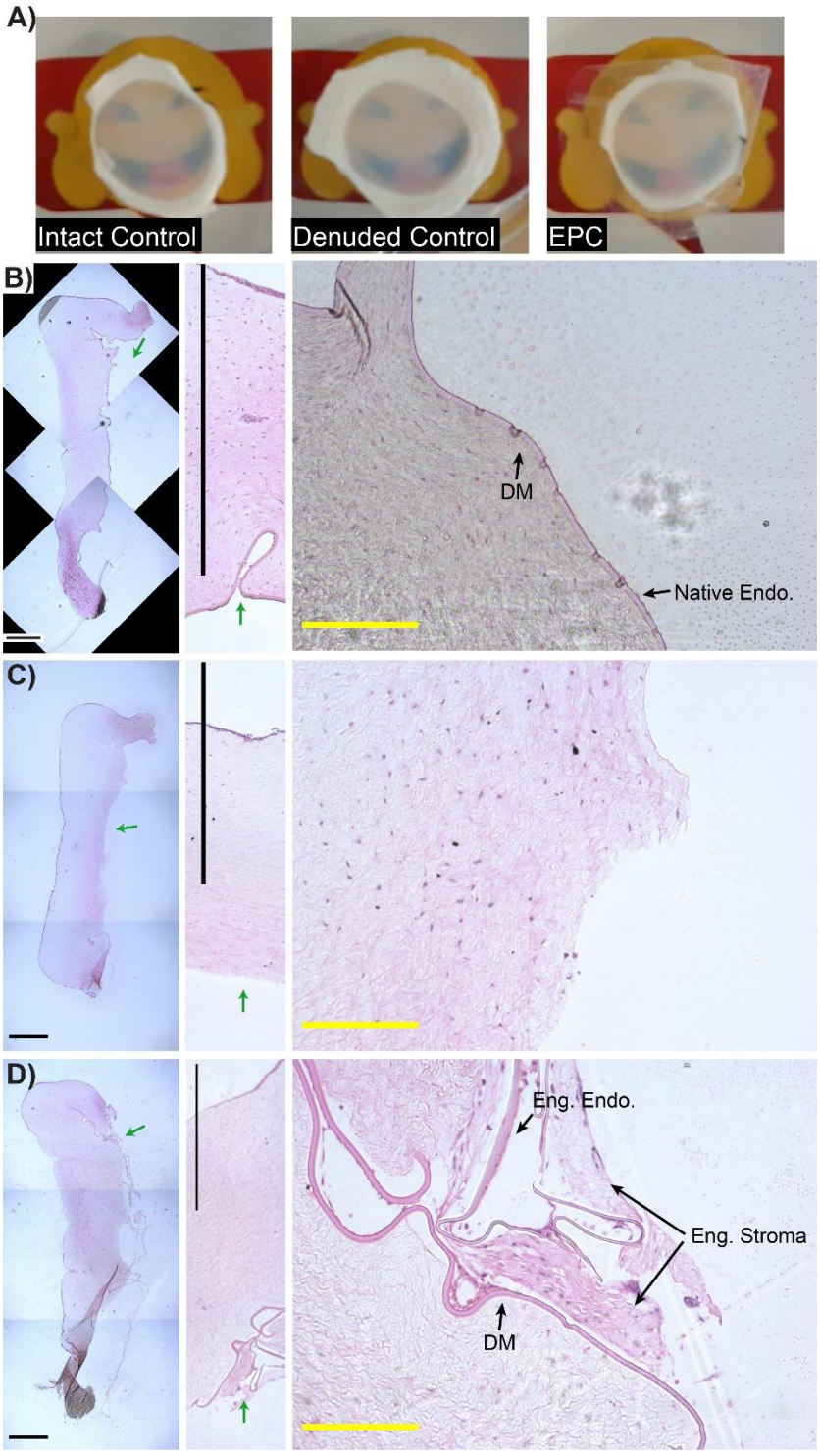

Figure 4.6. Transplantation of EPC to Ex-vivo Rabbit Corneas

(A) Photograph of intact, denuded controls, and ex-vivo cornea with EPC. H&E staining of the intact control (B), denuded control (C), and EPC (D). Green arrows: endothelial side. Scale bars: 1000 µm (black), 200 µm (yellow).

4.5. Discussion and Future Directions

Transplantation of the whole cornea was seen as the only solution for patients with damaged endothelium. Since over 40% of transplants are due to dysfunction of the cornea[57], there has been a rapid increase in the popularity of partial transplantation procedures such as DSEAK and DMEK, particularly for patients with a healthy stroma and epithelium. However, accessibility to donor-grade tissue and the probability of an immune response from the host to a foreign tissue remains a challenge.

Transplantable endothelial constructs can help to close the gap between the supply and demand of corneal donor tissue. Work by Kim, et al. shows an engineered endothelium made of a blend of aloe vera and silk fibroin. This silk fibroin scaffold was transplanted into an in-vivo rabbit cornea using a DMEK procedure. The scaffolds attached to the surface of the rabbit stroma and remained integrated into the native tissue without a significant inflammatory reaction after 4 weeks post-surgery[110].

Here, I presented an engineering approach to fabricating a corneal endothelium integrated to the various stromal construct of different thicknesses, EPC. The EPC was assessed in terms of the purity of each layer, as in whether only endothelial cells are present in the endothelial side, and on the transplantability of the engineered tissue. The EPC was composed of endothelium with consistent tight junctions and a regular cobblestone cell formation, suggesting a healthy endothelium. Similarly, in the experiment when the engineered endothelium was stacked with the single-sheet stroma, the stroma appeared to maintain a highly aligned and rotated cell bilayer. The stacking method and the engineered stroma construct used in this chapter were developed and assessed in Chapter 2 of this thesis.

To strengthen this study, I believe a more in-depth assessment and development of a co-culture maintenance media is needed. Here, my assessment metric, positive staining of ZO1 for endothelial cells, and negative staining of αSMA and cell shape and morphology for CSSC is limited and can be improved by assessing gene expression of the cells. For example, increased expression of ATP1A1 and ATP1B1, genes for the Na^+/K^+ ATPase pump, and n-cadherin, accompanied by decreased expression of αSMA are common markers that identify corneal endothelial cells[12,132]. Similarly, increased expression of keratocan and aldehyde dehydrogenase, and decrease expression of αSMA are suitable markers for healthy keratocytes[70,123]. A fluorescent stain of ZO1 for endothelial cells, and keratocan for keratocytes, can be complemented with αSMA with the expectation of a negative stain signaling a healthy cell phenotype.

This platform makes the development of a cornea construct with all 3 main layers accessible, however, the major limitation to developing a whole cornea construct would the optimization of the co-culture maintenance media. The ideal maintenance media would balance the differentiation of the CSSC to keratocytes and not having a fibroblastic response, prevent EMT of the endothelial cells, and, in the addition of epithelial cells, prevent epithelial-mesenchymal-transition from the epithelial cells. Furthermore, cytokines and growth factors secreted by cells in co-culture can influence cell growth and function, as it has been described in the formation of epithelial layers[159,238].

Nevertheless, including an epithelial layer to this platform to create a cornea construct with all three main corneal cell types and aiming to create transplantable tissue for full penetrating keratoplasty seems like a logical next step. Current multi-cell

constructs of the cornea have proposed the use of disease modeling or culture the epithelium and the stroma. Furthermore, it is common to see the stroma be replaced by an acellular gel, limiting the regenerative component of the tissue. The results presented here suggest that the platform is strong enough to withstand handling and has the potential to be used in DSEAK and DMEK procedures. I propose a timeline to grow and incorporate an epithelium into this platform (Fig. 4.7). Briefly, the engineered endothelium and the quad-stack or octo-stack (two quad-stacks together) are fabricated in parallel following the protocols in sections 3.3.5 and 4.3.6 of this thesis (Fig. 4.7A.i). The construct is then mounted on a CellCrown insert as described in section 3.3.5 and corneal epithelial cells are seeded on to COLI gel of the quad-stack stroma, the top side of the insert (Fig. 4.7A.ii-iii). To fabricate the whole cornea constructs, endothelial cells are seeded at least 10 days before stacking onto the quad-stack stroma, cultured for 5 days, and then mounted on the CellCrown insert, followed by seeding of the epithelial cells (Fig. 4.7B).

The current major limitation of this chapter is the method to test transplantation of the EPC, in particular the use of an agarose block to facilitate contact between the construct and the ex-vivo rabbit cornea. For example, the block might not have been heavy enough to displace media between the construct and the cornea that can inhibit contact between the tissues. Also, the block might have prevented the proper function of the endothelial cells since the block prevents the free flow of media into the endothelium. A future experiment might include partnering with corneal surgeons such as Dr. Deepinder Dhaliwal, M.D. and Dr. Gary Yam, Ph.D. at the University of Pittsburgh Medical Center, Department of Ophthalmology, to carry out an ex-vivo DMEK

procedure using the EPC.[96,192].

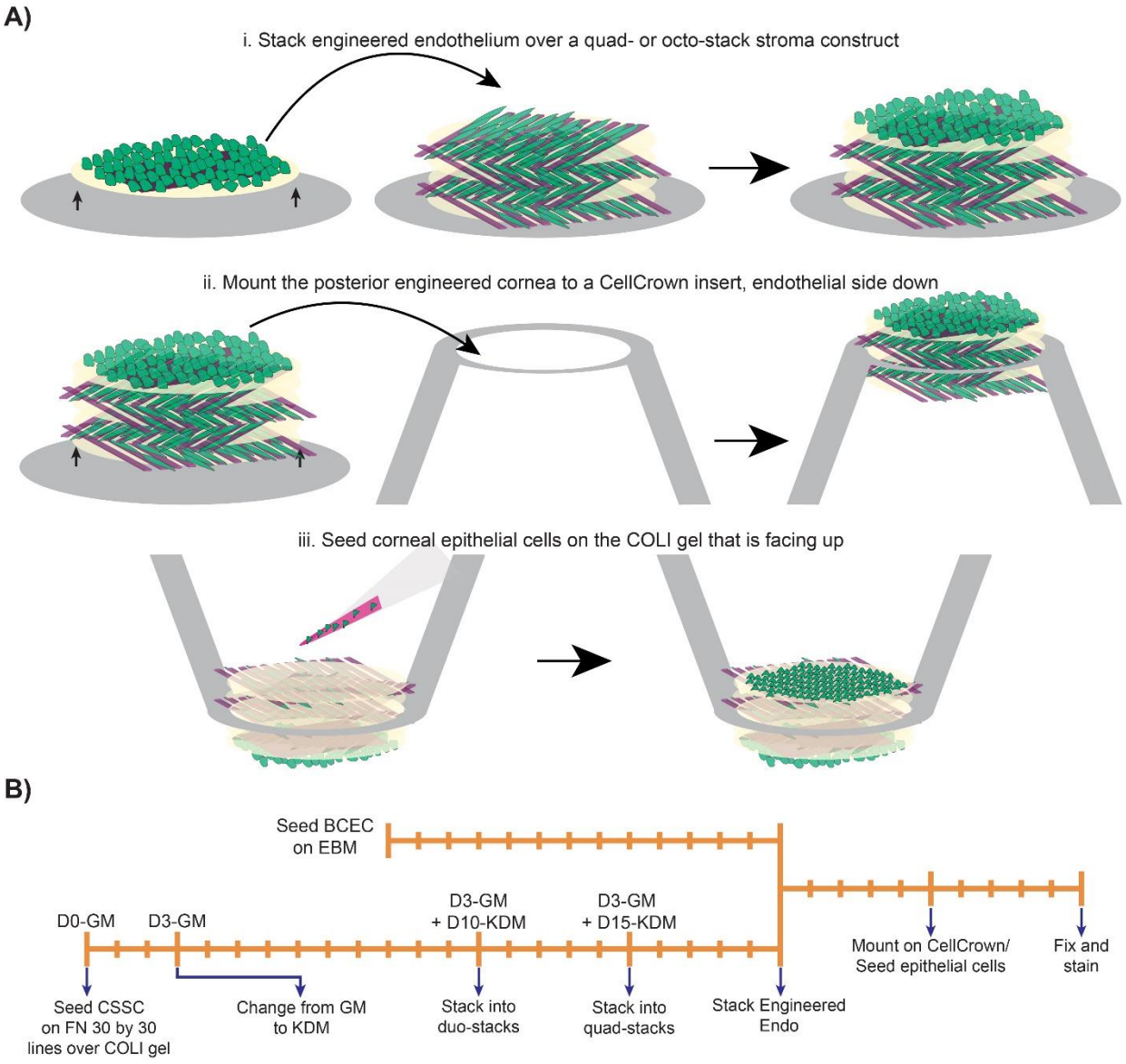

Figure 4.7. Schematic for Fabrication of Whole Cornea Construct.

(A) The engineered cornea endothelium and quad-stack stroma are fabricated parallelly and then stacked as previously done (i). The construct is then mounted on a CellCrown insert such that the endothelium is facing down (ii). Epithelial cells can be seeded on the top-most COLI gel from the quad-stack stroma. (B) Proposed timeline for the fabrication of a whole cornea construct.

4.6. Conclusion

In this chapter, I expanded on the stacking platform used in Chapter 3 to bring about the duo- and quad-stack stroma by integrating an engineered endothelium to stromal constructs of various thicknesses. The presence of tight junctions and regular cobblestone organization of the endothelium suggests that healthy endothelial cells were present and integrated with the various stroma constructs. An EPC, composed of the engineered endothelium and a single-sheet stroma, was transplanted onto an ex-vivo rabbit cornea and successfully integrated with the rabbit stroma tissue. It will be important to further characterize the co-culture conditions, in the form of a co-culture maintenance medium, that optimize a functional endothelium and healthy differentiated keratocytes. Taken together, the platform presented in Chapter 4 serves as proof of concept for engineered tissues suitable for DSEAK and DMEK procedures and a launchpad for the development of a whole cornea engineered construct.

Chapter 5: Effects of Strain on Corneal Extracellular Matrix Assembly and Corneal Stromal Stem Cell Differentiation and Development

5.1. Abstract

The cells in the body live in an active, always changing 3-dimensional environment and experience stimuli that include fluid flow, stretching, compression and load, electrical and biochemical signaling, and topographical cues. While in-vitro culture provides a controlled environment to study cells and biological phenomena, most in-vitro culture happens in a 2-dimensional system, which is by no means complex. Bioreactors are useful systems to study biological phenomena in a controlled environment. These can be used to study disease progression, pharmacological effects, and tissue development. Bioreactors attempt to mimic the minimum number of biological parameters needed to replicate native biological responses. Some examples of these have been developed for lung, heart, and kidney, among others. Corneal bioreactors can be useful to study the transportation of eye drops drug and the phenomena that give rise to transparency during corneal embryonic development. This chapter makes a point on the importance of corneal bioreactors, embryonic development. The chapter contains a section on my work and initial steps on the development of a corneal stroma bioreactor that harnesses the protocols used in Chapter 3. Lastly, it outlines the immediate and long-term steps to develop the corneal bioreactor and the next set of experiments needed to continue this work.

5.2. Introduction

5.2.1. A Note on the Need for Bioreactors

Bioreactor systems play an important role in tissue engineering. They provide a controlled environment that enables reproducibility and allows for the regulation of changes to specific factors. Bioreactors are widely used in tissue engineering for cell proliferation studies[30,198], understanding of disease progression and drug development[116,191], generation of 3D constructs[78], and as organ support devices[173,187,202]. In general, bioreactors should provide for control of oxygen tension, pH, and temperature, while bioreactors tailored for specific organs and tissue types might include control of fluid flow, electrical field, and mechanical stresses.

For example, organ-on-a-chip and other small engineered systems can be categorized as small bioreactors because these mimic the cellular architecture and physiological environment of an organ. Organ-on-a-chip devices have shown potential in investigating the physiological and disease cause, as well as toxicology and drug screening studies[230]. Lung-on-a-chip systems provide control over fluid flow as well as the air-fluid boundary native of the alveolar space[191].

5.2.2. Embryonic Development of the Stroma

The cornea is a unique, collagen (COL)-rich, transparent tissue. COL is organized into a complex lamellar architecture made of fibrils of uniform diameter and spacing. Key developmental steps and structural transformations happen in the embryo for the cornea to be transparent. Even though the origins of corneal transparency have been studies for well over 100 years (See work by Kessler in 1877)[109,177], there are developmental differences between species[85,136], many questions remain unanswered

on how cellular and organizational dynamics during the development of the cornea bring about transparency.

The cornea is made of three cellular layers from cranial ectoderm origin. The epithelium is a direct descendant of the ectoderm ocular surface ectoderm and is the anterior-most layer. The stroma is derived from neural crest cells and is the middle layer. Lastly, the endothelium is from neural crest origin and covers the posterior-most surface of the cornea. (Fig. 5.1A)

The first layer of the cornea to start to develop is the epithelium. After the formation of the lens vesicle, the overlying ectoderm joins together to make the early epithelium (Fig. 5.1B). Studies in chick embryonic models suggest that the interaction between the epithelium and the lens synthesizes the primary stroma[86,89,136]. Between E3 through E5, the epithelium is two-cell layers thick. By E6 and E7, the epithelium is three-cell thick and continues to increase to 4 to 5 cell layers, at which point K12 starts to be expressed (Fig. 5.1B)[38,201]. After E14, the epithelium is fully developed and consists of 6 to 8 cell layers[97].

Our current understanding of corneal stroma development stems from work by Hay and Revel, 1969[88,177]; in their research, a two-stage process for the assembly and deposition of COL is established. In the first stage, a cell-free primary stroma matrix of highly ordered COL is assembled by the early ectodermal epithelial cells. Through a two-wave process of mesenchymal cells, for which the endothelium is formed in the first wave[5,224], mesenchymal cells destined to become keratocytes and assembled the secondary stroma migrate in between the endothelium and the epithelium. The early keratocytes go on to synthesize most of the secondary stroma by assembling COL

fibrils into thick lamellae (Fig. 4.1C)[177].

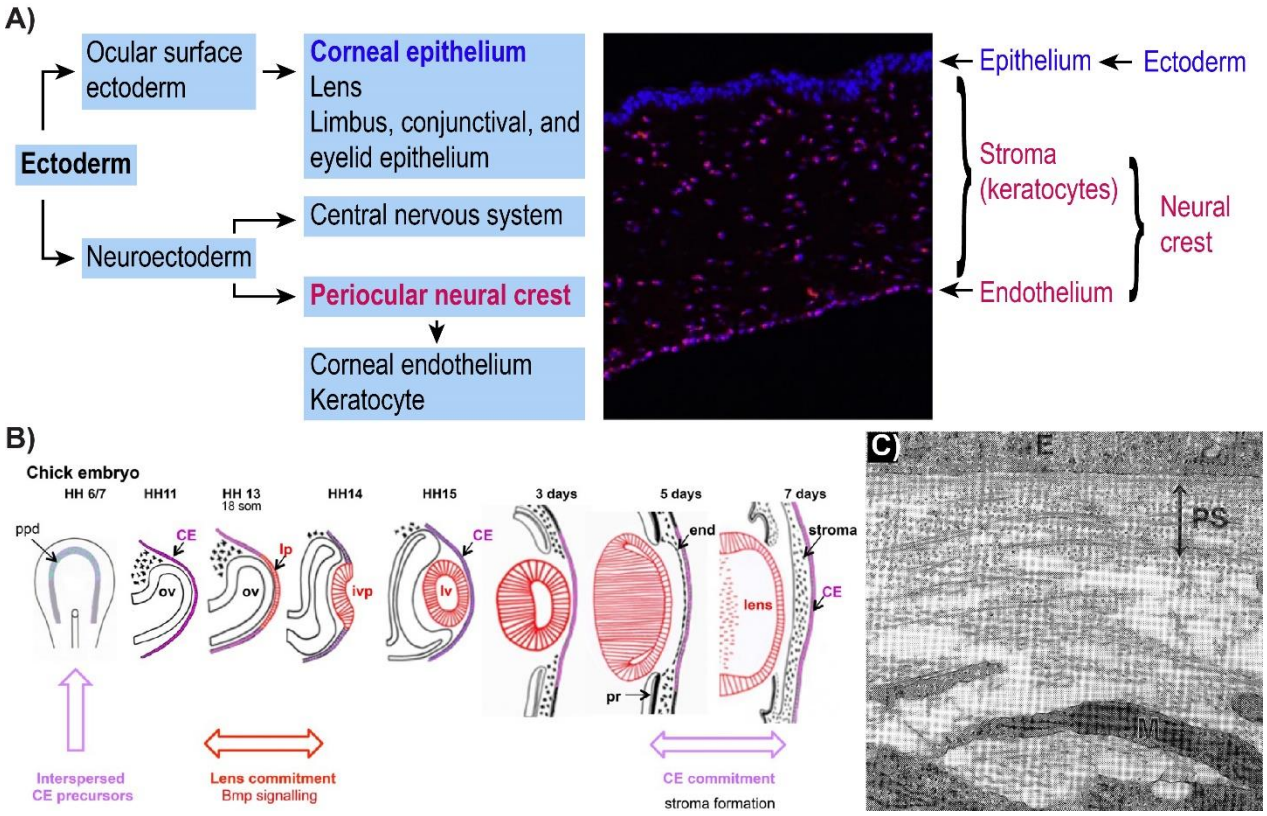

Figure 5.1. Structure of the early embryonic chick cornea.

(A) Diagram of the derivatives of the cranial ectoderm and cross-section through the cornea showing the epithelium, keratocytes, and endothelium. Reprinted from Lwigale, 2015[136], with permission from Elsevier. (B) Development of the chick corneal epithelium starting at the Hamburger and Hamilton (HH) stage6/7 to commitment cornea at embryonic day 7 (E7). Corneal endothelium (CE), invagination lens placode (ilp), endothelium (end), lens (le), lens vesicle (lv), optic vesicle (ov), pigmented retina (pr). Reprinted and modified from Dhouailly, et al. 2014[38], with permission from John Wiley and Sons. (C) Ultrastructure of the chick cornea stroma showing the basal epithelium (E), primary stroma (PS), and secondary stroma with an invading mesenchymal cell (M). Reprinted from Quantock and Young, 2008[177], with permission from John Wiley and Sons.

5.2.3. Types of Corneal Bioreactors

Note: for this text, the model is the combination of biological and biomedical components that made up the tissue, e.g., cells, extracellular components, engineered constructs, while the bioreactor is the system that provides an external stimulus to the model.

The cornea, from a bioreactor design point of view, appears to be simpler than other organs. The main characteristics include static pressure in the form of the intraocular pressure that ranges between 10 to 20 mmHg, a liquid-air interface found for the epithelium, and a liquid interface adjacent to the endothelium. Therefore, major considerations to fabricate a corneal bioreactor include (1) creating two distinct chambers for the epithelium and the endothelium, (2) biocompatibility of glues used to bind the different parts of the reactor, (3) maintain a supply of fresh medium and (4) pressure or strain mimicking the intraocular pressure[131,202].

A corneal bioreactor can be used to extend the long-term survival of donor corneas by preventing stromal swelling and Descemet membrane folding[202]. It can also be used to mimic in vivo conditions and provide insight into potential therapeutic approaches using in-vitro or ex-vivo corneal models. For example, Siran, et al., 2018, developed a bioreactor where a neural-innervated 3D corneal epithelium and stroma tissue model[209] could be grown in an environment mimicking the intraocular pressure and tear flow[193]. Here, the model is exposed to capsaicin, an irritant known to stimulate nociceptive neurons and induce pain.

Lastly, corneal bioreactors have been used to understand corneal fibroblast, as a proxy to keratocyte,[131,228], and endothelial cell behavior during development[199]. For

example, in work by Li, et al., 2017, Anney, et al., 2021., and Thériault, et al., 2019, highlights the importance of pressure in strengthening the formation of tight junctions in endothelial cells[6,133,199].

However, there is a gap in knowledge on how the unique architecture of the stroma forms during development. Here, I developed the principles behind a bioreactor for the engineered stroma models I developed in Chapter 3 that can mimic the intraocular pressure. Corneal stroma stem cells (CSSC) are a specialized group of mesenchymal cells located in the anterior limbal region of the human stroma [45,171]. In Chapter 3, I demonstrate that CSSC can assemble a stroma model expressing keratocyte-like genes and produce relevant ECM proteins. Current results suggest that CSSC could continue to assemble highly aligned, rotating cell layers past the cell bilayer shown in Chapter 3.

5.3. Materials and Methods

5.3.1. Fabrication of COLI Gels and Transferring of Fibronectin Features

Compressed COLI gels with FN lines were fabricated as previously described (section 3.3.2). Briefly, a 6 mg/mL COLI solution was prepared as manufacturer's protocol (BD Biosciences). A silicone ring of 20 mm diameter was placed over a glass coverslip and 200 µL of the COLI solution pipetted inside. The gel was placed inside a humidified incubator at 37°C for three hours to allow gel compression. After gelation, the silicone ring was removed, the COLI gel was rinsed with deionized water three times and then dried in a cell culture hood.

FN (Corning) protein was fluorescently labeled with AlexaFluor 555 SE tag (Thermo Fisher) according to the manufacturer's protocol. First, 30 by 30 µm FN were microcontact printed on a poly(N-isopropyl acrylamide) (PIPAAm, mixed 2% w/v in butanol, Scientific Polymer Products) coated coverslip. Next, 20% gelatin type A (Thermo Fisher) gels were prepared by pipetting 200 µL of gelatin solution warmed to 60°C on a 20 mm diameter silicone ring on a microscope slide. This was then followed by a 10-minute incubation at room temperature and the removal of the silicone ring. The coverslips prepared previously were placed ECM-side down over the gelatin gels and immersed in distilled water at room temperature to dissolve the PIPAAm and transfer the protein lines onto the gelatin. The gelatin was peeled off the microscope slide and placed protein-side down onto the compressed COLI. The completed COLI + FN lines constructs were then incubated in a humidified incubator at 37°C for 45 minutes, rinsed with warm 1xPBS thrice, and incubated again for 45 minutes to remove any residual gelatin. These were then dried in a biosafety hood and stored at room temperature.

5.3.2. Suspension of COLI Gels and Corneal Stroma Single Sheet on CellCrown

The COLI + FN lines constructs were mounted on a CellCorwn 24NX (Scaffdex) insert with the FN lines facing down. Briefly, the construct was submerged in 1xPBS and then peeled off the coverslip. Note that the COLI construct was peeled off such that the FN lines are facing down. Carefully, the construct was “fished out” using the CellCrown insert, and moved such that the FN lines are centered and taught. Finally, the construct is locked in place as manufacturers protocol. The mounted constructs were then sterilized in UV light for 15 minutes and rinsed with sterile PBS three times. The constructs were stored in PBS in an incubator for up to 48 hours before seeding.

5.3.3. Seeding and Culture of Corneal Stroma Stem Cells

Isolation of CSSC was performed as previously described [13,45,197]. Briefly, cornea-scleral tissues from human donors younger than 60 years with <5 days of preservation were obtained from the Center for Organ Recovery and Education (www.core.org), after the center corneal tissue had been removed for transplantation. The rims were rinsed, and the remaining endothelial cell layer, Descemet’s membrane, conjunctiva, and trabecular meshwork were removed. The limbal tissue was dissected, cut into 3 mm fragments, and digested overnight in 0.5 mg/mL collagenase L solution at 37°C. Fractions were pipetted and further digested for 30 to 45 minutes. The remaining digest was filtered through a cell strainer, and the cells were centrifuged at 1500 rpm for 5 minutes. The resulting CSSC were plated onto a 25 cm^2 tissue culture flask in stem cell growth medium (GM) containing 2% (v/v) fetal bovine serum, Dulbecco’s Modified Eagle Medium-LowGlucose-GlutaMax (Gibco), 400 mg/L MCDB-201 (Sigma Aldrich),

1mg/mL of AlbuMax Lipid-Rich BSA (Gibco), 0.1 mM L-ascorbic acid-2-phosphate (Sigma Aldrich), 0.1X insulin-transferring-selenium (Gibco), 10 ng/mL recombinant rat platelet-derived growth factor-BB protein (R&D Systems), 10 ng/mL recombinant human epidermal growth factor (R&D Systems), 100 nM dexamethasone (Sigma Aldrich), 1x penicillin-streptomycin 100x (Corning CellGro), and 1:1000 gentamycin (50 mg/mL) (Gibco) (Table 3.1). CSSC were expanded using TrypLe (Thermo Fisher) and passaged at ~1000 cells/cm^2. COLI scaffolds were seeded with CSSC derived from a single donor cornea at passage 2-5.

CSSC were seeded at 50,000 cells/cm^2 by diluting 50,000 cells in 100 µL and dispensing on the FN-side of the construct. CSSC were cultured in GM until confluency, and then the culture medium was switched to a keratocyte differentiation medium (KDM) containing advanced Dulbecco's Modified Eagle Medium (Gibco) with 1 mM L-ascorbate acid-2-phosphate (Sigma Aldrich), 10 ng/mL recombinant human fibroblast growth factor 2 (Cell Sciences), and 0.1 ng/mL recombinant human transforming growth factor β3 (R&D Systems) (Table 3.2; Fig. 3.2). KDM was replaced every 2 days for 10 days. The alignment of CSSC was calculated at the day of confluency and at the end of the differentiation.

5.3.4. Immunostaining and Microscopy

Samples were rinsed with 1xPBS, and then fixed with 4% paraformaldehyde in 1xPBS for 12 minutes and washed for 5 minutes with 1xPBS thrice. Samples were incubated in diamidino-2-phenylindole (DAPI, Thermo Fisher) to stain nuclei, and Phalloidin 488 (1:200 in 1% bovine serum albumin in 1xPBS, Thermo Fisher) to stain actin filaments for 1 hour. Samples were washed for 5 minutes with 1xPBS thrice again

and mounted on microscope glass slides with Prolong Anti-Fade (Life Technologies). Mounted samples were imaged on a Zeiss LSM 700 confocal microscope.

5.3.5. Orientational Order Parameter as a Measure of Alignment

The alignment was quantified by finding the largest eigenvalue of the orientational order tensor, defined as the 2D orientational order parameter (OOP) [81]. Actin alignment for all samples at D10-KDM was measured using a custom MATLAB (MathWorks) algorithm that calculates the OOP of the given image were 0 meaning isotropy and 1 perfect alignment, as in previously published methods [61]. To quantify the OOP, samples were imaged on the Zeiss LSM 700 confocal; 9 images per sample and 9 samples per condition.

5.4. Results

5.4.1. Effects of Strain on CSSC Alignment

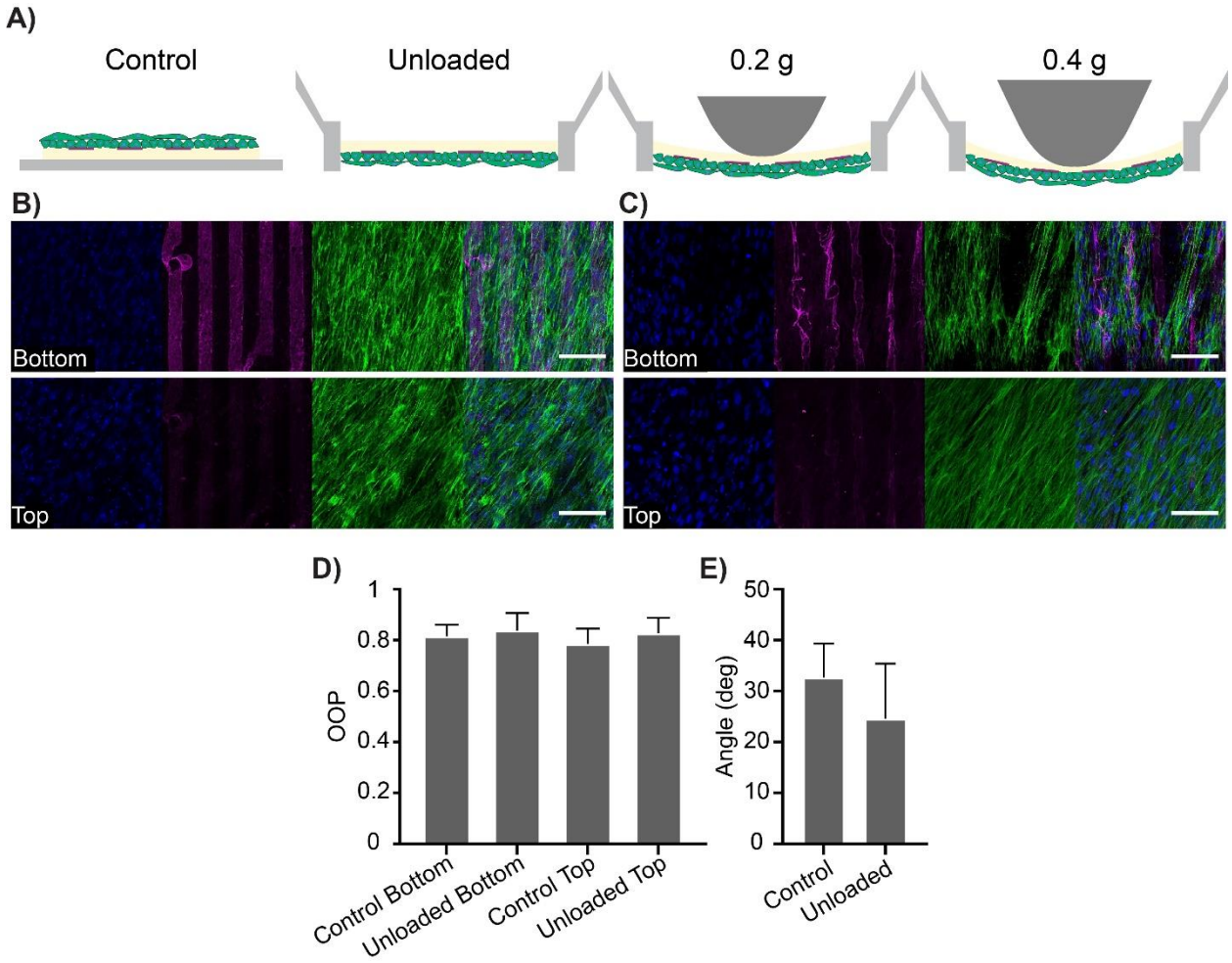

Figure 5.2. Alignment of CSSC to Different Indentation Weights

(A) Schematic of the different groups tested. In the control group, CSSC were cultured over a COLI+FN lines construct over a glass coverslip. In the unloaded group, CSSC were cultured over a COLI+FN lines construct mounted to a CellCrown insert. Note that for all groups mounted to the insert, CSSC were seeded on the underside of the gel. Fluorescent staining of the bottom and top cell layers for the control (B) and unloaded (C) groups. (D) The OOP for each cell layer. The scale bar is 100 µm. (E) The angle difference between the bottom and top cell layers for each group.

CSSC were cultured on COLI+FN lines construct, on a coverslip (control), and on

the underside of a COLI+FN lines constructs mounted to a CellCrown insert (unloaded). On both groups, CSSC formed a cell bilayer with highly aligned and rotated cells. Assessment of the actin cytoskeleton for both groups showed that for both groups the bottom and top cell bilayers are made of highly aligned CSSC, demonstrated by a high OOP (Fig. 5.3B-D). Also, the angle of rotation between the bottom and top cell layers was 32.70 $\pm$ 6.64 and 24.56 $\pm$ 10.84 degrees for the control and unloaded groups, respectively. No significant difference was found in OOP between the groups nor between the cell layers, and no significant difference in the rotational angle was found between the groups.

Interestingly, a construct was found to have three distinct CSSC layers in the unloaded group (Fig. 5.3). These layers had a slight clockwise rotation that went from being parallel to the FN lines to 90° clockwise on the last, third cell layer. This cell tri-layer was not observed in any of the control groups, nor any of the samples in Chapter 2, and only on a few (<25%) of the unloaded samples. This effect can be either a cause from the COLI construct being suspended or from uneven seeding on the unloaded samples that caused the cells to collect on one side of the COLI gel.

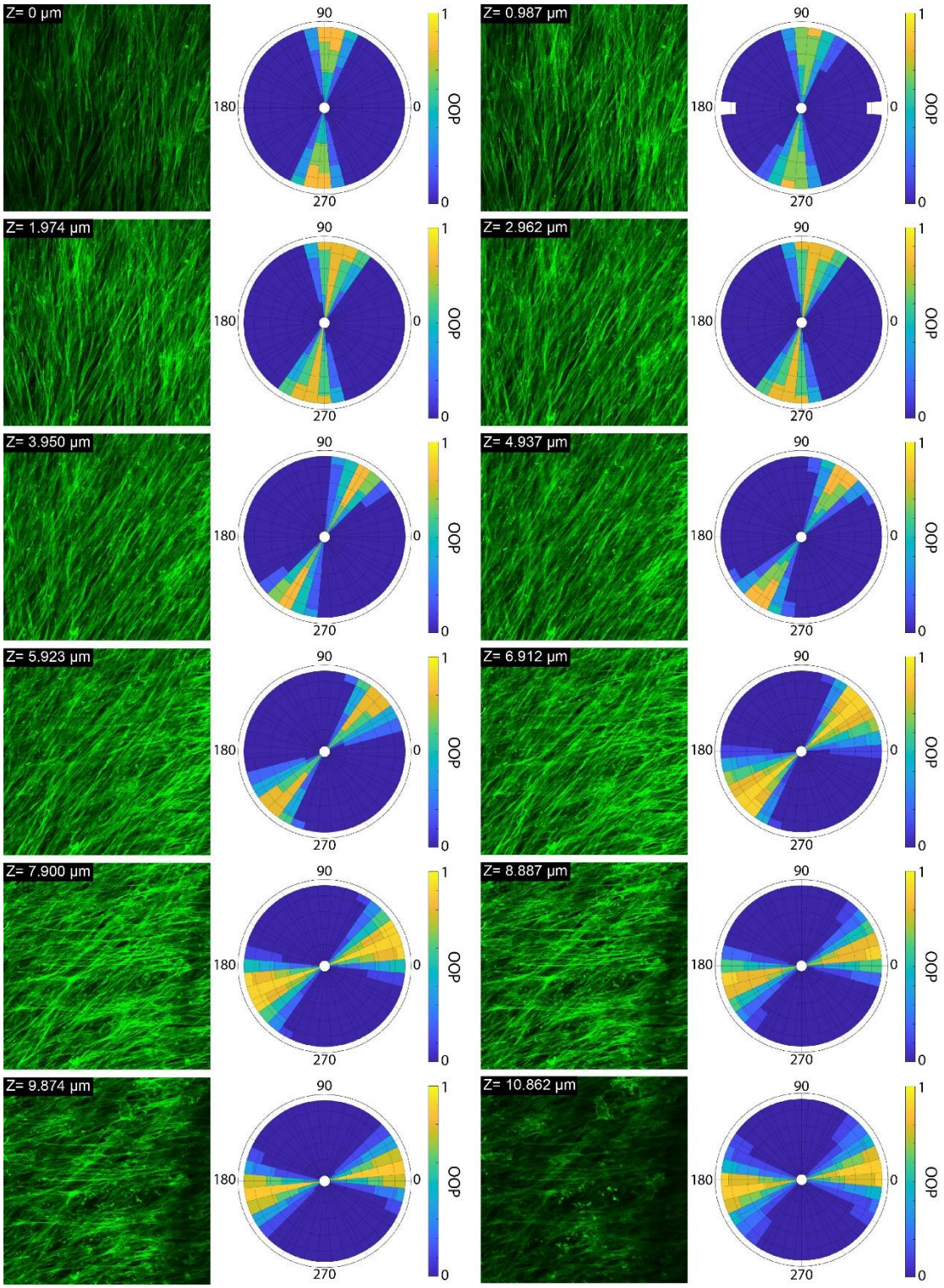

Figure 5.3. CSSC formed three rotating cell layers.

Fluorescent imaging of actin cytoskeleton of CSSC at different heights in the cell layers. A rose plot is shown along with the image. The scale bar is 100 µm

5.5. Discussion and Future Directions

5.5.1. Characterization of Mechanical Properties of the COLI gel and Constructs.

COLI can be characterized by indentation using PDMS weights. The weights can be shaped into a cone and placed over the mounted COLI gels. Note, the COLI will be submerged in 1xPBS. The deformation of the gel can be measured 1 hour, 24 hours, 3 days, and 7 days after placement of the PDMS weight to measure the viscoelastic behavior of the gels. Using the know parameters of the system (Fig. 5.4A.) the COLI can be characterized as described in Ahearne, et al 2005[2]. Reflectance microscopy on an inverse microscope can be used to observe the deformation of the (Fig. 5.4B-C).

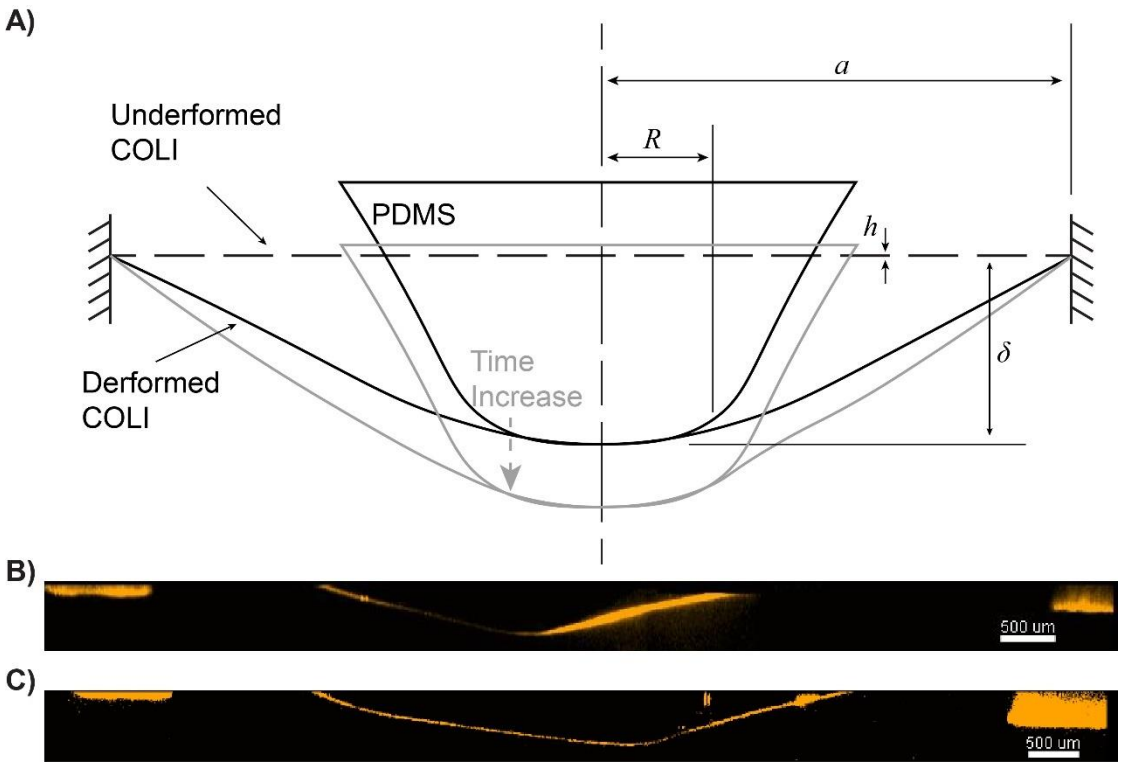

Figure 5.4. Indentation of COLI by PDMS cone.
Schematic (A) and actual indentation of mounted COLI gel on a CellCrown indent with 0.2 (B) and 0.4 g (C) PDMS weight.

Changes in the mechanical properties of the construct as the CSSC differentiated and assembled a COLI matrix will be assessed similarly. The CSSC will be seeded on mounted COLI gel and grown to confluency. PDMS weights will be placed over the constructs on the same day of medium change to KDM. The COLI gel will be imaged at 1 hour, 24 hours, 3 days, 7 days, and 10 days after placement of the PDMS weights. Much like above, the viscoelastic properties will be measured and calculated.

5.5.2. CSSC-assembled ECM under various strain conditions.

The consensus of corneal stroma development is that a primary stroma is synthesized by the cornea epithelium and neural crests cells migrate and deposit a secondary stroma after differentiation into keratocytes[87,88]. Also, studies by Coulombre and Coulombre, 1958, investigating the role of intraocular pressure in the development of the corneal curvature suggested that corneal curvature and growth are dominated by the intraocular pressure in the eye[32,33]. Furthermore, experiments reducing the intraocular pressure in developing chick corneas also affect the rate of neural crest migration and suggest that the assembly of the secondary stroma is affected by the growth of the cornea[15]. Recent studies in ex-vivo embryonic chick corneas further emphasize the role of neural crest keratocytes in the assembly of an intricate collagen-rich ECM and the assembly of the secondary stroma[227]. However, the relationship between interocular pressure and keratocyte biology and collagen assembly has been not studied extensively. Work by Koudouna, et al., 2018, suggests that keratocytes in the embryonic cornea control stromal organization through a mechanism not regulated by the intraocular pressure[122].

The main objective of this bioreactor is to identify the relationship between ECM

assembly, specifically the cell-assembled bilayer, and strain in an engineered stroma model. Here, CSSC will be grown to confluency on the mounted COLI gels as described in section 5.3.3. Then, a mechanical load using PDMS weights will be placed on the mounted COLI construct on the same day of the medium change to KDM. After 10 days of culture, the construct will be fixed, ECM stained, cell alignment assessed, and gene expression measured.

5.5.3. Improvements to the corneal bioreactor

The major limitation of the bioreactor used here is the mechanism of introducing strain into the system. There can be several limitations as well as unknowns to using the PDMS weight. For instance, there is variance between the masses, though I tried to maintain the standard deviation between the weight below 5%. Furthermore, some of the assumptions of the viscoelastic model used in Ahearne, et al. 2005, are violated by the PDMS weight.

The first major improvement in the bioreactor would be to induce strain via hydrostatic pressure. Bioreactors such as Boyce, et al. 2008[19] (Fig. 5.5A), and Thériault, et al. 2019[199] (Fig. 5.5B), use a sealed chamber that allows for controlled filling with medium and induce a known amount of pressure to the tissue. However, both are design for ex-vivo corneas and a bioreactor design for my engineered construct needs to be developed. I propose to build individual bioreactors that can accommodate CellCrown inserts. The pressure-induced on the engineered stroma construct would be controlled by the medium intake, pushing the stroma to construct outward in a fashion similar to the native cornea. Furthermore, work done by Nguyen and Boyce, 2011 can be expanded to determine the mechanical parameters of the stroma construct[155].

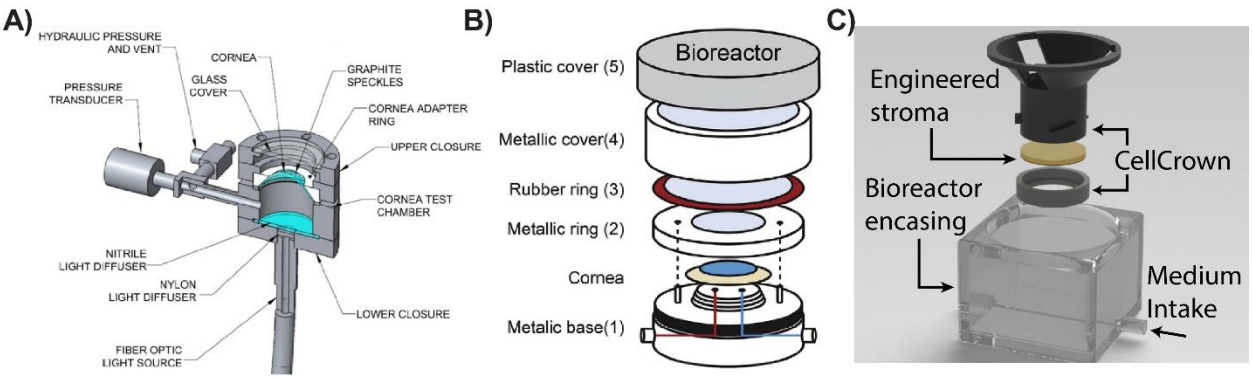

Figure 5.5. Schematic of bioreactors for ex vivo corneas and engineered cornea.
(A) Schematic of the cornea inflation bioreactor. Reprinted from Boyce, et al.[19] with permission from Elsevier. (B) Schematic of corneal bioreactor. Reprinted from Thériault, et al.[199] with permission from Elsevier. (C) Schematic of proposed bioreactor for engineered corneal stroma.

Chapter 6: Conclusions and Future Directions

6.1. Conclusions

The unique and intricate ECM architecture of the cornea allows for light transmittance where there is none. Disruption to this unique ECM causes opacities and refractive errors that can manifest into blindness. Transplantation of the donor whole cornea or partial transplantation selective layers of the cornea can restore vision. However, there is a shortage of transplantable donor tissue. Various engineering techniques using silk[37,73–75,110,111,138,144,208,209,223,232], the amniotic membrane[44,47,54,59,115,120,160,184,185,206,217,229,234,236], and decellularized tissue/ECM[3,77,82,94,113,114,160,165] have been used to fabricate corneal scaffolds with the potential for transplantation and study corneal cell behavior.

Here, I combine different engineering approaches to manipulate proteins found in the native cornea with the expertise in culturing corneal stroma stem cells from the Funderburgh Lab to engineer corneal stroma and posterior cornea tissues towards application in corneal transplantation. In Chapter 3 I built a highly aligned stromal scaffold that can be stacked into a multilayered scaffold. In Chapter 4, I stacked an engineered endothelium with the stroma scaffold to make an engineered posterior cornea (EPC) and integrated the EPC into an ex-vivo rabbit cornea. Finally, in Chapter 5, I designed a bioreactor that harbors the various engineered tissue developed before to better understand stromal ECM assembly.

In Chapter 3, surface-modified COLI gels were used to generate single-corneal stroma sheets (single-sheets) that can be easily stacked and handled without altering cell organization. I show that micropatterned FN and LAM lines on COLI scaffolds can

serve as an early guide for CSSC alignment and that this alignment guides assembly of a stromal-like ECM from differentiated keratocytes. CSSC-derived keratocytes expressed keratocan and assembled COLI and COLV, both found in the native stroma. Engineered stroma sheets and multilayered constructs were robust and capable of being handled, rolled, unrolled, and further stacked without tearing the constructs. These results make animal in-vivo studies and further understanding of the self-rotating assembled ECM possible next steps.

In Chapter 4, I expanded on the stacking platform used in Chapter 3 to bring about the duo- and quad-stack stroma by integrating an engineered endothelium to stromal constructs of various thicknesses. The presence of tight junctions and regular cobblestone organization of the endothelium suggests that healthy endothelial cells were present and integrated with the various stroma constructs. An EPC, composed of the engineered endothelium and a single-sheet stroma, was transplanted onto an ex-vivo rabbit cornea and successfully integrated with the rabbit stroma tissue. It will be important to further characterize the co-culture conditions, in the form of a co-culture maintenance medium, that optimize a functional endothelium and healthy differentiated keratocytes. Taken together, the platform presented in Chapter 4 serves as proof of concept for engineered tissues suitable for DSEAK and DMEK procedures and a launchpad for the development of a whole cornea engineered construct.

In Chapter 5, I put into context the benefits and challenges of building a corneal bioreactor. The bioreactor needs to (1) creating two distinct chambers for the epithelium and the endothelium, (2) biocompatibility of glues or methods used to bind the different parts of the reactor, (3) maintain a supply of fresh medium and (4) pressure or strain

mimicking the intraocular pressure[131,202]. I developed the principles behind a bioreactor with the potential to mimic the intraocular pressure for the engineered stroma models I developed in Chapter 3. I used a CellCrown insert to mount and suspend the stromal construct and propose placing a PDMS weight to put pressure on the mounted construct. Current results suggest no difference in alignment or cell bilayer formation between a control sample and samples mounted onto the CellCrown without any load. However, and interestingly, 3 highly aligned and rotated cell layers was observed on some of the unloaded samples. These initial results support the need for a better understanding between stromal ECM organization and intraocular pressure. Lastly, an improved design for the bioreactor based on hydrostatic pressure is presented.

Taken together, this thesis provides an engineering approach to build corneal stroma and posterior cornea tissues towards application in corneal transplantation (Fig. 6.1.).

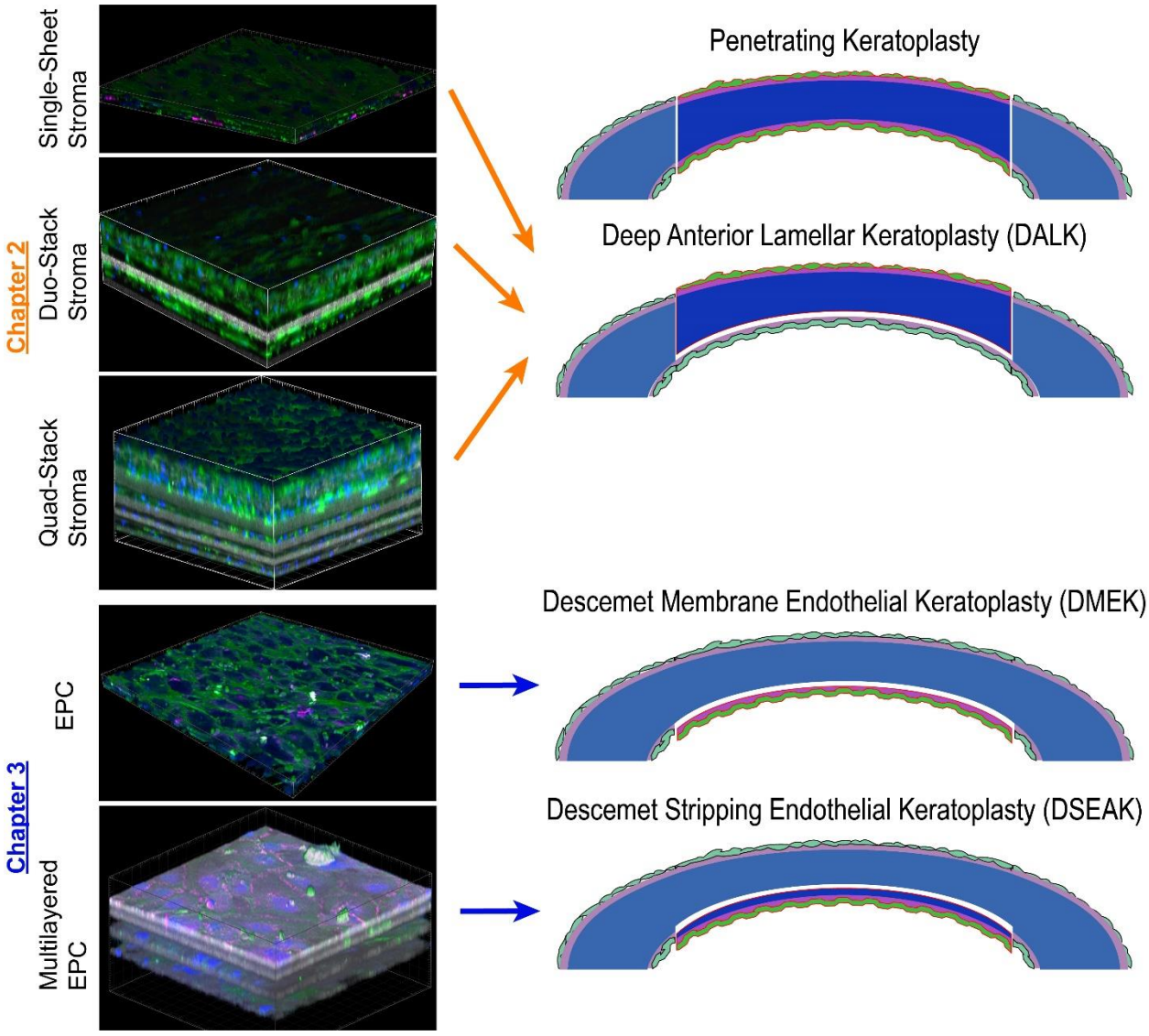

Figure 6.1. Proposed Transplantation Procedures for the Various Engineered Corneal Scaffolds Developed Throughout this Thesis.

6.2. Future directions

6.2.1. Generation of thicker multilayered corneal stroma constructs

In Chapter 3, I generated multi-layered stroma-like constructs of up to 90 µm in thickness. However, to target a wider array of transplantation procedures, including whole penetrating cornea, thicker stromal constructs will be needed. This can be accomplished by 1) increasing the number of CSSC-assembled layers and collagen synthesis in each single sheet stroma and 2) stacking up to 16 of these individual single sheets. To accomplish the first goal, I suggest taking advantage of the upregulation and assembly of corneal collagen by CSSC through the process of differentiation. FGF2 and TGFß-3 each increase the expression of cornea-specific ECM and the combination of the two of these factors, as is the case of the keratocyte differentiation medium (KDM), is synergistic to the generation of stroma-like tissue[221]. The presence of TGFß3 induces the production of non-fibrotic ECM production[93,157,176,213] and it stimulates differentiation of adult stem cells [11,102]. TGFß3, in combination with FGF2, stimulates chondrogenesis in hypoxic conditions[156,233]. HIF1-alpha induced by hypoxia, upregulates collagen crosslinking via lysyloxidases, lysylhydroxylases, and prolylhydroxylase domain enzymes[76,140,207]. I suggest examining how FGF2 and TGFß3 concentration and reduced oxygen increase the volume of the stroma-like ECM produced by CSSC-derived keratocytes on the sheets.

Similarly, a thicker construct can be using a multilayered stacking approach. Briefly, the bioengineered stromal sheets can be stacked into an 8-layered construct by generating two quad-stacks, while a 16-layered construct will be generated by stacking two 8-layered constructs. Although, the strength of adhesion between the stacks has

not been tested; however, my work shows that multi-layered stacks can be handled, rolled, and unrolled without damaging the cells or construct integrity.

6.2.2. Evaluation of the multilayered cornea stroma in a DALK procedure

The results from Chapter 3 suggest that multilayered stroma constructs, and to some extent, the single-sheet stroma can be handled and tested for transplantability. Deep anterior lamellar keratoplasty (DALK) is a partial-thickness transplantation procedure that involves only the stroma. If the patient has a functional endothelium and does not suffer from limbal stem cell deficiency, DALK can be an effective option to treat diseases and pathologies in the anterior cornea[180]. Alkali burn rabbit models are excellent surrogate pathology for DALK procedures because it causes extensive damage to the cornea stroma and epithelial layer and results in permanent visual impairment. I recommend transplanting, via DALK, a bioengineered multi-layered stroma and as a control an acellular collagen gel, each of equivalent thickness of ~20 to 80 µm. Follow-up of the construct and host cornea can be made by measuring the corneal thickness, light scatter, and cellularity using a Nidek Confoscan 3 corneal confocal microscopy[43] and ocular optical coherence tomography (OCT)[46]. These instruments generate noninvasive 3-D images of the cells and light scatter of the tissue providing both qualitative and quantitative analysis of the corneal transparency[46,84,112]. While the refractive power of the cornea will be examined using a corneal refractometer. Upon removal rabbit eyes transparency, corneal thickness, and refraction will be assessed as described above, as will histological sectioning of the tissue and gene expression of keratocytes.

6.2.3. Evaluation of the EPC in a rabbit model in a DSEK procedure

Between both Chapter 3 and Chapter 4, the results suggest that I can bioengineer the stroma (Chapter 3), endothelium[161], and I can combine these into an EPC that can integrate into a rabbit ex-vivo cornea. Descemet stripping endothelial Keratoplasty (DSEK) is a partial transplantation procedure of the posterior layers of the cornea (Descemet membrane and the endothelium) and the posterior stroma[174]. I recommend combining the multi-layered stroma and endothelium into a ~100 µm thick and assess surgical handling and function grafting into an ex vivo rabbit cornea and allow for at least 2 weeks of culture. Two weeks of ex vivo culture is appropriate based on published ex vivo models[23] and 3D in vitro models[73,144]. Next, I recommend an in vivo rabbit model where the endothelium and Descemet membrane will be removed and replaced via DSEK with an EPC, collagen gel (control), or no graft (control); non-treated controls will be the contralateral eyes. To assess the integration of the construct, I recommend assessing transplantation, transparency, corneal thickness, refraction, histology sectioning, and gene expression 1 week and 4 weeks after DMEK.

References

1. Agarwal, S., J. H. Wendorff, and A. Greiner. Progress in the Field of Electrospinning for Tissue Engineering Applications. *Adv. Mater.* 21:3343–3351, 2009.
2. Ahearne, M., Y. Yang, A. J. El Haj, K. Y. Then, and K.-K. Liu. Characterizing the viscoelastic properties of thin hydrogel-based constructs for tissue engineering applications. *J. R. Soc. Interface* 2:455–463, 2005.
3. Alió del Barrio, J. L., M. El Zarif, A. Azaar, N. Makdissy, C. Khalil, W. Harb, I. El Achkar, Z. A. Jawad, M. P. de Miguel, and J. L. Alió. Corneal Stroma Enhancement With Decellularized Stromal Laminas With or Without Stem Cell Recellularization for Advanced Keratoconus. *Am. J. Ophthalmol.* 186:47–58, 2018.
4. Altomare, L., M. Riehle, N. Gadegaard, M. Tanzi, and S. Farè. Microcontact Printing of Fibronectin on a Biodegradable Polymeric Surface for Skeletal Muscle Cell Orientation. *Int. J. Artif. Organs* 33:535–543, 2010.
5. Amano, S., S. Yamagami, T. Mimura, S. Uchida, and S. Yokoo. Corneal Stromal and Endothelial Cell Precursors. *Cornea* 25:S73–S77, 2006.
6. Anney, P., M. Thériault, and S. Proulx. Hydrodynamic forces influence the gene transcription of mechanosensitive intercellular junction associated genes in corneal endothelial cells. *Exp. Eye Res.* 206:108532, 2021.
7. Anshu, A., M. O. Price, and F. W. Price. Descemet's Stripping Endothelial Keratoplasty: Long-term Graft Survival and Risk Factors for Failure in Eyes with Preexisting Glaucoma. *Ophthalmology* 119:1982–1987, 2012.
8. Anwar, M., and K. D. Teichmann. Big-bubble technique to bare Descemet's membrane in anterior lamellar keratoplasty. *J. Cataract Refract. Surg.* 28:398–403, 2002.
9. Aristotle. On the Soul (350 BCE)
10. Barry, P. A., W. M. Petroll, P. M. Andrews, H. D. Cavanagh, and J. V Jester. The Spatial Organization of Corneal Endothelial Cytoskeletal Proteins and Their Relationship to the Apical Junctional Complex. *Investig. Opthalmology Vis. Sci.* 36:, 1995.
11. Barsby, T., and D. Guest. Transforming growth factor beta3 promotes tendon differentiation of equine embryo-derived stem cells. *Tissue Eng. Part A* 19:2156–65, 2013.
12. Bartakova, A., K. Alvarez-Delfin, A. D. Weisman, E. Salero, G. A. Raffa, R. M. Merkhofer, N. J. Kunzevitzky, and J. L. Goldberg. Novel Identity and Functional Markers for Human Corneal Endothelial Cells. *Investig. Opthalmology Vis. Sci.* 57:2749, 2016.
13. Basu, S., A. J. Hertsenberg, M. L. Funderburgh, M. K. Burrow, M. M. Mann, Y. Du, K. L. Lathrop, F. N. Syed-Picard, S. M. Adams, D. E. Birk, and J. L. Funderburgh. Human limbal biopsy-derived stromal stem cells prevent corneal scarring. *Sci. Transl. Med.* 6:266ra172-266ra172, 2014.
14. Baydoun, L., I. Dapena, and G. Melles. Current Treatment Options for Fuchs Endothelial Dystrophy. Cham: Springer International Publishing, 2017, 73–85 pp.doi:10.1007/978-3-319-43021-8
15. Bee, J. A., and S. M. Roche. Reducing intraocular pressure by intubation elicits precocious development and innervation of the embryonic chick cornea. *Invest. Ophthalmol. Vis. Sci.* 33:3469–78, 1992.
16. Bigger, S. An inquiry into the possibility of transplanting the corean with a view to relieving blindness. *Dublin J. Med. Sci.* 11:408–417, 1837.
17. Birk, D. E., J. M. Fitch, J. P. Babiarz, K. J. Doane, and T. F. Linsenmayer. Collagen fibrillogenesis in vitro: interaction of types I and V collagen regulates fibril diameter. *J. Cell Sci.* 95:649–657, 1990.
18. Bourne, W. M. Clinical estimation of corneal endothelial pump function. *Trans. Am. Ophthalmol. Soc.* 96:229–39; discussion 239-42, 1998.

19. Boyce, B. L., J. M. Grazier, R. E. Jones, and T. D. Nguyen. Full-field deformation of bovine cornea under constrained inflation conditions. *Biomaterials* 29:3896–3904, 2008.
20. Brown, R. A., M. Wiseman, C.-B. Chuo, U. Cheema, and S. N. Nazhat. Ultrarapid Engineering of Biomimetic Materials and Tissues: Fabrication of Nano- and Microstructures by Plastic Compression. *Adv. Funct. Mater.* 15:1762–1770, 2005.
21. Chae, J. J., W. McIntosh Ambrose, F. A. Espinoza, D. G. Mulreany, S. Ng, T. Takezawa, M. M. Trexler, O. D. Schein, R. S. Chuck, and J. H. Elisseeff. Regeneration of corneal epithelium utilizing a collagen vitrigel membrane in rabbit models for corneal stromal wound and limbal stem cell deficiency. *Acta Ophthalmol.* 93:e57–e66, 2015.
22. Chan, B. P., and K. W. Leong. Scaffolding in tissue engineering: general approaches and tissue-specific considerations. *Eur. Spine J.* 17:467–479, 2008.
23. Chen, K.-H. M. D., D. M. D. Azar, and N. C. Joyce. Transplantation of Adult Human Corneal Endothelium Ex Vivo: A Morphologic Study. *Cornea* 20:731–737, 2001.
24. Chen, S., Q. Zhu, H. Sun, Y. Zhang, S. Tighe, L. Xu, and Y. Zhu. Advances in culture, expansion and mechanistic studies of corneal endothelial cells: A systematic review. *J. Biomed. Sci.* 26:1–7, 2019.
25. Chirila, T. V, M. Chirila, Y. Ikada, H. Eguhi, and H. Shiota. A historical review of artificial cornea research in Japan. *Jpn. J. Ophthalmol.* 49:S1-13, 2005.
26. Chirila, T. V, and C. R. Hicks. The origins of the artificial cornea: Pellier de Quengsy and his contribution to the modern concept of keratoprosthesis. *Gesnerus* 56:96–106, 1999.
27. Choi, H. J., M. K. Kim, H. J. Lee, S. H. Jeong, H. J. Kang, C.-S. Park, C.-G. Park, S. Joon Kim, and W. R. Wee. Effect of αGal on corneal xenotransplantation in a mouse model. *Xenotransplantation* 18:176–182, 2011.
28. Choi, Y. S., J. Y. Kim, W. R. Wee, and J. H. Lee. Effect of the Application of Human Amniotic Membrane on Rabbit Corneal Wound Healing After Excimer Laser Photorefractive Keratectomy. *Cornea* 17:389, 1998.
29. Claesson, M., and W. J. Armitage. Ten-Year Follow-up of Graft Survival and Visual Outcome After Penetrating Keratoplasty in Sweden. *Cornea* 28:1124–1129, 2009.
30. Comhair, S. A. A., W. Xu, L. Mavrakis, M. A. Aldred, K. Asosingh, and S. C. Erzurum. Human Primary Lung Endothelial Cells in Culture. *Am. J. Respir. Cell Mol. Biol.* 46:723–730, 2012.
31. Correia, A. C. P., J.-R. A. J. Moonen, M. G. L. Brinker, and G. Krenning. FGF2 inhibits endothelial–mesenchymal transition through microRNA-20a-mediated repression of canonical TGF-β signaling. *J. Cell Sci.* 129:569–579, 2016.
32. Coulombre, A. J. The role of intraocular pressure in the development of the chick eye. I. Control of eye size. *J. Exp. Zool.* 133:211–225, 1956.
33. Coulombre, A. J., and J. L. Coulombre. The Role of Intraocular Pressure in the Development of the Chick Eye. *AMA. Arch. Ophthalmol.* 59:502, 1958.
34. Crawford, A., D. Patel, and C. McGhee. A brief history of corneal transplantation: From ancient to modern. *Oman J. Ophthalmol.* 6:, 2013.
35. Danforth, D. N., and R. W. Hull. The microscopic anatomy of the fetal membranes with particular reference to the detailed structure of the amnion. *Am. J. Obstet. Gynecol.* 75:536–550, 1958.
36. Dawson, D. G., J. L. Ubels, and H. F. Edelhauser. Cornea and Sclera. Elsevier Mosby, 2011, 71–130 pp.
37. Deardorff, P. M., T. B. McKay, S. Wang, C. E. Ghezzi, D. M. Cairns, R. D. Abbott, J. L. Funderburgh, K. R. Kenyon, and D. L. Kaplan. Modeling Diabetic Corneal Neuropathy in a 3D In Vitro Cornea System. *Sci. Reports 2018 81* 8:17294, 2018.
38. Dhouailly, D., D. J. Pearton, and F. Michon. The vertebrate corneal epithelium: From early specification to constant renewal. *Dev. Dyn.* 243:1226–1241, 2014.
39. van Diks, K., L. Baydoun, R. M. Konder, and G. R. Melles. Contact Lenses After

Keratoplasty. *Contact Lens Spectr.* 29:36-38,40,42, 2014.
40. Doane, K. J., W.-H. Ting, J. S. McLaughlin, and D. E. Birk. Spatial and Temporal Variations in Extracellular Matrix of Periocular and Corneal Regions During Corneal Stromal Development. *Exp. Eye Res.* 62:285–292, 1996.
41. Donaghy, C. L., J. M. Vislisel, and M. A. Greiner. An Introduction to Corneal Transplantation. , 2015.at <http://eyerounds.org/tutorials/cornea-transplant-intro/index.htm#history>
42. Drubaix, I., J.-M. Legeais, N. Malek-Chehire, M. Savoldelli, M. Ménasche, L. Robert, G. Renard, and Y. Pouliquen. Collagen Synthesized in Fluorocarbon Polymer Implant in the Rabbit Cornea. *Exp. Eye Res.* 62:367–376, 1996.
43. Du, Y., E. C. Carlson, M. L. Funderburgh, D. E. Birk, E. Pearlman, N. Guo, W. W.-Y. Kao, and J. L. Funderburgh. Stem cell therapy restores transparency to defective murine corneas. *Stem Cells* 27:1635–42, 2009.
44. Du, Y., J. Chen, J. L. Funderburgh, X. Zhu, and L. Li. Functional reconstruction of rabbit corneal epithelium by human limbal cells cultured on amniotic membrane. *Mol. Vis.* 9:635–43, 2003.
45. Du, Y., M. L. Funderburgh, M. M. Mann, N. SundarRaj, and J. L. Funderburgh. Multipotent Stem Cells in Human Corneal Stroma. *Stem Cells* 23:1266–1275, 2005.
46. Du, Y., D. S. Roh, M. M. Mann, M. L. Funderburgh, J. L. Funderburgh, and J. S. Schuman. Multipotent stem cells from trabecular meshwork become phagocytic TM cells. *Invest. Ophthalmol. Vis. Sci.* 53:1566–75, 2012.
47. Dua, H. S., J. A. . Gomes, A. J. King, and V. S. Maharajan. The amniotic membrane in ophthalmology. *Surv. Ophthalmol.* 49:51–77, 2004.
48. Duffy, R. M., Y. Sun, and A. W. Feinberg. Understanding the Role of ECM Protein Composition and Geometric Micropatterning for Engineering Human Skeletal Muscle. *Ann. Biomed. Eng.* 44:2076–2089, 2016.
49. Dupps, W. J., and S. E. Wilson. Biomechanics and wound healing in the cornea. *Exp. Eye Res.* 83:709–720, 2006.
50. Elhalis, H., B. Azizi, and U. V. Jurkunas. Fuchs Endothelial Corneal Dystrophy. *Ocul. Surf.* 8:173–184, 2010.
51. Elsheikh, A., S. Ross, D. Alhasso, and P. Rama. Numerical Study of the Effect of Corneal Layered Structure on Ocular Biomechanics. *Curr. Eye Res.* 34:26–35, 2009.
52. Engelmann, K., J. Bednarz, and M. Valtink. Prospects for endothelial transplantation. *Exp. Eye Res.* 78:573–578, 2004.
53. Engler, A. J., S. Sen, H. L. Sweeney, and D. E. Discher. Matrix Elasticity Directs Stem Cell Lineage Specification. *Cell* 126:677–689, 2006.
54. Espana, E. M., H. He, T. Kawakita, M. A. Di Pascuale, V. K. Raju, C.-Y. Y. Liu, and S. C. G. G. Tseng. Human Keratocytes Cultured on Amniotic Membrane Stroma Preserve Morphology and Express Keratocan. *Investig. Opthalmology Vis. Sci.* 44:5136–5141, 2003.
55. Etheredge, L., B. P. Kane, N. Valkov, S. Adams, D. E. Birk, and J. R. Hassell. Enhanced cell accumulation and collagen processing by keratocytes cultured under agarose and in media containing IGF-I, TGF-β or PDGF. *Matrix Biol.* 29:519–24, 2010.
56. Eye Bank Association of America. 2016 Eye Banking Statistical Report. 2017.at <www.restoresight.org>
57. Eye Bank Association of America. 2020 Eye Banking Statistical Report. 2020.
58. Fagerholm, P., N. S. Lagali, J. A. Ong, K. Merrett, W. B. Jackson, J. W. Polarek, E. J. Suuronen, Y. Liu, I. Brunette, and M. Griffith. Stable corneal regeneration four years after implantation of a cell-free recombinant human collagen scaffold. *Biomaterials* 35:2420–2427, 2014.
59. Fan, J., M. Wang, and F. Zhong. Improvement of Amniotic Membrane Method for the

Treatment of Corneal Perforation. *Biomed Res. Int.* 2016:1–8, 2016.
60. Fattet, L., H.-Y. Jung, M. W. Matsumoto, B. E. Aubol, A. Kumar, J. A. Adams, A. C. Chen, R. L. Sah, A. J. Engler, E. B. Pasquale, and J. Yang. Matrix Rigidity Controls Epithelial-Mesenchymal Plasticity and Tumor Metastasis via a Mechanoresponsive EPHA2/LYN Complex. *Dev. Cell* 54:302-316.e7, 2020.
61. Feinberg, A. W., P. W. Alford, H. Jin, C. M. Ripplinger, A. A. Werdich, S. P. Sheehy, A. Grosberg, and K. K. Parker. Controlling the contractile strength of engineered cardiac muscle by hierarchal tissue architecture. *Biomaterials* 33:5732–5741, 2012.
62. Feinberg, A. W., and K. K. Parker. Surface-Initiated Assembly of Protein Nanofabrics. *Nano Lett.* 10:2184–2191, 2010.
63. Feneck, E. M., P. N. Lewis, J. Ralphs, and K. M. Meek. A comparative study of the elastic fibre system within the mouse and human cornea. *Exp. Eye Res.* 177:35–44, 2018.
64. Fernández-Pérez, J., P. W. Madden, and M. Ahearne. Engineering a corneal stromal equivalent using a novel multi-layered fabrication assembly technique. *Tissue Eng. Part A* 60:ten.TEA.2020.0019, 2020.
65. Flaxman, S. R. *et al.* Global causes of blindness and distance vision impairment 1990–2020: a systematic review and meta-analysis. *Lancet Glob. Heal.* 5:e1221–e1234, 2017.
66. Fontana, L., G. Parente, and G. Tassinari. Clinical outcomes after deep anterior lamellar keratoplasty using the big-bubble technique in patients with keratoconus. *Am. J. Ophthalmol.* 143:117–124, 2007.
67. Forrester, J. V., A. D. Dick, P. G. McMenamin, F. Roberts, and E. Pearlman. Biochemistry and cell biology. *Eye* 157-268.e4, 2016.doi:10.1016/b978-0-7020-5554-6.00004-6
68. Fratzl, P. Collagen: Structure and mechanics, an introduction. In: Collagen: Structure and Mechanics, edited by P. Fratzl. Springer, 2008, pp. 1–13.doi:10.1007/978-0-387-73906-9_1
69. Freegard, T. J. The Physical Basis of Transparency of the Normal Cornea. *R. Coll. Ophthalmol.* 44:465–471, 1997.
70. Funderburgh, J. L., M. M. Mann, and M. L. Funderburgh. Keratocyte Phenotype Mediates Proteoglycan Structure. *J. Biol. Chem.* 278:45629–45637, 2003.
71. Galen. Galen on the Usefulness of the Parts of the Body. Cornell University Press, 1968, 802 pp.
72. Garg, P., P. V. Krishna, A. K. Stratis, and U. Gopinathan. The value of corneal transplantation in reducing blindness. *Eye* 19:1106–1114, 2005.
73. Ghezzi, C. E., B. Marelli, F. G. Omenetto, J. L. Funderburgh, and D. L. Kaplan. 3D functional corneal stromal tissue equivalent based on corneal stromal stem cells and multi-layered silk film architecture. *PLoS One* 12:1–18, 2017.
74. Gil, E. S., B. B. Mandal, S.-H. Park, J. K. Marchant, F. G. Omenetto, and D. L. Kaplan. Helicoidal multi-lamellar features of RGD-functionalized silk biomaterials for corneal tissue engineering. *Biomaterials* 31:8953–8963, 2010.
75. Gil, E. S., S. H. Park, J. Marchant, F. Omenetto, and D. L. Kaplan. Response of human corneal fibroblasts on silk film surface patterns. *Macromol. Biosci.* 10:664–673, 2010.
76. Gilkes, D. M., S. Bajpai, P. Chaturvedi, D. Wirtz, and G. L. Semenza. Hypoxia-inducible factor 1 (HIF-1) promotes extracellular matrix remodeling under hypoxic conditions by inducing P4HA1, P4HA2, and PLOD2 expression in fibroblasts. *J. Biol. Chem.* 288:10819–29, 2013.
77. Gonzalez-Andrades, M., J. de la Cruz Cardona, A. M. Ionescu, A. Campos, M. del Mar Perez, and M. Alaminos. Generation of Bioengineered Corneas with Decellularized Xenografts and Human Keratocytes. *Investig. Opthalmology Vis. Sci.* 52:215, 2011.
78. Gorman, D. E., T. Wu, S. E. Gilpin, and H. C. Ott. A Fully Automated High-Throughput Bioreactor System for Lung Regeneration. *Tissue Eng. Part C Methods* 24:671–678,

2018.
79. Goweida, M. B., A. Abuelkheir, W. El-Menawy, and S. Mahmoud. Dynamics of Big Bubble Formation During Deep Anterior Lamellar Keratoplasty in Eyes with Advanced Keratoconus. *Clin. Ophthalmol.* Volume 14:4305–4310, 2020.
80. Griffith, M., E. I. Alarcon, and I. Brunette. Regenerative approaches for the cornea. *J. Intern. Med.* 280:276–286, 2016.
81. Hamley, I. Introduction to Soft Matter: Revised Edition Synthetic and Biological Self-Assembling. John Wiley & Sons, 2007, 328 pp.
82. Hashimoto, Y., S. Funamoto, S. Sasaki, J. Negishi, S. Hattori, T. Honda, T. Kimura, H. Kobayashi, and A. Kishida. Re-epithelialization and remodeling of decellularized corneal matrix in a rabbit corneal epithelial wound model. *Mater. Sci. Eng. C* 102:238–246, 2019.
83. Hassell, J. R., and D. E. Birk. The molecular basis of corneal transparency. *Exp. Eye Res.* 91:326–35, 2010.
84. Hatou, S., S. Yoshida, K. Higa, H. Miyashita, E. Inagaki, H. Okano, K. Tsubota, and S. Shimmura. Functional Corneal Endothelium Derived from Corneal Stroma Stem Cells of Neural Crest Origin by Retinoic Acid and Wnt/β-Catenin Signaling. *Stem Cells Dev.* 22:828–39, 2013.
85. Haustein, J. On the ultrastructure of the developing and adult mouse corneal stroma. *Anat. Embryol. (Berl).* 168:291–305, 1983.
86. Hay, E. D. Development of the Vertebrate Cornea. 1980, pp. 263–322.doi:10.1016/S0074-7696(08)61760-X
87. Hay, E. D., and J. W. Dodson. SECRETION OF COLLAGEN BY CORNEAL EPITHELIUM. *J. Cell Biol.* 57:190–213, 1973.
88. Hay, E. D., and J. P. Revel. Fine structure of the developing avian cornea. *Monogr. Dev. Biol.* 1:1–144, 1969.
89. Hayashi, M., Y. Ninomiya, K. Hayashi, T. F. Linsenmayer, B. R. Olsen, and R. L. Trelstad. Secretion of collagen types I and II by epithelial and endothelial cells in the developing chick cornea demonstrated by in situ hybridization and immunohistochemistry. *Development* 103:27–36, 1988.
90. Hedbys, B. O. The role of polysaccharides in corneal swelling. *Exp. Eye Res.* 1:81–91, 1961.
91. Ho, W. T., C. C. Su, J. S. Chang, S. W. Chang, F. R. Hu, T. S. Jou, and I. J. Wang. In vitro and in vivo models to study corneal endothelial-mesenchymal transition. *J. Vis. Exp.* 2016:1–7, 2016.
92. Holland, C., K. Numata, J. Rnjak-Kovacina, and F. P. Seib. The Biomedical Use of Silk: Past, Present, Future. *Adv. Healthc. Mater.* 8:1800465, 2019.
93. Honardoust, D., M. Varkey, Y. Marcoux, H. A. Shankowsky, and E. E. Tredget. Reduced decorin, fibromodulin, and transforming growth factor-β3 in deep dermis leads to hypertrophic scarring. *J. Burn Care Res.* 33:218–27.
94. Hong, H., H. Kim, S. J. Han, J. Jang, H. K. Kim, D.-W. Cho, and D. S. Kim. Compressed collagen intermixed with cornea-derived decellularized extracellular matrix providing mechanical and biochemical niches for corneal stroma analogue. *Mater. Sci. Eng. C* 103:109837, 2019.
95. Hos, D., M. Matthaei, F. Bock, K. Maruyama, M. Notara, T. Clahsen, Y. Hou, V. N. H. Le, A. C. Salabarria, J. Horstmann, B. O. Bachmann, and C. Cursiefen. Immune reactions after modern lamellar (DALK, DSAEK, DMEK) versus conventional penetrating corneal transplantation. *Prog. Retin. Eye Res.* 73:100768, 2019.
96. Huang, M. J., S. Kane, and D. Dhaliwal. WEK vs DMEK for Treatment of Fuchs' Endothelial Corneal Dystrophy. *Investig. Opthalmology Vis. Sci.* 59:2904, 2018.
97. Ikeda, A., H. Maisel, and D. Waggoner. An immunofluorescent study of cornea development in the chick. *Development* 33:279–290, 1975.

98. Ing, J. J., H. H. Ing, L. R. Nelson, D. O. Hodge, and W. M. Bourne. Ten-year postoperative results of penetrating keratoplasty. *Ophthalmology* 105:1855–65, 1998.
99. Isaacson, A., S. Swioklo, and C. J. Connon. 3D bioprinting of a corneal stroma equivalent. *Exp. Eye Res.* 173:188–193, 2018.
100. Isenberg, B. C., P. A. DiMilla, M. Walker, S. Kim, and J. Y. Wong. Vascular Smooth Muscle Cell Durotaxis Depends on Substrate Stiffness Gradient Strength. *Biophys. J.* 97:1313–1322, 2009.
101. Islam, M. M., O. Buznyk, J. C. Reddy, N. Pasyechnikova, E. I. Alarcon, S. Hayes, P. Lewis, P. Fagerholm, C. He, S. Iakymenko, W. Liu, K. M. Meek, V. S. Sangwan, and M. Griffith. Biomaterials-enabled cornea regeneration in patients at high risk for rejection of donor tissue transplantation. *npj Regen. Med.* 3:, 2018.
102. Jester, J. V., J. Huang, W. Matthew Petroll, and H. Dwight Cavanagh. TGFβ Induced Myofibroblast Differentiation of Rabbit Keratocytes Requires Synergistic TGFβ, PDGF and Integrin Signaling. *Exp. Eye Res.* 75:645–657, 2002.
103. Johnson, D. H. The Ultrastructure of Descemet's Membrane. *Arch. Ophthalmol.* 100:1942, 1982.
104. Joyce, N. Proliferative capacity of the corneal endothelium. *Prog. Retin. Eye Res.* 22:359–389, 2003.
105. Joyce, N. C., B. Meklir, S. J. Joyce, and J. D. Zieske. Cell cycle protein expression and proliferative status in human corneal cells. *Invest. Ophthalmol. Vis. Sci.* 37:645–55, 1996.
106. Joyce, N. C., S. E. Navon, S. Roy, and J. D. Zieske. Expression of cell cycle-associated proteins in human and rabbit corneal endothelium in situ. *Invest. Ophthalmol. Vis. Sci.* 37:1566–75, 1996.
107. Karamichos, D., M. L. Funderburgh, A. E. K. K. Hutcheon, J. D. Zieske, Y. Du, J. Wu, and J. L. Funderburgh. A Role for Topographic Cues in the Organization of Collagenous Matrix by Corneal Fibroblasts and Stem Cells. *PLoS One* 9:1–11, 2014.
108. Kaufman, H. ., J. . Capella, and J. . Robbins. The Human Corneal Endothelium. *Am. J. Ophthalmol.* 61:835–841, 1966.
109. Kessler, L. Zur Entwicklung des Auges der Wibeltiere. Vogel, Leipzig: 1877.
110. Kim, D. K., B. R. Sim, and G. Khang. Nature-Derived Aloe Vera Gel Blended Silk Fibroin Film Scaffolds for Cornea Endothelial Cell Regeneration and Transplantation. *ACS Appl. Mater. Interfaces* 8:15160–15168, 2016.
111. Kim, D. K., B. R. Sim, J. I. Kim, and G. Khang. Functionalized silk fibroin film scaffold using β-Carotene for cornea endothelial cell regeneration. *Colloids Surfaces B Biointerfaces* 164:340–346, 2018.
112. Kim, E., K. Ehrmann, J. Choo, S. Franz, and J. Moilanen. The effect of inlay implantation on corneal thickness and radius of curvature in rabbit eyes. *Cornea* 32:e106-12, 2013.
113. Kim, H., J. Jang, J. Park, K.-P. Lee, S. Lee, D.-M. Lee, K. H. Kim, H. K. Kim, and D.-W. Cho. Shear-induced alignment of collagen fibrils using 3D cell printing for corneal stroma tissue engineering. *Biofabrication* 11:035017, 2019.
114. Kim, H., M.-N. Park, J. Kim, J. Jang, H.-K. Kim, and D.-W. Cho. Characterization of cornea-specific bioink: high transparency, improved in vivo safety. *J. Tissue Eng.* 10:204173141882338, 2019.
115. Kim, J. C., and S. C. G. Tseng. The effects on inhibition of corneal neovascularization after human amniotic membrane transplantation in severely damaged rabbit corneas. *Korean J. Ophthalmol.* 9:32, 1995.
116. Kim, S., W. Kim, S. Lim, and J. Jeon. Vasculature-On-A-Chip for In Vitro Disease Models. *Bioengineering* 4:8, 2017.
117. Kissam, R. Ceratoplastics in man. *New York J. Med.* 2:281–282, 1844.
118. Kivanany, P. B., K. C. Grose, N. Yonet-Tanyeri, S. Manohar, Y. Sunkara, K. H. Lam, D. W. Schmidtke, V. D. Varner, and W. M. Petroll. An In Vitro Model for Assessing Corneal

Keratocyte Spreading and Migration on Aligned Fibrillar Collagen. *J. Funct. Biomater.* 9:54, 2018.
119. Kohno, T., N. Sorgente, T. Ishibashi, R. Goodnight, and S. J. Ryan. Immunofluorescent studies of fibronectin and laminin in the human eye. *Invest. Ophthalmol. Vis. Sci.* 28:506–14, 1987.
120. Konomi, K., Y. Satake, S. Shimmura, K. Tsubota, and J. Shimazaki. Long-term results of amniotic membrane transplantation for partial limbal deficiency. *Cornea* 32:1110–5, 2013.
121. Koo, S., S. J. Ahn, H. Zhang, J. C. Wang, and E. K. F. Yim. Human Corneal Keratocyte Response to Micro- and Nano-Gratings on Chitosan and PDMS. *Cell. Mol. Bioeng.* 4:399–410, 2011.
122. Koudouna, E., E. Mikula, D. J. Brown, R. D. Young, A. J. Quantock, and J. V. Jester. Cell regulation of collagen fibril macrostructure during corneal morphogenesis. *Acta Biomater.* 79:96–112, 2018.
123. Kumar, P., A. Pandit, and D. I. Zeugolis. Progress in Corneal Stromal Repair: From Tissue Grafts and Biomaterials to Modular Supramolecular Tissue-Like Assemblies. *Adv. Mater.* 28:5381–99, 2016.
124. Kurkinen, M., K. Alitalo, ~ Antti Vaheri, ~andlaurisaxi ? Svantestenman, A. Vaheri, S. Stenman, L. Saxén, ~ Antti Vaheri, ~andlaurisaxi ? Svantestenman, A. Vaheri, S. Stenman, and L. Saxén. Fibronectin in the development of embryonic chick eye. *Dev. Biol.* 69:589–600, 1979.
125. Lamm, V., H. Hara, A. Mammen, D. Dhaliwal, and D. K. C. Cooper. Corneal blindness and xenotransplantation. *Xenotransplantation* 21:99–114, 2014.
126. Lawrenson, J. G. Anterior Eye. In: Contact Lens Practice. Elsevier, 2018, pp. 10-27.e2.doi:10.1016/B978-0-7020-6660-3.00002-2
127. Lee, H. T., and E. D. P. Kay. FGF-2 induced reorganization and disruption of actin cytoskeleton through PI 3-kinase, Rho, and Cdc42 in corneal endothelial cells. *Mol. Vis.* 9:624–634, 2003.
128. Lee, H. T., J. G. Lee, M. Na, and E. D. P. Kay. FGF-2 induced by interleukin-1β through the action of phosphatidylinositol 3-kinase mediates endothelial mesenchymal transformation in corneal endothelial cells. *J. Biol. Chem.* 279:32325–32332, 2004.
129. Lee, J. G., M. H. K. Ko, and E. D. P. Kay. Endothelial mesenchymal transformation mediated by IL-1β-induced FGF-2 in corneal endothelial cells. *Exp. Eye Res.* 95:35–39, 2012.
130. De Leo, D., P. A. Hickey, G. Meneghel, and C. H. Cantor. Blindness, Fear of Sight Loss, and Suicide. *Psychosomatics* 40:339–344, 1999.
131. Leonard, E. K., V. H. Pai, P. Amberg, J. Gardner, and E. J. Orwin. Design and validation of a corneal bioreactor. *Biotechnol. Bioeng.* 109:3189–3198, 2012.
132. Li, S., Y. Han, H. Lei, Y. Zeng, Z. Cui, Q. Zeng, D. Zhu, R. Lian, J. Zhang, Z. Chen, and J. Chen. In vitro biomimetic platforms featuring a perfusion system and 3D spheroid culture promote the construction of tissue-engineered corneal endothelial layers. *Sci. Rep.* 7:1–17, 2017.
133. Li, S., Y. Han, H. Lei, Y. Zeng, Z. Cui, Q. Zeng, D. Zhu, R. Lian, J. Zhang, Z. Chen, and J. Chen. In vitro biomimetic platforms featuring a perfusion system and 3D spheroid culture promote the construction of tissue-engineered corneal endothelial layers. *Sci. Rep.* 7:777, 2017.
134. Livingston, P. M., C. A. McCarty, and H. R. Taylor. Knowledge, attitudes, and self care practices associated with age related eye disease in Australia. *Br. J. Ophthalmol.* 82:780–785, 1998.
135. Lo, C.-M., H.-B. Wang, M. Dembo, and Y. Wang. Cell Movement Is Guided by the Rigidity of the Substrate. *Biophys. J.* 79:144–152, 2000.
136. Lwigale, P. Y. Corneal Development. In: Progress in Molecular Biology and Translational

Science. Elsevier Inc., 2015, pp. 43–59.
137. Madden, P. W., I. Klyubin, and M. J. Ahearne. Silk fibroin safety in the eye: a review that highlights a concern. *BMJ Open Ophthalmol.* 5:e000510, 2020.
138. Madden, P. W., J. N. X. Lai, K. A. George, T. Giovenco, D. G. Harkin, and T. V. Chirila. Human corneal endothelial cell growth on a silk fibroin membrane. *Biomaterials* 32:4076–4084, 2011.
139. Maghsoudlou, P., G. Sood, and H. Akhondi. Cornea Transplantation. 2021.at <http://www.ncbi.nlm.nih.gov/pubmed/30969512>
140. Makris, E. A., J. C. Hu, and K. A. Athanasiou. Hypoxia-induced collagen crosslinking as a mechanism for enhancing mechanical properties of engineered articular cartilage. *Osteoarthr. Cartil.* 21:634–41, 2013.
141. Matthyssen, S., B. Van den Bogerd, S. N. Dhubhghaill, C. Koppen, and N. Zakaria. Corneal regeneration: A review of stromal replacements. *Acta Biomater.* 69:31–41, 2018.
142. Maurice, D. M. The structure and transparency of the cornea. *J. Physiol.* 136:263–286, 1957.
143. McKay, T. B., A. Ford, S. Wang, D. M. Cairns, R. N. Parker, P. M. Deardorff, C. E. Ghezzi, and D. L. Kaplan. Assembly and Application of a Three-Dimensional Human Corneal Tissue Model. *Curr. Protoc. Toxicol.* 81:1–36, 2019.
144. McKay, T. B., A. Ford, S. Wang, D. M. Cairns, R. N. Parker, P. M. Deardorff, C. E. Ghezzi, and D. L. Kaplan. Assembly and Application of a Three-Dimensional Human Corneal Tissue Model. *Curr. Protoc. Toxicol.* 81:, 2019.
145. Meek, K. M. The Cornea and Sclera. In: Collagen. Boston, MA: Springer US, 2008, pp. 359–396.doi:10.1007/978-0-387-73906-9_13
146. Meek, K. M., and C. Boote. The use of X-ray scattering techniques to quantify the orientation and distribution of collagen in the corneal stroma. *Prog. Retin. Eye Res.* 28:369–392, 2009.
147. Meek, K. M., and C. Knupp. Corneal structure and transparency. *Prog. Retin. Eye Res.* 49:1–16, 2015.
148. Michelacci, Y. M. Y. M. Collagens and proteoglycans of the corneal extracellular matrix. *Brazilian J. Med. Biol. Res.* 36:1037–46, 2003.
149. Moffatt, S. L., V. A. Cartwright, and T. H. Stumpf. Centennial review of corneal transplantation. *Clin. Exp. Ophthalmol.* 33:642–657, 2005.
150. Müller, L. J., E. Pels, and G. F. J M Vrensen. The specific architecture of the anterior stroma accounts for maintenance of corneal curvature. 2001.
151. Müller, L. J., E. Pels, L. R. H. M. Schurmans, and G. F. J. M. Vrensen. A new three-dimensional model of the organization of proteoglycans and collagen fibrils in the human corneal stroma. *Exp. Eye Res.* 78:493–501, 2004.
152. Müller, L. J., E. Pels, and G. F. J. M. Vrensen. The specific architecture of the anterior stroma accounts for maintenance of corneal curvature. *Br. J. Ophthalmol.* 85:437–443, 2001.
153. Musselmann, K., B. Alexandrou, B. Kane, and J. R. Hassell. Maintenance of the keratocyte phenotype during cell proliferation stimulated by insulin. *J. Biol. Chem.* 280:32634–9, 2005.
154. Nam, E., W. C. Lee, and S. Takeuchi. Formation of Highly Aligned Collagen Nanofibers by Continuous Cyclic Stretch of a Collagen Hydrogel Sheet. *Macromol. Biosci.* 16:995–1000, 2016.
155. Nguyen, T. D., and B. L. Boyce. An inverse finite element method for determining the anisotropic properties of the cornea. *Biomech. Model. Mechanobiol.* 10:323–337, 2011.
156. O'hEireamhoin, S., C. T. Buckley, E. Jones, D. McGonagle, K. J. Mulhall, and D. J. Kelly. Recapitulating aspects of the oxygen and substrate environment of the damaged joint milieu for stem cell-based cartilage tissue engineering. *Tissue Eng. Part C. Methods*

19:117–27, 2013.
157. Ohno, S., S. Hirano, S. Kanemaru, Y. Kitani, T. Kojima, S. Ishikawa, M. Mizuta, I. Tateya, T. Nakamura, and J. Ito. Transforming growth factor β3 for the prevention of vocal fold scarring. *Laryngoscope* 122:583–9, 2012.
158. Oliva, M. S., M. Gulati, T. Schottman, M. Gulati, and T. Schottman. Turning the tide of corneal blindness. *Indian J. Ophthalmol.* 60:423, 2012.
159. Orwin, E. J., and A. Hubel. In vitro culture characteristics of corneal epithelial, endothelial, and keratocyte cells in a native collagen matrix. *Tissue Eng.* 6:307–19, 2000.
160. Palchesko, R. N., S. D. Carrasquilla, and A. W. Feinberg. Natural Biomaterials for Corneal Tissue Engineering, Repair, and Regeneration. *Adv. Healthc. Mater.* 7:1–18, 2018.
161. Palchesko, R. N., J. L. Funderburgh, and A. W. Feinberg. Engineered Basement Membranes for Regenerating the Corneal Endothelium. *Adv. Healthc. Mater.* 5:2942–2950, 2016.
162. Palchesko, R. N., K. L. Lathrop, J. L. Funderburgh, and A. W. Feinberg. In Vitro Expansion of Corneal Endothelial Cells on Biomimetic Substrates. *Sci. Rep.* 5:32–34, 2015.
163. Palchesko, R. N., J. M. Szymanski, A. Sahu, and A. W. Feinberg. Shrink wrapping cells in a defined extracellular matrix to modulate the chemo-mechanical microenvironment. *Cell. Mol. Bioeng.* 7:355–368, 2014.
164. Panda, A., M. S. Pangtey, P. Sony, and S. Khokhar. Big Bubble Technique in Anterior Lamellar Keratoplasty. *J. Cataract Refract. Surg.* 28:2067, 2002.
165. Park, J., K. Lee, H. Kim, S. Park, R. E. Wijesinghe, J. Lee, S. Han, S. Lee, P. Kim, D. Cho, J. Jang, H. K. Kim, M. Jeon, and J. Kim. Biocompatibility evaluation of bioprinted decellularized collagen sheet implanted in vivo cornea using swept-source optical coherence tomography. *J. Biophotonics* 12:e201900098, 2019.
166. Pascolini, D., and S. P. Mariotti. Global estimates of visual impairment: 2010. *Br. J. Ophthalmol.* 96:614–618, 2012.
167. Patel, S., J. McLaren, D. Hodge, and W. Bourne. Normal human keratocyte density and corneal thickness measurement by using confocal microscopy in vivo. *Invest. Ophthalmol. Vis. Sci.* 42:333–9, 2001.
168. Peh, G. S. L., R. W. Beuerman, A. Colman, D. T. Tan, and J. S. Mehta. Human Corneal Endothelial Cell Expansion for Corneal Endothelium Transplantation: An Overview. *Transplantation* 91:811–819, 2011.
169. Perotto, G., Y. Zhang, D. Naskar, N. Patel, D. L. Kaplan, S. C. Kundu, and F. G. Omenetto. The optical properties of regenerated silk fibroin films obtained from different sources. *Appl. Phys. Lett.* 111:103702, 2017.
170. Petsche, S. J., D. Chernyak, J. Martiz, M. E. Levenston, and P. M. Pinsky. Depth-Dependent Transverse Shear Properties of the Human Corneal Stroma. *Investig. Opthalmology Vis. Sci.* 53:873, 2012.
171. Pinnamaneni, N., and J. L. Funderburgh. Concise review: Stem cells in the corneal stroma. , 2012.
172. Pinnock, A., N. Shivshetty, S. Roy, S. Rimmer, I. Douglas, S. MacNeil, and P. Garg. Ex vivo rabbit and human corneas as models for bacterial and fungal keratitis. *Graefe's Arch. Clin. Exp. Ophthalmol.* 255:333–342, 2017.
173. Pörtner, R., S. Nagel-Heyer, C. Goepfert, P. Adamietz, and N. M. Meenen. Bioreactor design for tissue engineering. *J. Biosci. Bioeng.* 100:235–245, 2005.
174. Price, M. O., P. Gupta, J. Lass, and F. W. Price. EK (DLEK, DSEK, DMEK): New Frontier in Cornea Surgery. *Annu. Rev. Vis. Sci.* 3:69–90, 2017.
175. Priyadarsini, S., A. Sarker-Nag, T. G. Rowsey, J.-X. X. Ma, and D. Karamichos. Establishment of a 3D In Vitro Model to Accelerate the Development of Human Therapies

against Corneal Diabetes. *PLoS One* 11:e0168845, 2016.
176. Qi, Y., D. Jiang, A. Sindrilaru, A. Stegemann, S. Schatz, N. Treiber, M. Rojewski, H. Schrezenmeier, S. Vander Beken, M. Wlaschek, M. Böhm, A. Seitz, N. Scholz, L. Dürselen, J. Brinckmann, A. Ignatius, and K. Scharffetter-Kochanek. TSG-6 released from intradermally injected mesenchymal stem cells accelerates wound healing and reduces tissue fibrosis in murine full-thickness skin wounds. *J. Invest. Dermatol.* 134:526–537, 2014.
177. Quantock, A. J., and R. D. Young. Development of the corneal stroma, and the collagen-proteoglycan associations that help define its structure and function. *Dev. Dyn.* 237:2607–2621, 2008.
178. de Quengsy, G. P. Précis ue Cours d'Opérations sur la Chirurgie des Yeux. Didot, Paris, France, Paris, France: 1789.
179. Radner, W., M. Zehetmayer, R. Aufreiter, and R. Mallinger. Interlacing and Cross-Angle Distribution of Collagen Lamellae in the Human Cornea. *Cornea* 17:537–543, 1998.
180. Reinhart, W. J., D. C. Musch, D. S. Jacobs, W. B. Lee, S. C. Kaufman, and R. M. Shtein. Deep anterior lamellar keratoplasty as an alternative to penetrating keratoplasty: A report by the American academy of ophthalmology. *Ophthalmology* 118:209–218, 2011.
181. Reisinger, F. Die keratoplastik, ein versuch zur enweiterund der augenheilkunde. *Bayer. Ann.* 1:, 1824.
182. Rönkkö, S., K.-S. S. Vellonen, K. Järvinen, E. Toropainen, and A. Urtti. Human corneal cell culture models for drug toxicity studies. *Drug Deliv. Transl. Res.* 6:660–675, 2016.
183. Ruberti, J. W., A. Sinha Roy, and C. J. Roberts. Corneal Biomechanics and Biomaterials. *Annu. Rev. Biomed. Eng.* 13:269–295, 2011.
184. Sangwan, V. S. Current Ophthalmology Amniotic membrane transplantation: A review of current indications in the management of ophthalmic disorders Scientific Basis of Clinical Application. 2007.
185. Sangwan, V. S., S. Burman, S. Tejwani, S. P. Mahesh, and R. Murthy. Amniotic membrane transplantation: A review of current indications in the management of ophthalmic disorders. *Indian J. Ophthalmol.* 55:251–60, 2007.
186. Sevcik, E. N., J. M. Szymanski, Q. Jallerat, and A. W. Feinberg. Patterning on topography for generation of cell culture substrates with independent nanoscale control of chemical and topographical extracellular matrix cues. *Curr. Protoc. Cell Biol.* 2017:10.23.1-10.23.25, 2017.
187. Shachar, M., and S. Cohen. Cardiac tissue engineering, ex-vivo: design principles in biomaterials and bioreactors. *Heart Fail. Rev.* 8:271–6, 2003.
188. Shafaie, S., V. Hutter, M. T. Cook, M. B. Brown, and D. Y. S. Chau. In Vitro Cell Models for Ophthalmic Drug Development Applications. *Biores. Open Access* 5:94–108, 2016.
189. Sharif, R., S. Priyadarsini, T. G. Rowsey, J. X. Ma, and D. Karamichos. Corneal Tissue Engineering: An In Vitro Model of the Stromal-nerve Interactions of the Human Cornea. *J. Vis. Exp.* 2018:1–5, 2018.
190. Shimmura, S., J. Shimazaki, Y. Ohashi, and K. Tsubota. Antiinflammatory Effects of Amniotic Membrane Transplantation in Ocular Surface Disorders. *Cornea* 20:, 2001.
191. Shrestha, J., S. Razavi Bazaz, H. Aboulkheyr Es, D. Yaghobian Azari, B. Thierry, M. Ebrahimi Warkiani, and M. Ghadiri. Lung-on-a-chip: the future of respiratory disease models and pharmacological studies. *Crit. Rev. Biotechnol.* 40:213–230, 2020.
192. Sie, N. M., G. H.-F. Yam, Y. Q. Soh, M. Lovatt, D. Dhaliwal, V. Kocaba, and J. S. Mehta. Regenerative capacity of the corneal transition zone for endothelial cell therapy. *Stem Cell Res. Ther.* 11:523, 2020.
193. Siran, W., C. E. Ghezzi, D. M. Cairns, R. E. Pollard, Y. Chen, R. Gomes, T. B. McKay, D. Pouli, A. Jamali, I. Georgakoudi, J. L. Funderburgh, K. Kenyon, P. Hamrah, and D. L. Kaplan. Human Corneal Tissue Model for Nociceptive Assessments. *Adv. Healthc. Mater.*

7:1800488, 2018.
194. Steinmetz, J. D. *et al.* Causes of blindness and vision impairment in 2020 and trends over 30 years, and prevalence of avoidable blindness in relation to VISION 2020: the Right to Sight: an analysis for the Global Burden of Disease Study. *Lancet Glob. Heal.* 9:e144–e160, 2021.
195. Stepp, M. A. Corneal integrins and their functions. *Exp. Eye Res.* 83:3–15, 2006.
196. Sun, Y., Q. Jallerat, J. M. Szymanski, and A. W. Feinberg. Conformal nanopatterning of extracellular matrix proteins onto topographically complex surfaces. *Nat. Methods* 12:134–136, 2015.
197. Syed-Picard, F. N., Y. Du, A. J. Hertsenberg, R. Palchesko, M. L. Funderburgh, A. W. Feinberg, and J. L. Funderburgh. Scaffold-free tissue engineering of functional corneal stromal tissue. *J. Tissue Eng. Regen. Med.* 12:59–69, 2017.
198. Tadakuma, K., N. Tanaka, Y. Haraguchi, M. Higashimori, M. Kaneko, T. Shimizu, M. Yamato, and T. Okano. A device for the rapid transfer/transplantation of living cell sheets with the absence of cell damage. *Biomaterials* 34:9018–25, 2013.
199. Thériault, M., O. Roy, I. Brunette, and S. Proulx. Physiological pressure enhances the formation of tight junctions in engineered and native corneal endothelium. *Exp. Eye Res.* 179:102–105, 2019.
200. Thurston, M., A. Thurston, and J. Mcleod. Socio-emotional effects of the transition from sight to blindness. *Br. J. Vis. Impair.* 28:90–112, 2010.
201. Trelstad, R. L. The Golgi Apparatus in Chick Corneal Epithelium: Changes in Intracellular Position During Development. *J. Cell Biol.* 45:34–42, 1970.
202. Trone, M., N. Campolmi, A. Guthier, C. Nefzaoui, A. Bernard, N. Naigeon, T. Nangoum-Fosso, S. Piselli, O. Garraud, S. Acquart, G. Thuret, P. Gain, A. Gauthier, C. Nefzaoui, A. Bernard, N. Naigeon, T. Nangoum-Fosso, S. Piselli, O. Garraud, S. Acquart, G. Thuret, and P. Gain. Conception and optimization of a corneal bioreactor. *Acta Ophthalmol.* 91:0–0, 2013.
203. Vajpayee, R. B., J. Tyagi, N. Sharma, N. Kumar, V. Jhanji, and J. S. Titiyal. Deep anterior lamellar keratoplasty by big-bubble technique for treatment corneal stromal opacities. *Am. J. Ophthalmol.* 143:954–957, 2007.
204. Velling, T., J. Risteli, K. Wennerberg, D. F. Mosher, and S. Johansson. Polymerization of type I and III collagens is dependent on fibronectin and enhanced by integrins alpha 11beta 1 and alpha 2beta 1. *J. Biol. Chem.* 277:37377–81, 2002.
205. Vepari, C., and D. L. Kaplan. Silk as a biomaterial. *Prog. Polym. Sci.* 32:991–1007, 2007.
206. Vlasov, A., R. K. Sia, D. S. Ryan, M. J. Mines, R. D. Stutzman, B. A. Rivers, S. C. G. Tseng, and K. S. Bower. Sutureless cryopreserved amniotic membrane graft and wound healing after photorefractive keratectomy. *J. Cataract Refract. Surg.* 42:435–443, 2016.
207. van Vlimmeren, M. A. A., A. Driessen-Mol, M. van den Broek, C. V. C. Bouten, and F. P. T. Baaijens. Controlling matrix formation and cross-linking by hypoxia in cardiovascular tissue engineering. *J. Appl. Physiol.* 109:1483–91, 2010.
208. Wang, L., R. Ma, G. Du, H. Guo, and Y. Huang. Biocompatibility of helicoidal multilamellar arginine-glycine-aspartic acid-functionalized silk biomaterials in a rabbit corneal model. *J. Biomed. Mater. Res. - Part B Appl. Biomater.* 103:204–211, 2015.
209. Wang, S., C. E. Ghezzi, R. Gomes, R. E. Pollard, J. L. Funderburgh, and D. L. Kaplan. In vitro 3D corneal tissue model with epithelium, stroma, and innervation. *Biomaterials* 112:1–9, 2017.
210. Wang, W., K. D. Tran, X. Wang, C. Stoeger, C. Patzer, Elisseeff, Jennifer H., and A. S. Jun. Cultured human corneal endothelial cells on a collagen vitrigel carrier as a donor tissue for endothelial keratoplasty. *Investig. Opthalmology Vis. Sci.* 67:1192, 2020.
211. Wang, X., S. Majumdar, U. Soiberman, J. N. Webb, L. Chung, G. Scarcelli, and J. H. Elisseeff. Multifunctional synthetic Bowman's membrane-stromal biomimetic for corneal

reconstruction. *Biomaterials* 241:119880, 2020.
212. Waring, G. O., W. M. Bourne, H. F. Edelhauser, and K. R. Kenyon. The Corneal Endothelium. *Ophthalmology* 89:531–590, 1982.
213. Weng, L., J. L. Funderburgh, I. Khandaker, M. L. Geary, T. Yang, R. Basu, M. L. Funderburgh, Y. Du, and G. H.-F. Yam. The anti-scarring effect of corneal stromal stem cell therapy is mediated by transforming growth factor β3. *Eye Vis.* 7:52, 2020.
214. West-Mays, J. A., and D. J. Dwivedi. The keratocyte: corneal stromal cell with variable repair phenotypes. *Int. J. Biochem. Cell Biol.* 38:1625–31, 2006.
215. Whitcher, J. P., M. Srinivasan, and M. P. Upadhyay. Corneal blindness: a global perspective. *Bull. World Health Organ.* 79:214–21, 2001.
216. Wilson, S. L., I. Wimpenny, M. Ahearne, S. Rauz, A. J. El Haj, and Y. Yang. Chemical and Topographical Effects on Cell Differentiation and Matrix Elasticity in a Corneal Stromal Layer Model. *Adv. Funct. Mater.* 22:3641–3649, 2012.
217. Woo, H.-M., M. Kim, O.-K. Kweon, D.-Y. Kim, T.-C. Nam, and J. H. Kim. Effects of amniotic membrane on epithelial wound healing and stromal remodelling after excimer laser keratectomy in rabbit cornea. *Br. J. Ophthalmol.* 85:345–349, 2001.
218. World Health Organization. World report on vision. 2019, 1–160 pp.
219. Wray, L. S., and E. J. Orwin. Recreating the Microenvironment of the Native Cornea for Tissue Engineering Applications. *Tissue Eng. Part A* 15:1463–1472, 2009.
220. Wu, J., Y. Du, M. M. Mann, J. L. Funderburgh, and W. R. Wagner. Corneal stromal stem cells versus corneal fibroblasts in generating structurally appropriate corneal stromal tissue. *Exp. Eye Res.* 120:71–81, 2014.
221. Wu, J., Y. Du, M. M. Mann, E. Yang, J. L. Funderburgh, and W. R. Wagner. Bioengineering Organized, Multilamellar Human Corneal Stromal Tissue by Growth Factor Supplementation on Highly Aligned Synthetic Substrates. *Tissue Eng. Part A* 19:2063–2075, 2013.
222. Wu, J., Y. Du, S. C. Watkins, J. L. Funderburgh, and W. R. Wagner. The engineering of organized human corneal tissue through the spatial guidance of corneal stromal stem cells. *Biomaterials* 33:1343–1352, 2012.
223. Wu, J., J. Rnjak-Kovacina, Y. Du, M. L. Funderburgh, D. L. Kaplan, and J. L. Funderburgh. Corneal stromal bioequivalents secreted on patterned silk substrates. *Biomaterials* 35:3744–3755, 2014.
224. Wulle, K. G. Electron microscopy of the fetal development of the corneal endothelium and Descemet's membrane of the human eye. *Invest. Ophthalmol.* 11:897–904, 1972.
225. Yamashita, K., S. Hatou, E. Inagaki, K. Higa, K. Tsubota, and S. Shimmura. A Rabbit Corneal Endothelial Dysfunction Model Using Endothelial-Mesenchymal Transformed Cells. *Sci. Rep.* 8:16868, 2018.
226. Young, R. D., C. Knupp, E. Koudouna, J. R. Ralphs, Y. Ma, P. Y. Lwigale, J. V. Jester, and A. J. Quantock. Cell-independent matrix configuration in early corneal development. *Exp. Eye Res.* 187:107772, 2019.
227. Young, R. D., C. Knupp, C. Pinali, K. M. Y. Png, J. R. Ralphs, A. J. Bushby, T. Starborg, K. E. Kadler, and A. J. Quantock. Three-dimensional aspects of matrix assembly by cellsin the developing cornea. *Proc. Natl. Acad. Sci. U. S. A.* 111:687–692, 2014.
228. Zareian, R., M. E. Susilo, J. A. Paten, J. P. McLean, J. Hollmann, D. Karamichos, C. S. Messer, D. T. Tambe, N. Saeidi, J. D. Zieske, and J. W. Ruberti. Human Corneal Fibroblast Pattern Evolution and Matrix Synthesis on Mechanically Biased Substrates. *Tissue Eng. Part A* 22:1204–1217, 2016.
229. Zeng, B., P. Wang, L.-J. Xu, X.-Y. Li, H. Zhang, and G.-G. Li. Amniotic membrane covering promotes healing of cornea epithelium and improves visual acuity after debridement for fungal keratitis. *Int. J. Ophthalmol.* 7:785–9, 2014.
230. Zhang, B., A. Korolj, B. F. L. Lai, and M. Radisic. Advances in organ-on-a-chip

engineering. *Nat. Rev. Mater.* 3:257–278, 2018.
231. Zhang, G., S. Chen, S. Goldoni, B. W. Calder, H. C. Simpson, R. T. Owens, D. J. McQuillan, M. F. Young, R. V. Iozzo, and D. E. Birk. Genetic Evidence for the Coordinated Regulation of Collagen Fibrillogenesis in the Cornea by Decorin and Biglycan. *J. Biol. Chem.* 284:8888–8897, 2009.
232. Zhang, W., J. Chen, L. J. Backman, A. D. Malm, and P. Danielson. Surface Topography and Mechanical Strain Promote Keratocyte Phenotype and Extracellular Matrix Formation in a Biomimetic 3D Corneal Model. *Adv. Healthc. Mater.* 6:1–11, 2017.
233. Zhao, H., Y. Jiang, Q. Cao, Y. Hou, and C. Wang. Role of integrin switch and transforming growth factor Beta 3 in hypoxia-induced invasion inhibition of human extravillous trophoblast cells. *Biol. Reprod.* 87:47, 2012.
234. Zhao, J., T. Fan, X. Ma, and X. Hu. Construction of a high cell density human corneal endothelial equivalent and its transplantation in primate models. *Xenotransplantation* 26:1–9, 2019.
235. Zhao, J., X.-Y. Ma, and T.-J. Fan. Construction of a tissue-engineered human corneal endothelium and its transplantation in rabbit models. *TURKISH J. Biol.* 40:420–429, 2016.
236. Zhao, X., W. Song, Y. Chen, S. Liu, and L. Ren. Collagen-based materials combined with microRNA for repairing cornea wounds and inhibiting scar formation. *Biomater. Sci.* 7:51–62, 2019.
237. Zhong, S., W. E. Teo, X. Zhu, R. W. Beuerman, S. Ramakrishna, and L. Y. L. Yung. An aligned nanofibrous collagen scaffold by electrospinning and its effects onin vitro fibroblast culture. *J. Biomed. Mater. Res. Part A* 79A:456–463, 2006.
238. Zieske, J. D., V. S. Mason, M. E. Wasson, S. F. Meunier, C. J. M. Nolte, N. Fukai, B. R. Olsen, and N. L. Parenteau. Basement Membrane Assembly and Differentiation of Cultured Corneal Cells: Importance of Culture Environment and Endothelial Cell Interaction. *Exp. Cell Res.* 214:621–633, 1994.
239. Zirm, E. K. Eine erfolgreiche rorale keratoplastik. *Arch Ophthalmol* 4:895–899, 1906.

Appendix A: Alternative Cell Alignment Method by Fabrication of COLI Microgrooves

Note: This appendix serves as a registry of an alternative methods that I found valuable to record and I think has potential for future experiments. It was developed in conjunction to the experiments presented in Chapter 3. I am presenting the introduction, methods, results, and a future considerations section as if it was a research article. This was done to make it easy to follow and perhaps encourage the reader to continue this work.

Summary: CSSC were cultured on COLI gels with molded microgrooves to guide cell orientation. The COLI microgrooves are produced by first casting a sacrificial gelatin gel over a PDMS mold with the desired pattern. Then, the gelatin is peeled off and COLI is cast over the gelatin mold with the desired microgrooves. Lastly, the gelatin construct is flipped, and the gelatin is melted and washed away. By using gelatin as a sacrificial mold, I can replicate PDMS channels and triangular features onto the COLI surface with a planar x-y-resolution of up to 2 µm planar-resolution and z-resolution of 1 µm. CSSC showed a high degree of alignment when seeded over the COLI microgrooves, regardless of initial seeding concentration. CSSC easily attached to the surface and assembled an aligned FN matrix parallel to the cell orientation. This further supports the idea that aligned CSSC assembled an aligned ECM. Overall, COLI microgrooves present an efficient method to align CSSC. COLI surfaces do not require chemical modifications to promote cell adhesion, and unlike other commonly used topographical-based guiding mechanisms, PDMS and gelatin, most cells can reassemble and readily modify the COLI surface. I recommend that future experiments

explore the role of other proteins, such as COLVI and COLIV, in conjunction with COLI to aid in the differentiation of CSSC. Finally, the use of a gelatin sacrificial mold to make COLI scaffold can be expanded to be used in organ-on-a-chip approaches.

Introduction

Soluble factors, the ECM composition, surface and matrix structure, mechanical loads and other forces, and cell-cell interactions are some examples of environmental cues that can affect cell behavior and fate. Surface-cell interactions are of special interest because several important cell behaviors can be affected by adjusting the surface composition, topography, or structure. For example, stiffness can be used exclusively to guide stem cell differentiation[53], affect cell migration (durotaxis)[100,135], cause cell metastasis[60], or induce ECM remodeling[76].

Similarly, by adjusting the topography of the surface, cells can be organized into highly aligned monolayers. Popular examples of surface modifications to align and affect cell behavior include soft-silicone or natural channels and grooves[73,121,197,208], electrospinning of synthetic and natural fibrils[1,220,237], and use of protein lines or features to create a biased surface[4,48,196].

Here, I present a method to bring about micron-level topographical features onto a COLI gel. A gelatin sacrificial gel is used to copy the desired features on the surface of a PDMS surface. The gelatin was able to accurately copy and transfer on the COLI gel channels with a width of 10 µm and a spacing of 10 µm. Similarly, 2 µm triangles arranged in a hexagonal pattern were also successfully copied on the COLI surface. Channel height on the COLI surface was ~1 µm from an original channel height of ~2.5 µm on the PDMS surface.

Following, CSSC were seeded at various concentrations to assess how the COLI microgrooves affect cell alignment and matrix assembly. CSSC cultured at 10,500, 30,000, 50,000 and 100,000 cells/cm^2 reached a high degree of alignment, measures as an orientational order parameter (OOP), and assembled an aligned FN matrix parallel to the cell orientation.

Materials and Methods

Fabrication of COLI Microgrooves

COLI microgrooves are produced by first casting sacrificial gelatin over the desired PDMS mold, followed by the casting of COLI over the sacrificial gelatin mold. First, sonicate the PDMS stamp or surface in 50% ethanol solution for 30 min and dry with air or nitrogen. Then, evenly spread a 20% gelatin type A (ThermoFisher) solution over the PDMS surface with the feature facing up and allow the gelatin to gel at room temperature, ~15 min (Fig. 1i). Then, carefully peel off the gelatin from the PDMS and place feature-side up. Evenly distribute a 6 mg/mL COLI solution over the gelatin and allow the COLI to gel at room temperature, ~1 hour (Fig. 1ii). Flipped the COLI-gelatin such that the COLI is in the bottom, and placed the whole construct in a 37°C incubator for 1 hour to melt the gelatin away. Rinse the COLI with warm di-water to wash away any remaining gelatin (Fig. 1iii). Seed cells over the COLI microgrooves as desired (Fig. 1iv).

Characterization of COLI Microgrooves

Planar x-y-resolution was assessed by imaging the surface of a PDMS stamp with 10 by 10 by 2.5 μm (width by spacing by depth) channels or custom 2 μm triangles

in a hexagonal, the surface of the gelatin sacrificial mold, and the final COLI microgroove using a phase microscope (). Similarly, the z-resolution was assessed by imaging the side of the PDMS channels and the side of the gelatin channel using the phase microscope. Z-resolution of the COLI microgrooves was assessed by tile scanning using a Nikon Eclipse Ti2 multiphoton microscope at a wavelength of 810-830 nm for the generation of second-harmonic signaling. Lastly, atomic force microscopy () was used to assess the detailed COLI channel of the COLI microgroove.

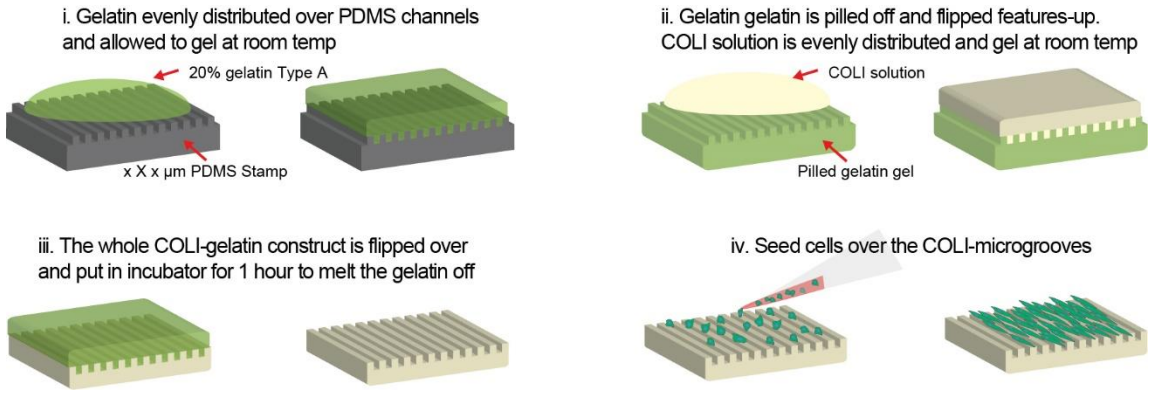

Figure 1. Fabrication of COLI microgrooves.
(i) A gelatin solution is evenly distributed over a PDMS surface with the desired features. The gelatin is allowed to gel at room temperature. (ii) The gelatin is then peeled-off and placed feature-side up. A COLI solution is evenly distributed across the gelatin surface. The COLI is allowed to gel at room temperature. (iii) The whole construct is flipped over, COLI gel below, and placed in an incubator. The gelatin is melted away and rinsed with warm di-water. (iv) Cells can then be seeded directly on the COLI microgroove surface.

Seeding and Culture of Corneal Stroma Stem Cells on COLI Microgrooves

CSSC were seeded onto COLI microgrooves of dimensions 10 by 10 by 1 µm (width by spacing by depth) at 10,500, 30,000, 50,000, or 100,000 cells/cm^2. CSSC were cultured in GM until confluency as described in section 2.3.4. The alignment, as measured by OOP, of CSSC was calculated at the end of the differentiation process. As

described in section 2.3.8.

Immunostaining and Microscopy

CSSC were imaged 1 hour, 1 day, 2 days, and 4 days after seeding using a phase microscope. On the days of confluency, CSSC were stained for FN, actin cytoskeleton, and nuclei. To stain the samples. the construct was rinsed with 1xPBS, and then fixed with 4% paraformaldehyde in 1xPBS for 12 minutes and washed for 5 minutes with 1xPBS thrice. Five percent normal goat serum in 1xPBS was used to block any non-specific binding. Samples were incubated mouse anti-human fibronectin (1:200, HFN 7.1, Development Studies Hybridoma Bank), in 1% bovine serum albumin in 1xPBS overnight at 4°C. Following, the samples were washed for 5 minutes with 1xPBS thrice and incubated with secondary antibody AlexaFluor 633 goat anti-mouse (1:200, Thermo Fisher), diamidino-2-phenylindole (DAPI, Thermo Fisher) to stain nuclei, and Phalloidin 488 (1:200, Thermo Fisher) to stain actin filaments for 1 hour. Samples were washed for 5 minutes with 1xPBS thrice again and mounted on microscope glass slides with Prolong Anti-Fade (Life Technologies). Mounted samples were imaged on a Zeiss LSM 700 confocal microscope.

OOP as a measurement of alignment

The alignment was quantified by finding the largest eigenvalue of the orientational order tensor, defined as the 2D orientational order parameter (OOP) [81]. Actin alignment for all samples at D10-KDM was measured using a custom MATLAB (MathWorks) algorithm that calculates the OOP of the given image were 0 meaning isotropy and 1 perfect alignment, as in previously published methods [61]. To quantify the

OOP, samples were imaged on the Zeiss LSM 700 confocal; 9 images per sample and 5 samples per condition.

Statistical Analysis

All the results are expressed as mean ± sample standard deviation. One-way ANOVA was used to compare the OOP of CSSC seeded at the various seeding concentration on the COLI microgrooves. $p<0.05$ was deemed significant. All statistical analysis was performed on GraphPad Prism 8.3.0.

Results

Gelatin and COLI microgrooves integrity

The accuracy of transferring PDMS features to the surface of a COLI gel was assessed by visually comparing the COLI surface to the surface of the original PDMS stamp. Phase microscopy was used to image the PDMS, gelatin, and COLI surface. The gelatin and COLI surface appear to have a similar topography to the original PDMS stamp. The 10 by 10 µm channels and the custom hexagonal 2 µm triangles were transferred successfully from the PDMS to the gelatin and from the gelatin to the COLI (Fig. 2.11A).

Similarly, I tested the shape and z-resolution by comparing the height of the channels between the PDMS, gelatin, and COLI, and an atomic force microscope was used to further assess the resolution of the COLI microgroove. The original PDMS channel height was 2.5 µm Although the channels are distinguishable, the channels on the gelatin surface seem to lack detail and appear to be shallower than the original PDMS channels and might have affected the final height of the COLI microgrooves (Fig.

2B). Using atomic force microscopy, I was able to characterize the surface and depth of the COLI microgrooves. The COLI microgrooves appear to have a width of 10 µm and a spacing of 10 µm width a depth of up to 1 µm (Fig. 2C). Taken together, these results suggest that the resolution of the final COLI microgrooves is dependent on how well the gelatin sacrificial layer “copied” the PDMS channels or features.

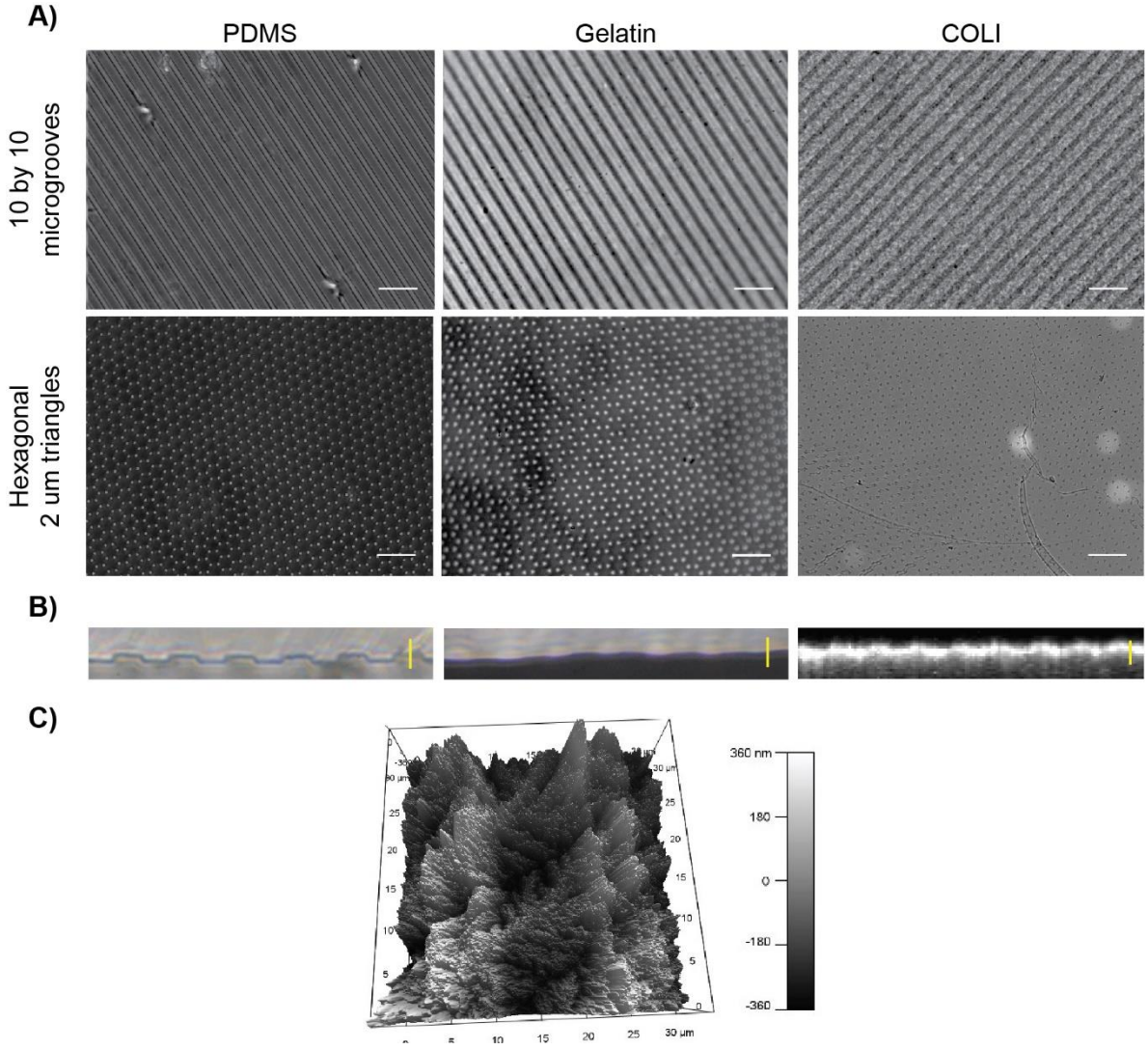

Figure 2. Comparison between initial PDMS features and final COLI gel.
(A) Phase imaged of PDMS, gelatin, and COLI surfaces using 10 by 10 µm PDMS channels and custom 2 µm triangles hexagonal PDMS features. (B) Side view of the PDMS and gelatin channels using a phase microscope, and COLI microgrooves using multiphoton microscopy.

(C) Map of the topography of a COLI microgroove using atomic force microscopy.

Alignment of CSSC over COLI microgrooves

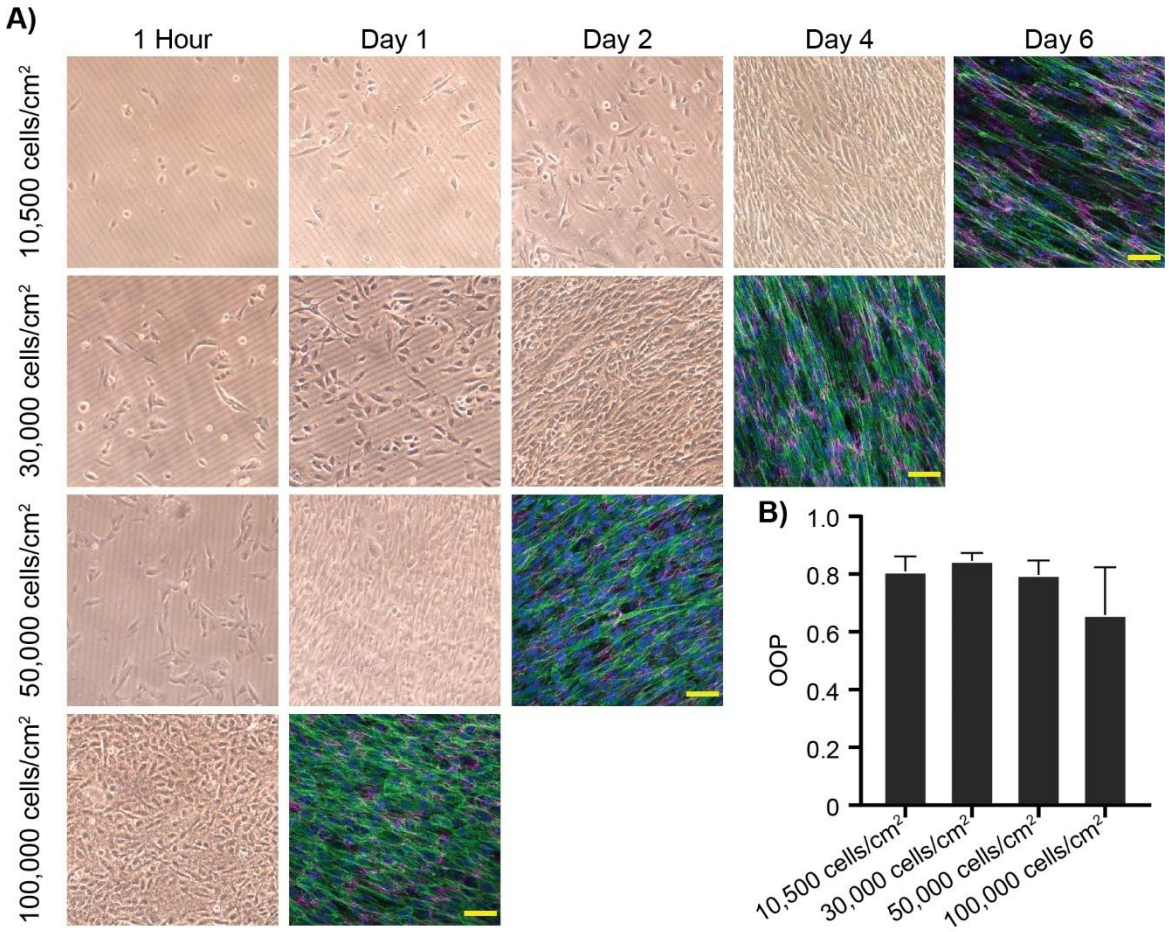

Figure 3. CSSC alignment as a function of seeding density on 10 by 10 COLI microgrooves. (A) Phase and fluorescent images of CSSC growth and alignment over the COLI microgrooves. The scale bar is 25 µm. Nuclei (blue), actin (green), FN (magenta). (B) OOP of CSSC at the end of the differentiation process. No statistical significance was found between the group (n=5).

To determine if the COLI microgrooves can be used to make an aligned cell-assembled ECM, CSSC were seeded at 10,500, 30,000, 50,000, 100,000 cells/cm^2 over the COLI microgrooves. At all seeding densities, CSSC are observed to align

parallel to the COLI microgrooves once they reach high confluency. Similarly, immunostaining of the FN matrix and the actin cytoskeleton show that the assembled FN runs parallel to the cell body (Fig. 3A). Furthermore, quantification of the OOP at full confluency shows that CSSC achieved a high degree of alignment, and an ANOVA test showed no significant difference in OOP (Fig. 3B).

Future Directions and Considerations

Cell alignment to topographical cues has been vastly researched on synthetic and natural biomaterials. COLI is the most abundant ECM protein in the body and there has is widespread interest in using COLI as a building material for engineered cell culture systems. Here, I present a method to bring about micron-level topographical features onto a COLI gel. A gelatin sacrificial gel is used to copy the desired features on the surface of a PDMS surface and then this is transferred onto a COLI gel. The gelatin was able to accurately copy and transfer on the COLI gel channels with a width of 10 µm and a spacing of 10 µm. Similarly, 2 µm triangles arranged in a hexagonal pattern were also successfully copied on the COLI surface. However, the channel height on the COLI surface was ~1 µm from an original channel height of ~2.5 µm on the PDMS surface. As shown in figure 2.10B, the gelatin lacks sharp edges and, unlike the sharp PDMS channels, the gelatin appears wave-like instead. This error in z-resolution can be attributed to the gelatin not being able to fully penetrate the PDMS channels; either from air trapped between the PDMS channels or from the viscosity of the gelatin not being able to flow into the full depth of the channel, or tearing of the gelatin channels as this is peeled off the PDMS surface. These can be easily addressed by adding a degassing step before gelatin gelation and testing a few different gelatin concentrations to lower

viscosity and facilitate penetration into the PDMS channels. It will be important to keep in mind that if a lower gelatin concentration is used, in here I used 20% gelatin in water, the gelatin might be more prone to tearing. Lastly, I recommend staying away from surface additives to prevent the addition of toxic chemicals into the cell culture.

Following, CSSC were seeded at various concentrations to assess how the COLI microgrooves affect cell alignment and matrix assembly. CSSC were cultured at 10,500, 30,000, 50,000 and 100,000 cells/cm^2 over 10 by 10 µm COLI microgrooves. CSSC are a group of specialized corneal stem cells found in the limbus of the cornea. These cells were chosen because I had them readily available and are very susceptible to their environment for proper alignment and differentiation. For example, in Chapter 2, CSSC were cultured using the same seeding concentration over FN lines of the same dimension as the COLI microgrooves. CSSC only showed a high degree of alignment when cultured at 50,000 cells/cm^2. In comparison here, CSSC reached a high degree of alignment, measured as orientational order parameter (OOP), and assembled an aligned FN matrix parallel to the cell orientation in all seeding concentrations.

These results corroborate the results done in channels or electrospun synthetic and naturals materials using the same type of cell. Syed-Picard, et al. achieved a highly aligned stromal matrix by seeded 10,500 CSSC/cm^2 over PDMS channels 10 µm wide, 10 equal µm apart, and 5 µm deep[197]. Similarly, dimensions as the ones presented in this paper. Similarly, Guezzi, et al. and Deardorff, et al. used a patterned silk film to align CSSC seeded at 50,000 cells/cm^2 and 15,000 cells/cm^2, respectively, that then assemble a highly aligned matrix[37,73]. Other examples of CSSC alignment due to topography include, but are not limited to, work by Karamichos, et al.[107], Wu, et

al.[220,221,223], and Wilson, et al.[216].

COLI surfaces are an attractive tool to understand the effects of topography on cell order, binding, and differentiation. COLI surfaces do not require chemical modifications to promote cell adhesion, and unlike other commonly used topographical-based guiding mechanisms e.g. PDMS and gelatin, most cells can reassemble and readily modify the COLI surface. Additionally, the COLI channels can be coated or mixed with other ECM proteins of interest including fibronectin and other collagen types. Finally, the COLI stiffness is far closer to the stiffness of native tissue. Most synthetic biomaterials possess a stiffness order of magnitude higher than the one present in soft tissue; and as discussed before, stiffness can have a great impact on cell behavior and, in the case of stem cells, differentiation.

Future experiments for the development of this technology include improving the height/depth resolution of the COLI microgrooves. This can be accomplished by removing any air trapped between the PDMS channels and the gelatin gel so that sharp edges can be copied to the gelatin and then to the COLI. Also, it will be important to understand how will cells reassemble the COLI in long-term culture (>30 days). Finally, creating COLI microgrooves and features could allow researchers to think about how to incorporate COLI surfaces into organ-on-a-chip systems, thus making these chips, which are traditionally made from coated PDMS, more accurate to the native tissue.

Appendix B: Alternative Method to Co-culture Engineered Endothelium and Stroma Layers Using Double-Surface Initiated Assembly and Suspension of Collagen Gels

Note: This appendix serves as a registry of an alternative methods that I found valuable to record and I think has potential for future experiments. It was developed in conjunction to the experiments presented in Chapter 4. I am presenting the introduction, methods, results, and a future considerations section as if it was a research article. This was done to make it easy to follow and perhaps encourage the reader to continue this work.

Summary: Here I present a method to readily fabricate a thin (<40 µm) posterior cornea toward applications in partial corneal transplantation. A COLI gel was stamped with laminin (LAM) and COLIV (COLIV) on one side, to mimic Descemet's membrane composition, and fibronectin (FN) lines on the opposite side to align corneal stroma stem cells and assemble a highly aligned extracellular matrix. Although endothelial cell density was sub-optimal after 4 days of culture, ZO1 was present only on the endothelial side of the construct. Additionally, CSSC aligned to the FN lines. Taken together these results serve as a proof of concept for thin posterior cornea models and can be further explored to develop a transplantable tissue for DSEAK or DMEK procedures.

Introduction

Corneal endothelial cells form a delicate monolayer in the posterior of the cornea and regulate the hydration of the stroma, resulting in the transparency of the cornea. Damage to this tissue can be addressed via transplantation of the cornea. Descemet's

Membrane Endothelial Keratoplasty (DMEK) and Descemet's Stripping Endothelial Keratoplasty (DSEAK) procedures are partial corneal transplantation procedures that target the endothelium and Descemet's membrane, and the endothelium Descemet's membrane and the posterior stroma, respectively. DSEAK and DMEK are becoming more popular to address corneal damage because these do not cause insult to a patient's healthy stroma and epithelium, specifically target the endothelium, and have more successful and shorter recovery than a whole cornea transplant. However, there is an unmet demand for transplantable endothelial corneal tissue.

The engineered constructs of the corneal endothelium might present as an alternative to transplantable tissue. Work using the amniotic membrane as a scaffold to culture and create a healthy endothelial cell monolayer shows promising applications in in-vivo animal studies[160,234,235]. Similarly, vitrified collagen I (COLI) has become a popular and promising material for endothelial cell work to build a transplantable tissue[210,211].

Here, I provide a procedure using collagen type 1 (COLI) gel to co-culture endothelial cells and keratocytes on different sides of the same gel and serve as a pseudo-Descemet's membrane. Collagen type 4 (COLIV) and laminin (LAM), and 30 by 30 µm fibronectin lines (FN30) were stamped on opposite sides of the COLI. The double-sided gel was then suspended such that there is access to both surfaces for cell seeding. Endothelial cells were seeded on the LAM-COLIV side, while corneal stromal stem cells (CSSC) were seeded on the FN30 side. Fluorescent staining showed a low endothelial cell and keratocyte density. This can be attributed to a short culture period, a small seeding density, or problems in selecting a suitable co-culture media.

Materials and Methods

Fabrication of Double-Sided Surface Initiated Assembly on a COLI gel

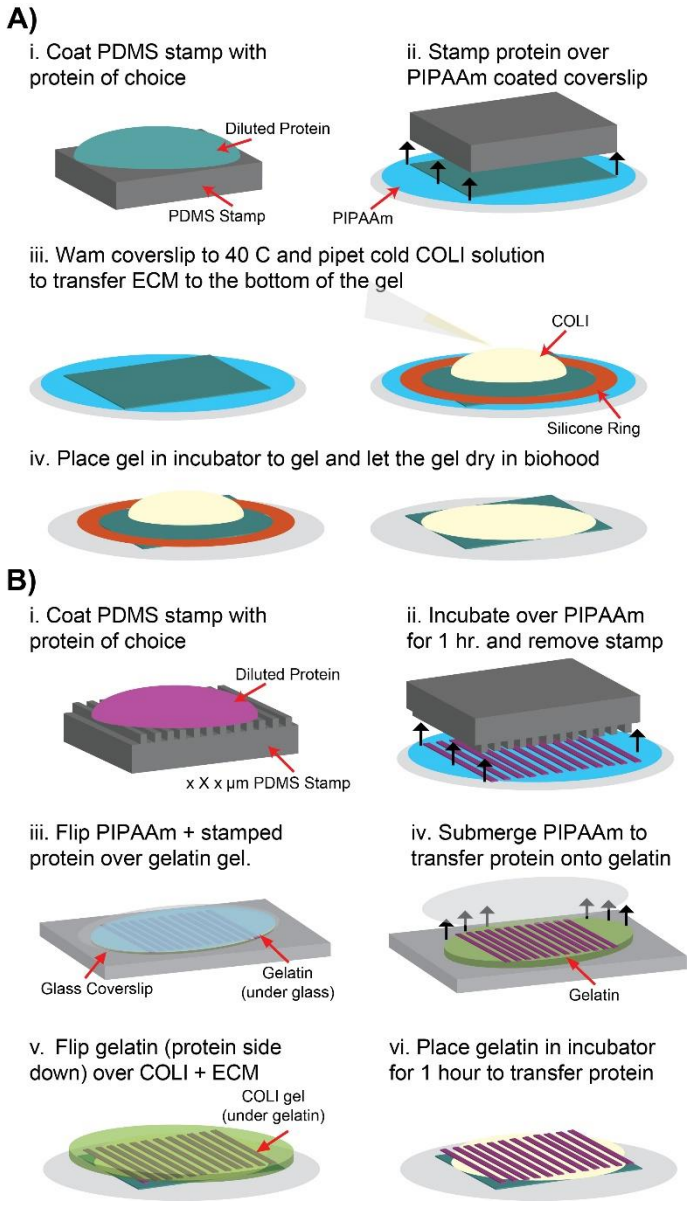

Figure 1 Fabrication of double-sided SIA on a COLI gel.

Detailed schematic to transfer protein features to the bottom (A) and top (B) of the COLI gel.

First, microcontact printing of featureless LAM-COLIV stamps were made over poly(N-isopropylacrylamide) (PIPAAm) coated coverslips. This was done by coating featureless polydimethylsiloxane (PDMS) stamp with a LAM (poly10% in butanol; Polysciences). Flat, featureless polydimethylsiloxane (PDMS) stamps were coated with LAM (50 µg/mL; Life Technologies) and COLIV (50 µg/mL; From the human placenta; Sigma Aldrich) solution for 1 hour (Fig. 1A.i). The stamps were rinsed and flip over, protein side down, over a coverslip coated with 10% PIPAAm in butanol. After 1 hour, the PDMS stamps were carefully removed (Fig. 3.8A.ii).

To transfer the LAM+COLIV stamp to the bottom side of a COLI gel, the PIPAAm coverslips with the LAM+COLIV proteins were warmed up to 40°C. A 20 mm silicone ring was placed over the coverslip and cold COLI solution was pipetted and rapidly evenly distributed inside the silicone ring (Fig. 3.8A.iii). This was done, carefully, without touching the surface of the coverslip to not disturb the protein stamp. The COLI+LAM+COLIV construct was then placed in the incubator for 1 hour and then in a laminar flow biohood to dry the COLI gel.

Parallelly, fibronectin (FN; Corning) lines of width by the spacing of 30 by 30 µm (FN30) were microcontact printed onto another PIPAAm coated coverslip using a PDMS with 30 by 30 µm channels as described above (Fig. 1B.i-ii). The FN30 stamp was transferred to a 20% gelatin A (Thermo Fisher) gel by flipping the PIPAAm with FN30 over the gelatin and submerging it in water to allow for the dissolution of PIPAAm (Fig. 1B.iii-iv). Lastly, the FN30 were transferred to the COLI+LAM+COLIV gel produced previously by peeling off and flipping the gelatin gel, FN30 side down) over the COLI gel. The construct was placed in the incubator at 37°C for one hour, rinsed with warm 1xPBS three times, and placed in the incubator for another hour to remove any remaining gelatin.

Mounting of Double-sided COLI Scaffold onto a CellCrown Insert

To be able to access both sides of the scaffold, the COLI gel was mounted onto a Transwell-like insert, CellCrown (CellCrown 24NX, Scaffdex). Briefly, the construct is submerged in 1xPBS and then peeled off the coverslip. The construct is then flipped over such that the LAM+COLIV is facing down. Carefully, the construct is “fished out” using the CellCrown insert, and the gel is moved such that the stamps are centered,

and the gel taught. Finally, the construct is locked in place as manufacturers protocol.

4.6.1.1. Seeding of BCEC Over the Mounted COLI Scaffold

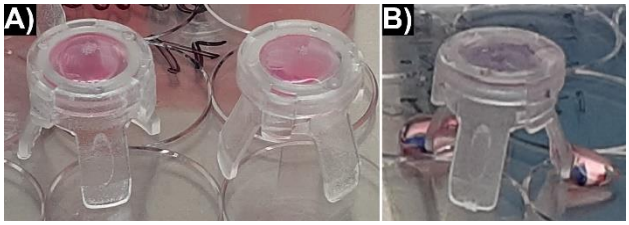

Figure 2. Seeding of BCEC on the Mounted COLI Gel.

(A) Dispensing 100 µL of 100,000 BCEC on a well-mounted gel after 30 minutes. (B) Any holes or tears on the gel or imperfect mounting can cause the medium to pass through the gel and affect cell seeding.

Bovine corneal endothelial cells (BCEC), passage 2 to 5, were seeded on the LAM+COLIV side of the mounted COLI scaffold at 100,000 cells per gel. To facilitate seeding, and because this side will be facing downward, dilute 100,000 cells in 100 µL, dispense on the mounted COLI gel, and let the cells attach for 30 minutes (Fig. 2A). Note that tearing of the COLI gel or an imperfect seal in the CellCrown insert can cause media to go through the gel and change the seeding count (Fig. 2B). Endothelial cells were culture in low glucose DMEM with 10% FBS, 1 penicillin-streptomycin - amphotericin B, and 0.5% gentamicin overnight.

Seeding of CSSC Over the Mounted COLI Scaffold

Corneal stroma stem cells (CSSC), passage 2 to 4, were cultured on a stem cell growth medium (GM) containing 2% (v/v) fetal bovine serum, Dulbecco's Modified Eagle Medium-LowGlucose-GlutaMax (Gibco), 400 mg/L MCDB-201 (Sigma Aldrich), 1mg/mL of AlbuMax Lipid-Rich BSA (Gibco), 0.1 mM L-ascorbic acid-2-phosphate (Sigma Aldrich), 0.1X insulin-transferring-selenium (Gibco), 10 ng/mL recombinant rat platelet-derived growth factor-BB protein (R&D Systems), 10 ng/mL recombinant human epidermal growth factor (R&D Systems), 100 nM dexamethasone (Sigma Aldrich), 1x

penicillin-streptomycin 100x (Corning CellGro), and 1:1000 gentamycin (50 mg/mL) (Gibco). CSSC were seeded at a density of 50,000 cells per gel (50,000 cells/cm^2) by diluting 50,000 cells in 100 µL and dispensing on the FN30 side of the construct. CSSC were seeded 1 days after seeding of BCEC and GM was used to co-culture the cells for 3 more days.

Staining and Imaging

CSSC and BCEC were fixed and imaged after 3 days of CSSC seeding. Construct were rinsed with 1xPBS supplemented with Ca and Mg ($1xPBS^{++}$), and then fixed with 4% paraformaldehyde in $1xPBS^{++}$ for 12 minutes and washed for 5 minutes with $1xPBS^{++}$ thrice. Tight junctions were stained using a primary antibody cocktail of mouse anti-ZO1 (1:200; Thermo Fisher) in 1% Bovine Serum Albumin in 1xPBS overnight at 4°C. The following day, samples were rinsed for 5 minutes three times with $1xPBS^{++}$ and stained using a second antibody cocktail containing AlexaFluor 555 goat anti-mouse (1:200; Thermo Fisher), Phalloidin 488 for staining of actin filaments, and diamidino-2-phenylindole (DAPI, Thermo Fisher) for staining of cell nuclei for 1 hour at room temperature. Finally, samples were washed for 5 minutes with $1xPBS^{++}$, demounted from the CellCrown, and mounted on a microscope glass slide and glass coverslip with Prolong Anti-Fade (Life Technologies).

Mounted samples were imaged on a Zeiss LSM 700 confocal microscope. Two-photon microscopy was perform using a Nikon Eclipse Ti2 multiphoton microscope at a wavelength of 810-830 nm for the generation of second-harmonic signaling from aligned COLI fibrils.

Results

Double-sided SIA in a COLI gel

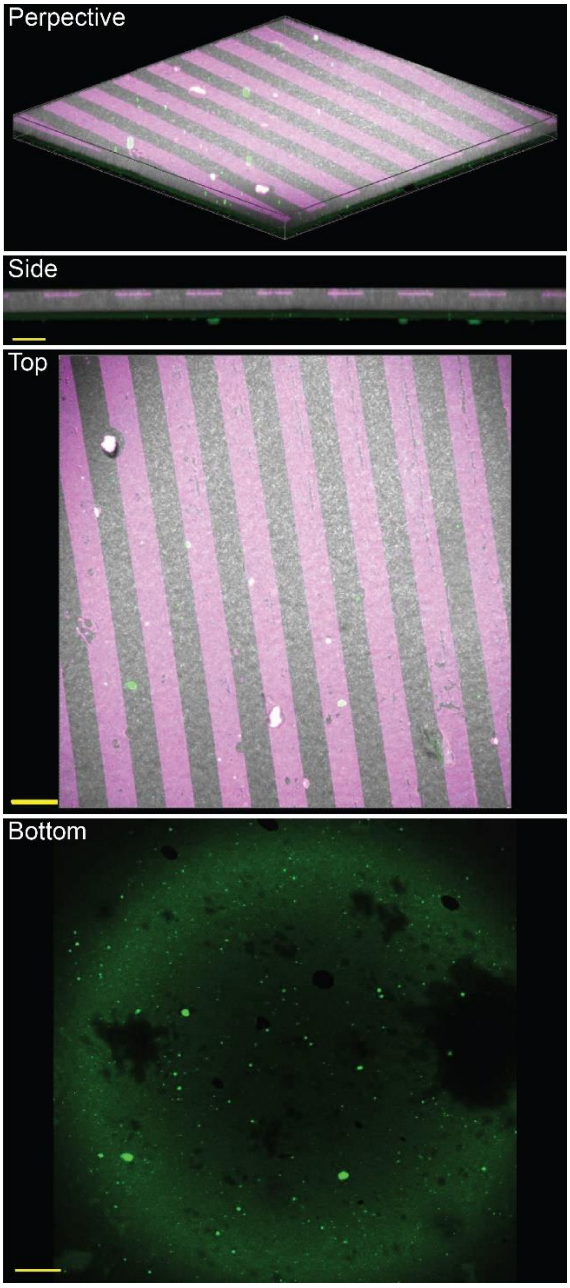

Figure 3. Imaging of double-sided SIA on a COLI gel.
Fluorescent staining of the bottom (green) and top (magenta) proteins transferred to the COLI gel (white). The scale bar is 25 µm.

Using second harmonic generation, tagged LAM+COLIV and FN30, the different layers of the construct were observed. The FN30 was attached to the whole COLI gel (Fig. 3. magenta). Similarly, the LAM+COLIV attached to the COLI gel with very little damage to the stamp (Fig. 3. green). Although tears on the stamp of less than 20 µm in diameter were observed, cell attachment might not be compromised because the supporting gel is COLI. The COLI scaffold had a total thickness of 20 µm and was strong enough to be moved around and mounted on the CellCrown insert without tearing. Note that it is easier to first stamp the LAM+COLIV on the bottom of the COLI gel instead of the other

way around.

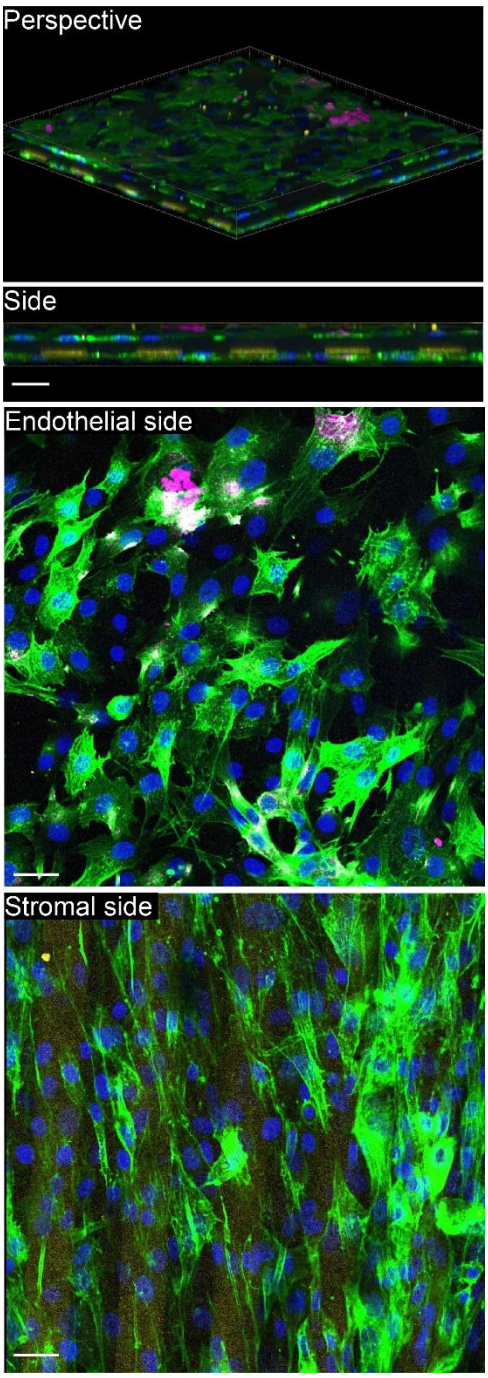

Figure 4. Co-culture of corneal endothelial and CSSC on a suspended COLI gel. Fluorescent images of BCEC and CSSC showing actin (green), nuclei (blue), ZO1 (magenta), and FN lines (yellow). Scale bars are 30 μm

Co-culture of BCEC and CSSC on COLI scaffold

BCEC and CSSC were seeded on the LAM+COLIV and FN30 sides of the COLI scaffold, respectively, and co-culture for 3 days in GM. Fluorescent staining of the cells shows that BCEC and CSSC were cultured on their respective sides of the COLI scaffold. Tight junction staining, in the form of ZO1, was only present on the BCEC side. Although ZO1 was not present throughout the whole monolayer, probably due to lack of cell-cell contact, there was some tight junction between BCEC (Fig. 4). Comparison of the BCEC and CSSC morphology, from the actin stain, it seems that the BCEC and CSSC remained separated and there was no mixing between the cell types nor migration of one cell from one side of the COLI gel onto the opposite side. As in other experiments with CSSC culture over

protein line, CSSC appear to have aligned parallel to the FN30, however, a second cell bilayer was not observed.

Future Considerations

Here, I provide a procedure to co-culture endothelial cells and keratocytes on different sides of a COLI gel that serves as a pseudo-Descemet's membrane. This work can be expanded by growing the BCEC to confluency before seeding of CSSC. Previous work done in the Feinberg lab suggests that BCEC can grow and maintain tight junctions when cultured in GM. However, if CSSC are to be differentiated into keratocytes, a medium that serves as keratocyte differentiation media and BCEC maintenance will be needed.